Structural Dynamics of Wild Type and Mutant Forms of CLIC4 and Ezrin

by

Merve Yığın

A Dissertation Submitted to the
Graduate School of Sciences and Engineering
in Partial Fulfillment of the Requirements for
the Degree of

Master of Science

in

Molecular Biology and Genetics

June 18, 2021

Structural Dynamics of Wild Type and Mutant Forms of CLIC4 and Ezrin

Koç University

Graduate School of Sciences and Engineering

This is to certify that I have examined this copy of a master's thesis by

Merve Yığın

and have found that it is complete and satisfactory in all respects,
and that any and all revisions required by the final
examining committee have been made.

Committee Members:

_____

Asst. Prof. Hasan Demirci (Advisor)

_____

Assoc. Prof. Nurhan Özlü

_____

Asst. Prof. Burcu Kaplan Türköz

Date: _____

To My Dearest Family

ABSTRACT

Structural Dynamics of Wild Type and Mutant Forms of CLIC4 and Ezrin

Merve Yığın

Master of Science in Molecular Biology and Genetics

June 18, 2021

Cell division is an extremely vital process in life that occurs continuously within all living beings to maintain genomic integrity, cell growth, reproduction and regeneration. It enables the cells to survive by replacing old, damaged, or dead ones with newly formed healthy daughter cells. Therefore, various types of cellular proteins have a role in this process to ensure to complete the division successfully. It has been demonstrated that during cytokinesis, the interaction of ezrin with Chloride Intracellular Channel 4 (CLIC4) protein at the plasma membrane is required for the completion of cytoplasmic division. Their co-localization anchors the plasma membrane and actin cytoskeleton at the cleavage furrow and the midbody providing cortical stability. The successful translocation of CLIC4 to the cleavage furrow and the midbody requires its conserved residues Cys35 and Phe37. When these two residues are mutated to C35A and F37D, respectively, the localization of CLIC4 to the mitotic cell surface and cleavage furrow is abolished. Moreover, ezrin needs to be activated to interact with CLIC4. First, it should bind to phosphatidylinositol-(4,5)-biphosphate (PIP2) and then be phosphorylated from its conserved residue threonine (Thr567) at the carboxyl terminus. However, the mutual interaction between ezrin and CLIC4 is still not well understood. Also, it is not clear how a mutation at the conserved residue Cys35 of CLIC4 or at the phosphorylation site of ezrin changes their structures. Since this interaction might have an important role in cancer therapy, this study aimed at unveiling the mystery behind structural information of these two proteins. Although the wild type structures of CLIC4 and ezrin proteins were previously determined, the structures of their mutant forms, CLIC4 C35A and ezrin T567D, are not available. Thus, this study has been motivated to analyze the structural dynamics of wild type and mutant forms of CLIC4 and ezrin with their mutual interaction.

ÖZETÇE

CLIC4 ve Ezrin'in Yabanıl ve Mutant Formlarının Yapısal Dinamikleri

Merve Yığın

Moleküler Biyoloji ve Genetik, Yüksek Lisans

18 Haziran 2021

Hücre bölünmesi genomik bütünlüğü, hücre büyümesini, üremeyi ve yenilenmeyi sürdürmek için tüm canlılarda sürekli olarak meydana gelen yaşamın içindeki son derece hayati bir süreçtir. Yaşlı, hasarlı veya ölü olanları yeni oluşan sağlıklı yavru hücreler ile değiştirerek hücrelerin hayatta kalmasını sağlar. Bu nedenle, çeşitli hücresel protein türleri bölünmenin başarılı bir şekilde tamamlanmasını sağlamak için bu süreçte rol oynar. Sitokinez sırasında sitoplazmik bölünmenin tamamlanması için ezrin ile Chloride Intracellular Channel 4 (CLIC4) proteinin plazma zarındaki etkileşiminin gerekli olduğu gösterilmiştir. Ortak lokalizasyonları plazma zarını ve aktin hücre iskeletini bölünme oluğuna ve orta gövdeye sabitleyerek kortikal stabilite sağlar. CLIC4'ün bölünme oluğuna ve orta gövdeye başarılı bir şekilde translokasyonu korunmuş kalıntıları olan Cys35 and Phe37'ye ihtiyaç duyar. Bu iki kalıntı sırasıyla C35A ve F37D'ye mutasyona uğratıldığında, CLIC4'ün mitotic hücre yüzeyine ve bölünme oluğuna lokalizasyonu ortadan kalkar. Ayrıca, CLIC4 ile etkileşime geçmek için ezrin'in etkinleştirilmesi gerekidir. İlk olarak fosfatidilinositol-(4,5)-bifosfata (PIP2) bağlanmalı ve daha sonra karboksil ucundaki korunmuş kalıntısı treoninden (Thr567) fosforile edilmelidir. Ancak, ezrin ve CLIC4 arasındaki karşılıklı etkileşim hala tam olarak anlaşılamamıştır. Ayrıca, CLIC4'ün korunmuş kalıntısı Cys35'teki veya ezrin'in fosforilasyon bölgesindeki bir mutasyonun yapılarını nasıl değiştirdiği açık değildir. Bu etkileşimin kanser tedavisinde önemli bir rolü olabileceğinden, bu çalışma, bu iki proteinin yapısal bilgilerinin ardındaki gizemi ortaya çıkarmayı amaçlamıştır. CLIC4 ve ezrin proteinlerinin yabanıl yapıları önceden belirlenmiş olmasına rağmen, mutant formlarının, CLIC4 C35A and ezrin T567D, yapıları mevcut değildir. Bu nedenle, bu çalışma CLIC4 ve ezrin'in yabanıl ve mutant formlarının karşılıklı etkileşimleri ile yapısal dinamiklerini analiz etmek için motive edilmiştir.

ACKNOWLEDGEMENTS

I would like to express my special thanks to my thesis advisor Assistant Professor Hasan Demirci for giving me the opportunity to conduct my Master education and research in his laboratory. Also, I really appreciate for his guidance, support and encouragement throughout this journey that improved my science career in the invaluable way.

Moreover, I would like to thank the rest of my Master thesis committee members: Assoc. Prof. Nurhan Özlü and Asst. Prof. Burcu Kaplan Türköz for giving their time and important comments on my thesis. Meanwhile, I want to thank Koç University and the Scientific and Technological Research Council of Turkey (TÜBİTAK) 2232 for their financial supports during my Master education and research.

I would like to thank all the Koç University Structural Biology Knowledge Center (KUYBIM) members especially Fatma Betül Ertem, Sabri Özkan Besler, Günseli Yıldırım and Ebru Destan for their friendship, cooperation, and help. I also want to thank Dr. Nazan Saner for sharing her crucial comments with me.

Last but not least, I would like to show my deep sense of gratitude to my mother Berrin, my father Hamdi and my brother Mertcan. I also would like to show my gratefulness to my dearest friend Batu Toledo for his endless patience and encouragement. They were always there as amazing supporters to help and push me to pursue my dreams. I would not be me or here without them.

TABLE OF CONTENTS

List of Tables ix

List of Figures x

Abbreviations xii

Chapter 1: Introduction 1

1.1 Cell Cycle 1

1.1.1 Interphase 2

1.1.2 Mitosis 3

1.2 The Cell Cycle Control 5

1.3 Chloride Intracellular Channel 4 (CLIC4) 7

1.4 Ezrin 14

1.5 X-ray Crystallography 16

1.5.1 Protein Crystallization 16

Chapter 2: Methods 19

2.1 Gene Construct Design and Cloning 19

2.1.1 Construct 1 and 2: CLIC4 and CLIC4 C35A 19

2.1.2 Construct 3 and 4: Ezrin and Ezrin T567D 19

2.2 Recombinant Protein Expression 21

2.2.1 CLIC4 WT and CLIC4 C35A Protein Expression in small scale 21

2.2.2 Ezrin WT and Ezrin T567D Protein Expression in small scale 21

2.2.3 Protein Expression in large scale 21

2.3 Pulldown Experiments 22

2.4 SDS-PAGE 22

2.5 Protein Purification 23

2.6 Reverse Chromatography 24

2.7 Crystallization 25

2.7.1 CLIC4 WT and Ezrin T567D Co-crystallization 25

2.8 Native PAGE Gel 27
Chapter 3: Results 28
3.1 Mini Expression Test for CLIC4 WT and CLIC4 C35A 28
3.2 Overexpression, Purification and Crystallization of CLIC4 C35A 32
3.3 Overexpression, Purification and Crystallization of CLIC4 WT 38
3.4 Mini Expression Test for Ezrin WT and Ezrin T567D 44
3.5 Overexpression, Purification and Crystallization of Ezrin 46
3.6 Overexpression, Purification and Crystallization of Ezrin T567D 53
3.7 Native Gel for CLIC and Ezrin Proteins 55
3.8 Co-Crystallization of CLIC4 WT and Ezrin T567D 56
3.9 CLIC4 and Ezrin Docking Study 57
Chapter 4: Conclusion/Discussions 59
Bibliography 67

LIST OF TABLES

Table 2.1: The Ingredients of the 41st Condition of Crystal Screen II 26
Table 2.2: The Ingredients of the 8th Condition of Midas II 26
Table 2.3: The Ingredients of the 12th Condition of Crystal Cryo II 26
Table 2.4: The Ingredients of the 38th Condition of Wizard I 27
Table 2.5: The Ingredients of the 24th Condition of Helix II 27

LIST OF FIGURES

Figure 1.1: The Cell Cycle Stages of Eukaryotic Cells 2
Figure 1.2: The Stages of Mitosis 4
Figure 1.3: The Cell Cycle Checkpoints 6
Figure 1.4: Structural Representation of CLIC4 and omega-class GST. PDB IDs: 2AHE and 1EEM, respectively. 9
Figure 1.5: CLIC4 Localization during Mitosis 11
Figure 1.6: The Phenotypic Effect of CLIC1/4 Knockout during Mitosis 12
Figure 1.7: Co-localization of CLIC4 and Ezrin during Mitosis 13
Figure 1.8: Basic Structural Motifs of Ezrin Protein 15
Figure 1.9: Schematic Illustration of Protein Crystallization Phase Diagram 17
Figure 2.1: pET28a(+) Plasmid Map 20
Figure 2.2: Schematic Representation of Nickel Affinity Chromatography 23
Figure 2.3: Experimental Flow of Reverse Chromatography 24
Figure 2.4: Schematic Representation of Crystallization 25
Figure 3.1: Mini Expression Test Results for Supernatant Samples of CLICs 29
Figure 3.2: Mini Expression Test Results for Pellet Samples of CLICs 30
Figure 3.3: Pulldown Results for CLICs 31
Figure 3.4: CLIC4 C35A Elution 33
Figure 3.5: Nickel Affinity Chromatography Graph for CLIC4 C35A 33
Figure 3.6: Thrombin Cut Check for CLIC4 C35A 34
Figure 3.7: Crystals of CLIC4 C35A obtained at the 41st Condition of Crystal Screen II 35
Figure 3.8: Reverse Chromatography Results for CLIC4 C35A 36
Figure 3.9: Reverse Chromatography Graph for CLIC4 C35A 37
Figure 3.10: Concentrated CLIC4 C35A 37
Figure 3.11: CLIC4 WT Elution 39
Figure 3.12: Nickel Affinity Chromatography Graph for CLIC4 WT 39
Figure 3.13: Reverse Chromatography for CLIC4 WT 41
Figure 3.14: Reverse Chromatography Graph for CLIC4 WT 41
Figure 3.15: Concentrated CLIC4 WT 42
Figure 3.16: Crystals of CLIC4 WT obtained at the 8th Condition of Midas II 43

Figure 3.17: Crystals of CLIC4 WT obtained at the 12th Condition of Crystal Cryo II 43
Figure 3.18: Mini Expression Test for Ezrin WT 45
Figure 3.19: Mini Expression Test for Ezrin T567D 45
Figure 3.20: Ezrin WT Elution 47
Figure 3.21: Nickel Affinity Chromatography Graph for Ezrin WT 47
Figure 3.22: Crystals of Ezrin WT obtained at the 8th Condition of Midas II 48
Figure 3.23: Reverse Chromatography for Ezrin WT 50
Figure 3.24: Reverse Chromatography Graph for Ezrin WT 50
Figure 3.25: Thrombin Cut Check for Ezrin WT 51
Figure 3.26: Concentrated Ezrin WT 52
Figure 3.27: Ezrin T567D Elution 54
Figure 3.28: Nickel Affinity Chromatography Graph of Ezrin T567D 54
Figure 3.29: Native Gel Result for CLIC and Ezrin Proteins 55
Figure 3.30: Co-crystals of CLIC4 WT and Ezrin T567D obtained at the 38th Condition of Wizard I 56
Figure 3.31: Co-crystals of CLIC4 WT and Ezrin T567D obtained at the 24th Condition of Helix II 56
Figure 3.32: Docked Structure of CLIC4 and Ezrin 57
Figure 3.33: Representation of Interaction between Ezrin-PIP2 and Ezrin-CLIC4 58
Figure 4.1: Cartoon Representation of CLIC4 PDB ID: 2AHE 59
Figure 4.2: Representation of Side Chain of Cys35 in CLIC4 WT and CLIC4 C35A 60
Figure 4.3: Cartoon Representation of Ezrin FERM:C-terminal Domain Complex PDB ID: 4RM9 61
Figure 4.4: Representation of Side Chain of Thr567 in Ezrin WT and Ezrin T567D 62
Figure 4.5: Interaction Model for CLIC4 and Ezrin 66

ABBREVIATIONS

APS	Ammonium persulfate
CLIC4	Chloride Intracellular Channel Protein 4
CLIC4 C35A	Amino acid 35 (Cysteine, C) is mutated to Alanine (A)
DNA	Deoxyribonucleic acid
E. coli	*Escherichia coli*
ERM	Ezrin, Radixin, Moesin
Ezrin T567D	Amino acid 567 (Threonine, T) is mutated to Aspartate (D)
G_0	Gap Zero
G_1	Gap One
G_2	Gap Two
IPTG	Isopropyl β-D-1-thiogalactopyranoside
kDa	Kilodalton
LB	Luria-Bertani medium / Lysogeny broth
M	Mitosis
mM	Millimolar
NaCl	Sodium Chloride
Ni-NTA	Nickel-Nitrilotriacetic acid
rpm	Revolutions per minute
S	Synthesis
SDS	Sodium Dodecyl Sulphate
SDS-PAGE	Sodium Dodecyl Sulphate Polyacrylamide Gel Electrophoresis
TEMED	Tetramethylethylenediamine
Tris-HAc	Tris buffer with free chloride ions
UV	Ultraviolet
WT	Wild Type

Chapter 1:
INTRODUCTION

1.1 Cell Cycle

Cell division is an extremely vital process in life that occurs every day, every hour, every second within all living beings. All organisms start life as one cell, called the parent cell, which divides into two new daughter cells before giving rise to four and more progeny. This ability to divide enables the cells to survive by replacing old, damaged, or dead ones with newly formed healthy daughter cells. The purpose of the cell division may vary from organism to organism. Unicellular species, such as yeasts and bacteria, utilize cell division for reproduction. In multicellular organisms, the division process provides cell growth, maintenance, and regeneration. For example, since tissues and organs are made up of numerous cells and cell types, there are also non-dividing cells. These non-dividing cells such as neurons, adipocytes and myocytes are functionally and structurally differentiated during the development. Also, their biochemical properties and roles are specialized to higher-order functions such as memory, learning, thinking, and language in the brain. Although they cannot divide, their configurations and numbers should be maintained by the dividing cells required for being properly functional (Iyama & Wilson III, 2013). Ultimately, for all species, the division has to occur at high fidelity to preserve a stable genetic substance in the offspring (Vader & Lens, 2008).

Cell division consists of an ordered series of events, that are collectively called the cell cycle. This cycle consists of two major steps: interphase and mitosis. Interphase is the first stage of the cell cycle. During interphase, cells prepare themselves for the cell division by duplicating their contents including the genetic material, DNA (deoxyribonucleic acid) (Vermeulen et al., 2003). The second phase is mitosis where the genetic material and cytoplasm of the cells divide (Figure 1.1). In order to ensure maintenance of chromosome content in the progeny, interphase takes more time than mitosis to complete the cycle. This is due to the fact that if the genetic integrity is not preserved, the dividing cells become abnormal, turning cancerous.

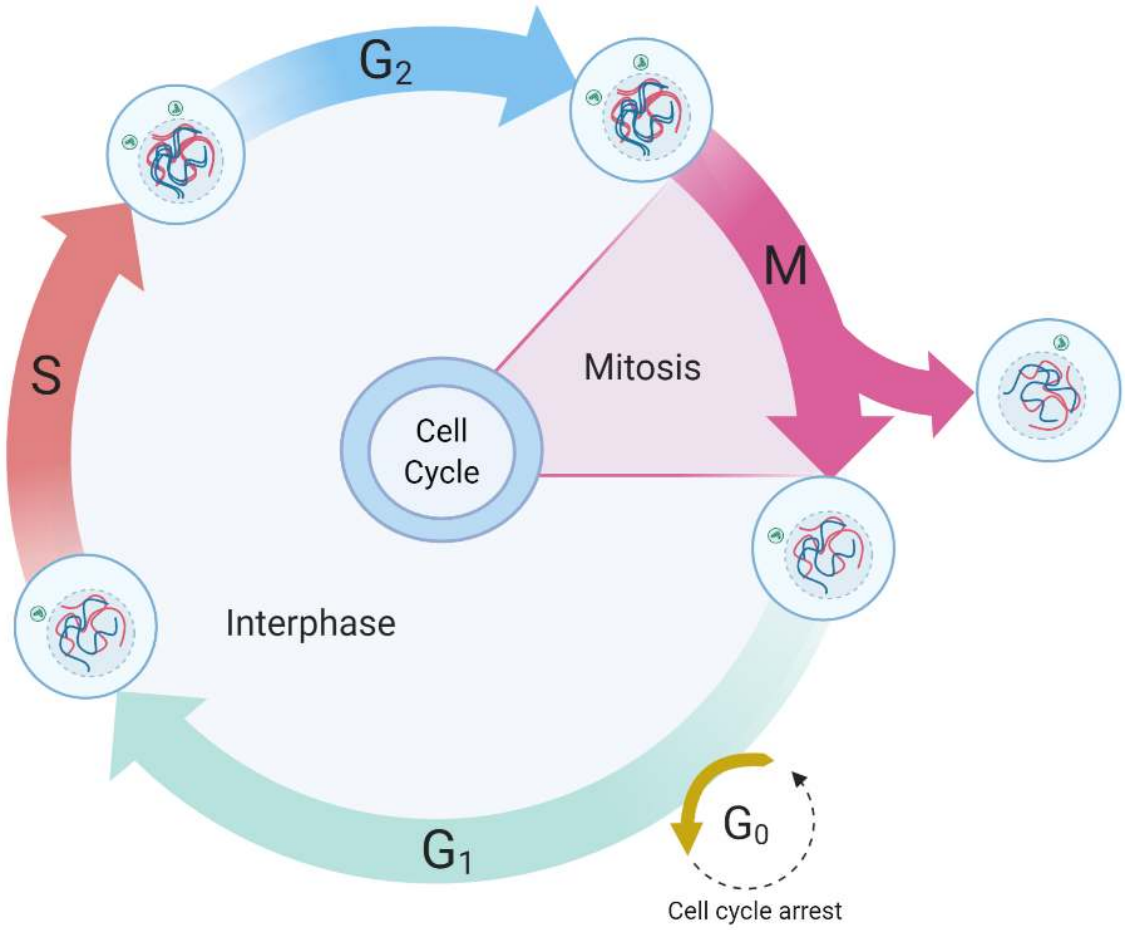

Figure 1.1: The Cell Cycle Stages of Eukaryotic Cells

In normal human cells, which are cultured in cell culture, interphase may be completed in approximately 23 hours of a 24-hour cycle while mitosis occupies 1 hour.

1.1.1 Interphase

Interphase comprises three phases called: Gap 1 (G_1), Synthesis (S), and Gap 2 (G_2). The G_1 is a gap between the end of mitosis and the start of DNA synthesis (Hunt et al., 2011). During G_1, cells become bigger and duplicate their organelles and proteins including the enzymes required for genome replication (Salazar-Roa & Malumbres, 2017). The G_1 phase contains a resting state called Gap 0 (G_0). Non-dividing cells, especially those which do not grow and proliferate, stay in this phase. Moreover, if the extracellular conditions are unfavorable, cells do not want to commit themselves to DNA

replication, so that they can enter the G_0 (Vermeulen et al., 2003). In this phase, cells can stay for days, weeks, or even years and re-enter into the cell cycle such as glial cells. In fact, many cells such as neurons, adipocytes, and myocytes permanently reside in the resting state until they die (Iyama & Wilson III, 2013). Cells in G_1 proceed with the Synthesis (S) phase where DNA synthesis occurs. During the G_1/S phase transition, centrosomes are also duplicated. Then, the G_2 follows the S phase. In the G_2 phase, cells grow more and prepare themselves for mitosis. Furthermore, in order to organize the mitotic spindle, duplicated centrosomes mature (Salazar-Roa & Malumbres, 2017; Vader & Lens, 2008).

1.1.2 Mitosis

Mitosis, also called the M phase, is the shortest but one of the important phases of the cell cycle. It comprises two main events: mitosis and cytokinesis. During mitosis, the newly duplicated chromosomes are equally segregated and divided to newly formed two daughter nuclei called karyokinesis (Álvarez-Fernández & Malumbres, 2014). Then, cells undergo a cytoplasmic division called cytokinesis. The five consecutive processes orchestrate mitosis: Prophase, prometaphase, metaphase, anaphase, and telophase (Figure 1.2). During eukaryotic cell division especially passing from interphase to mitosis, dividing cells encounter extensive structural alterations such as *de novo* mitotic spindle assembly, nuclear envelope break down and chromosome condensation (Álvarez-Fernández & Malumbres, 2014; Pines & Rieder, 2001). During prophase, the separation of matured centrosomes, an increase in microtubule nucleation, and chromosome condensation are achieved by enabling the bipolar mitotic spindle formation. Then, the nuclear envelope disassembles to enable cytoplasmic microtubules to interact with chromosomes to provide kinetochore-microtubule attachments (Burke & Ellenberg, 2002; Güttinger et al., 2009). These connections take place at the centromere of the chromosomes including two identical macromolecular complexes called kinetochores (Walczak et al., 2010). With the breakdown of the nuclear envelope, cells enter prometaphase. In prometaphase, the attachment of the mitotic spindles to the two kinetochores of each sister chromatid starts to align chromosomes at the equator of the cell. The cells are thought to be in metaphase once all condensed chromosomes finally

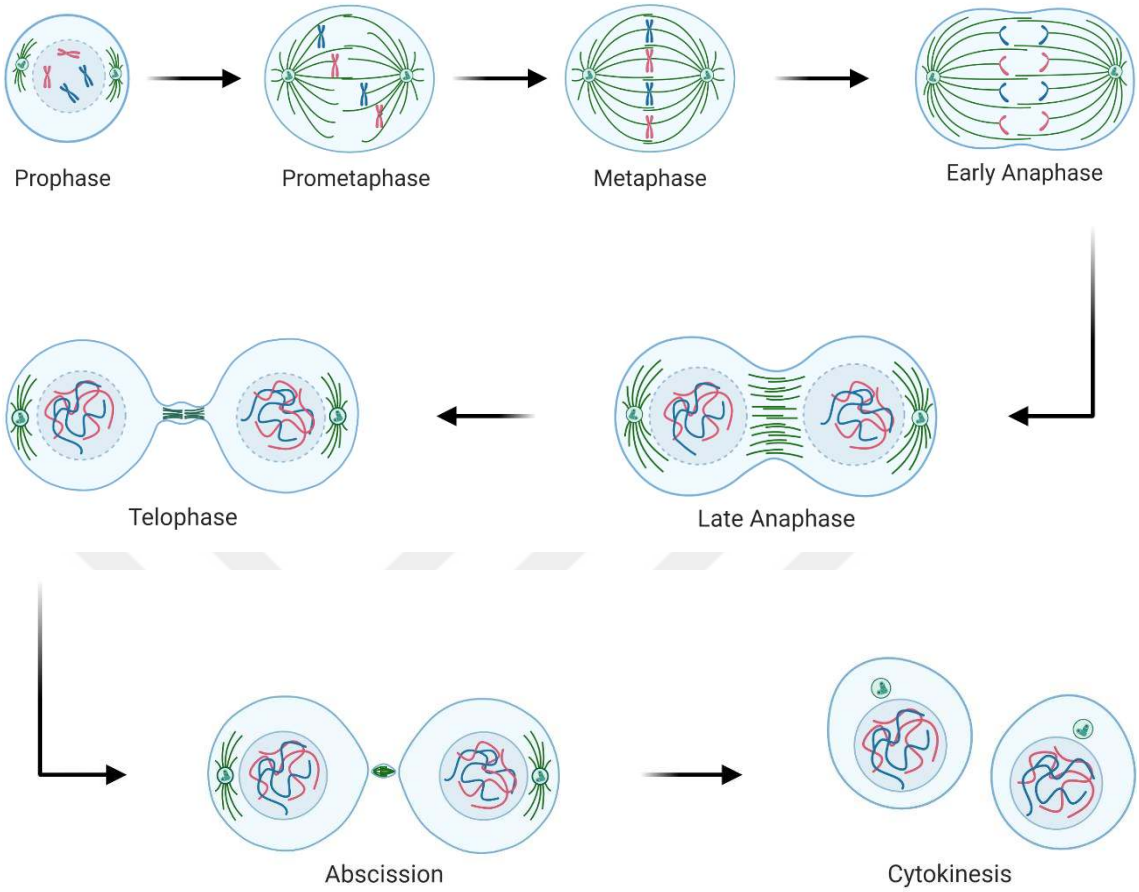

Figure 1.2: The Stages of Mitosis

align at the metaphase plate which is near the spindle equator (Pines & Rieder, 2001; Walczak et al., 2010). When all mitotic spindle fibers successfully attach to the kinetochores of each chromosome, during anaphase paired sister chromatids separate and segregate towards opposite poles. In telophase, two nuclear envelopes reform at two sites of the cell and chromatids start to decondense in the new daughter nuclei (Vader & Lens, 2008). As the final step, cytokinesis completes the cell cycle. During this process, the first cleavage furrow occurs at the middle of the dividing cell perpendicular to the axis of sister chromatid segregation to ensure even distribution of the mother's genetic content and cytoplasm. After furrow contraction, the midbody forms which consists of many proteins

and microtubules. The last stage of cytokinesis is abscission, also called completion and scission. In this step, the cytoplasm of the mother cell physically separates into two identical daughter cells. Prior to abscission, cleavage furrow ingression is fully extended forming an intercellular bridge between two daughter cells termed the midbody. Completion of actomyosin ring contraction and abscission of the midbody result in successful cytokinesis (Eggert et al., 2006; Vader & Lens, 2008; Walczak et al., 2010).

1.2 The Cell Cycle Control

The transition through cell cycle stages is monitored at specific checkpoints by a network of signaling pathways to make sure that each phase occurs precisely and in an orderly fashion. Also, the major aims of the cells are to replicate their genome error-free and transmit the chromosomes to daughter cells by preserving genomic integrity. Therefore, checkpoints are extremely important for cell division. The control of the cell cycle occurs at three major checkpoints: G_1-S checkpoint, G_2-M checkpoint and spindle checkpoint (Figure 1.3) (Harashima et al., 2013). During the transition from G_1 to S phase, the G_1-S checkpoint occurs to arrest the cell cycle in response to genomic instability and/or DNA damage. If the dividing cells with unrepaired damaged genome escape from the G_1-S checkpoint and continue to the cycle, the G_2-M checkpoint senses DNA damage and prevents the initiation of mitosis. In response to DNA replication stress, and/or DNA damage, these checkpoints provide time for the preparation of DNA replication machinery and chromatin assembly. When these checkpoints experience DNA damage, cell cycle arrest is induced, activating DNA replication machinery until the repair is fulfilled. With the completion of the repair, cell cycle progression is initiated. In the case of irreversible DNA damage, those potentially harmful cells are eliminated by permanent cell cycle delay or cell death (Bartek & Lukas, 2001; Lukas et al., 2004). The spindle checkpoint controls the chromosomal alignment in metaphase. If there is a problem with chromosome-mitotic spindle attachment, such as improperly aligned chromosomes on the mitotic spindle, the transition from metaphase to anaphase is prevented by spindle checkpoint (Vermeulen et al., 2003).

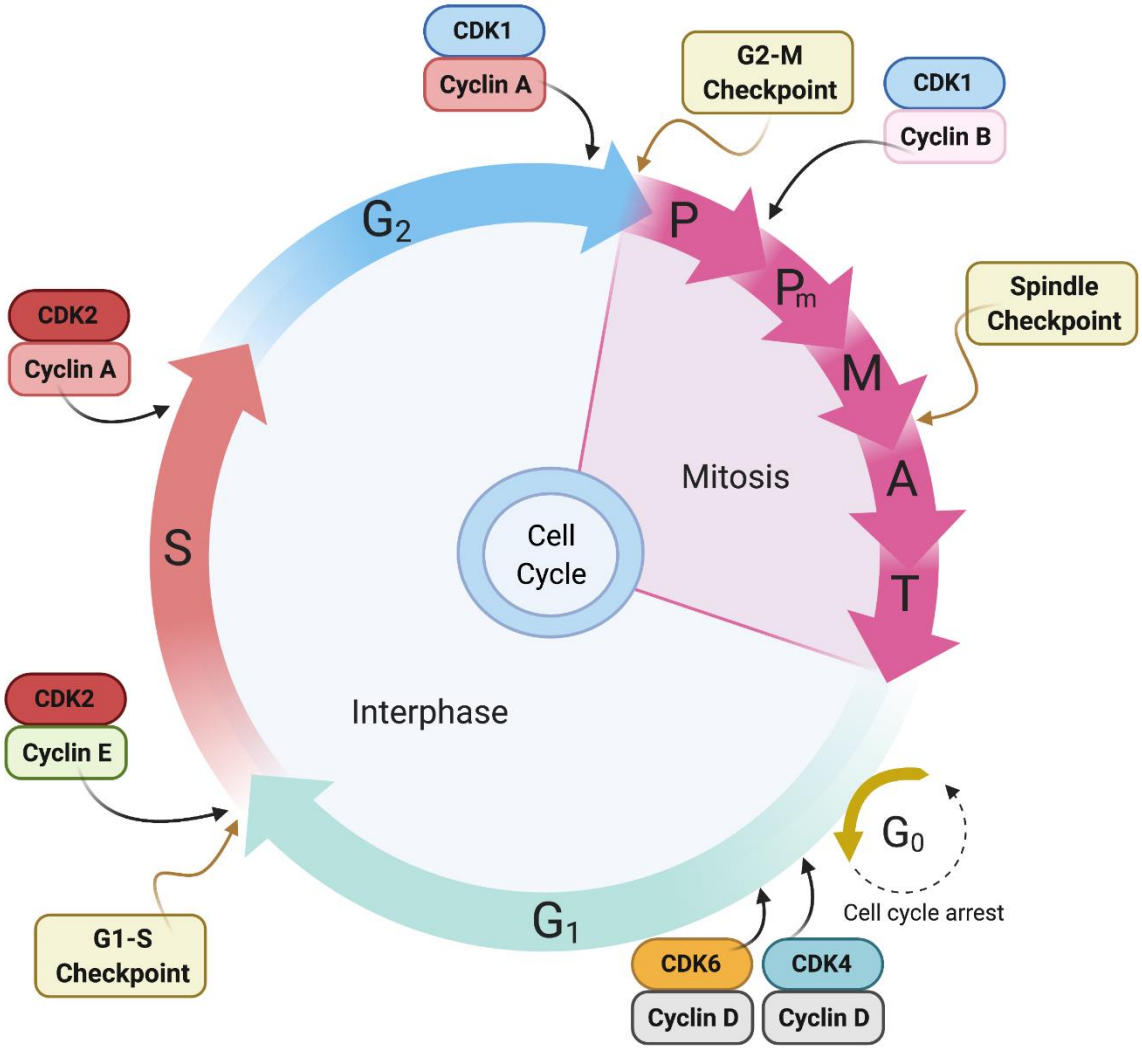

Figure 1.3: The Cell Cycle Checkpoints

Many different cellular proteins are recruited at certain points of the cell cycle stages to maintain the sequential progress of the cell cycle. Cyclin-dependent kinases (CDKs) are cell cycle regulatory proteins, which are a specific class of serine/threonine kinases. CDKs need interaction with cyclin proteins for their activation. The activity of CDKs periodically changes in response to their activating proteins since the amount of cyclin proteins oscillates during the cycle while CDK levels are kept constant. The affinity towards the substrates and the functions of CDK-cyclin complexes differ from one complex to another. When CDKs are activated, their targets are phosphorylated inducing downstream pathways. Different cyclins are involved in different cell cycle stages and

interact with corresponding CDKs. The D-type cyclin proteins interact with CDK4 and CDK6 enabling progression from G_0 to G_1 phase. Then, the formation of the CDK2-cyclin E complex promotes the transition from G_1 into the S phase. During the S phase, the CDK2-cyclin E complex dissociates and CDK2 is engaged with cyclin A. In late G_2 and early mitosis, cyclin A is required for the initiation of mitosis. It binds to CDK1 and regulates the changeover. The CDK1 further forms a complex with cyclin B to drive mitosis (Figure 1.3) (Evans et al., 1983; Harashima et al., 2013; Vermeulen et al., 2003). Subsequently, the anaphase-promoting complex/cyclosome (APC/C) targets mitotic A- and B-type cyclins for their degradation. The proteolysis activity of APC/C results in CDK inactivation and exits from mitosis inducing cytokinesis (Harashima et al., 2013; Peters, 2006).

1.3 Chloride Intracellular Channel 4 (CLIC4)

Chloride Intracellular Channel 4 (CLIC4), also termed as HuH1, RS43, p64H1, and mtCLIC, is a member of the chloride intracellular channel (CLIC) protein family, which is composed of six members, CLIC1-6. The CLIC proteins are highly conserved throughout metazoan and, extraordinarily, exist in both membrane-integrated and soluble forms. In contrast to their original names, CLICs are mostly found in soluble form in the resting cells where they are structurally homologous to the omega class of glutathione *S*-transferase (GST) proteins. Soluble CLIC proteins have distinct cellular functions from GSTs, though they are not well-known. Alternatively, in lipid bilayers, they might possess a selective chloride ion channel but, unfortunately, the transition mechanism between soluble and membrane-integrated states and its regulation has remained elusive (Dulhunty et al., 2001; Edwards & Kahl, 2010; Littler et al., 2010; Ponsioen et al., 2009).

Among the CLIC family members, the biological activity of CLIC4 has been the most extensively studied. It is a ubiquitously expressed small globular protein containing 253 amino acids. Its molecular weight is 29 kDa with a predicted isoelectric point (pI) of 5.45 (Chuang et al., 1999; Suh et al., 2005). The CLIC4 consists of nuclear localization signal (NLS), SH3 binding domain, transmembrane domain at the N-terminus and putative phosphorylation sites for protein kinase A (PKA), protein kinase C (PKC) and tyrosine kinases (Suginta et al., 2001; Suh et al., 2005).

Similar to other CLIC proteins, cytosolic CLIC4 is also capable of translocating to the plasma membrane. The activation of $G\alpha_{13}$-mediated RhoA by lysophosphatidic acid (LPA) and F-actin integrity enable the transient displacement of the cytosolic CLIC4 in the membrane. Moreover, mutational analysis has been demonstrated that for the purpose of the translocation in the plasma membrane, CLIC4 needs its conserved residues whose equivalents are essential for the substrate processing in omega-class GSTs (Figure 1.4). The Cys35 is the most important one among these residues. Its equivalent in the GSTomega (GSTΩ) proteins is Cys32, which is a reactive cysteine located in the active site. The Cys35 serves as a putative enzymatic site for CLIC4 promoting a cysteine-dependent transferase activity. When this residue is mutated to C35A in the CLIC4 structure, the translocation ability of CLIC4 to the plasma membrane is completely lost even in RhoA stimulation. For this reason, since this reactive cysteine residue provides the potential-substrate binding site at the enzymatically active cleft and membrane localization, it is extremely critical for the CLIC4 function.

Furthermore, there are other conserved residues in the CLIC4 structure, which are Phe37, Pro76, and Asp87. The equivalents of these residues are found in the glutathione-binding site of GSTΩ structures. This site is composed of Cys32, Phe34, Lys59, Leu71, Val72, Glu85, and Ser86. However, omega-GSTs only interact with glutathione (GSH) with Cys32, Lys59, Val72, Glu85, and Ser86 residues. Among the CLIC proteins, Phe122 and Tyr244 are also highly conserved whose equivalents, Arg183 and Trp222, position at the substrate-binding site of the GSTs. In the same manner with C35A, the membrane localization ability of CLIC4 is impaired when these GST activity-related residues are respectively mutated to F37D, P76A, D87A, F122R and Y244A (Argenzio et al., 2018; Board et al., 2000; Jiang et al., 2014; Ponsioen et al., 2009).

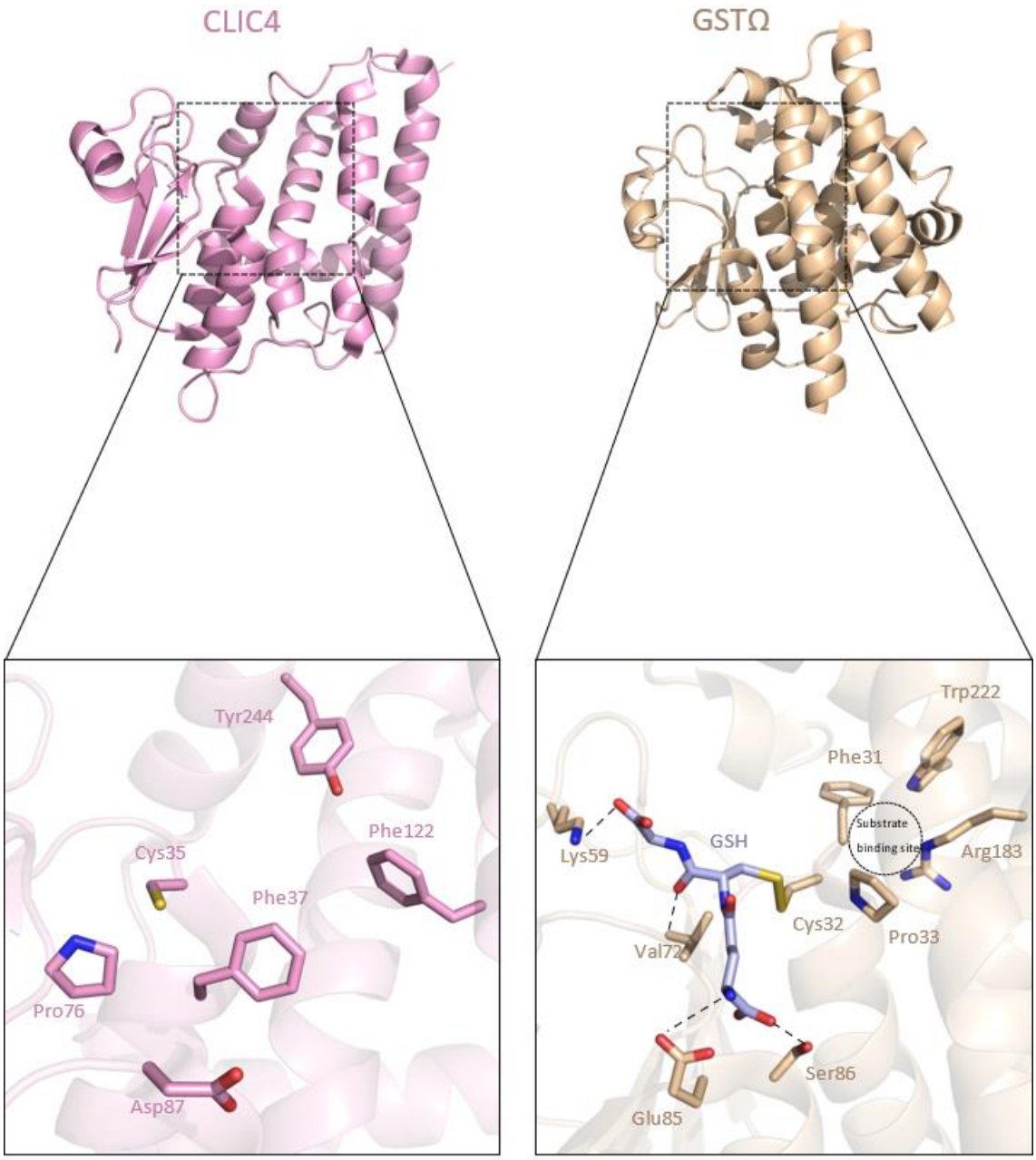

Figure 1.4: Structural Representation of CLIC4 and omega-class GST. PDB IDs: 2AHE and 1EEM, respectively.

In addition to the plasma membrane incorporation, CLIC4 has been implicated to localize organelles such as mitochondria and endoplasmic reticulum, nucleus, centrosomes, large dense-core vesicles and cortical actin cytoskeleton regarding the cell types. It is also highly expressed in the brain, heart, liver, kidney and lung (Berryman & Goldenring, 2003; Chuang et al., 1999; Duncan et al., 1997; Fernández-Salas et al., 1999; Ponsioen et al., 2009; Proutski et al., 2002; Shukla et al., 2009; Suh et al., 2004). Additionally, CLIC4 has been linked to various biological processes. It provides protein trafficking, migration, cell differentiation, and actin-mediated cellular processes including G-protein-coupled receptor signaling. Integrin signaling, cell spreading and cell-matrix adhesion are also induced by the activity of CLIC4 (Argenzio et al., 2014, 2018; Chou et al., 2016; Ponsioen et al., 2009). However, defective CLIC4 or its deletion causes different impairments in different cell types. For instance, the homozygous knockout of CLIC4 in mice results in delayed wound healing in the cornea and skin, as well as loss of microvilli in the mouse kidney. In addition to these consequences, spontaneous skin erosions and decreased angiogenesis activity have been observed. The depletion of CLIC4 also causes loss of vacuole formation and tubulogenesis in both renal and endothelial epithelial cells (Chou et al., 2016; Padmakumar et al., 2012; Ulmasov et al., 2009). In retinal pigment epithelium (RPE) cells, the silencing of CLIC4 induces retinal atrophy and retinal detachment (Chuang et al., 2010). Despite these studies, the activity of CLIC4 in these diverse cellular processes has not been completely elucidated.

In a recent study, it has been demonstrated that CLIC4 is extremely crucial for successful cell division. When the dividing cells move from interphase to mitosis, it is during the metaphase that CLIC4 is enriched at the mitotic cell surface (Özlü et al., 2015). As the cells progress into cytokinesis at the onset of anaphase, sister chromatids are pulled to opposite poles and CLIC4 begins to gradually accumulate at the cleavage furrow. At anaphase, the contractile ring becomes constricted causing blebbing. By the localization of CLIC4 at the polar blebs, this fast bleb expansion is followed by the bleb retraction resulting in its disappearance. Then, CLIC4 localizes the midbody enabling successful completion of cytokinesis (Figure 1.5) (Berryman & Goldenring, 2003; Kagiali et al., 2020).

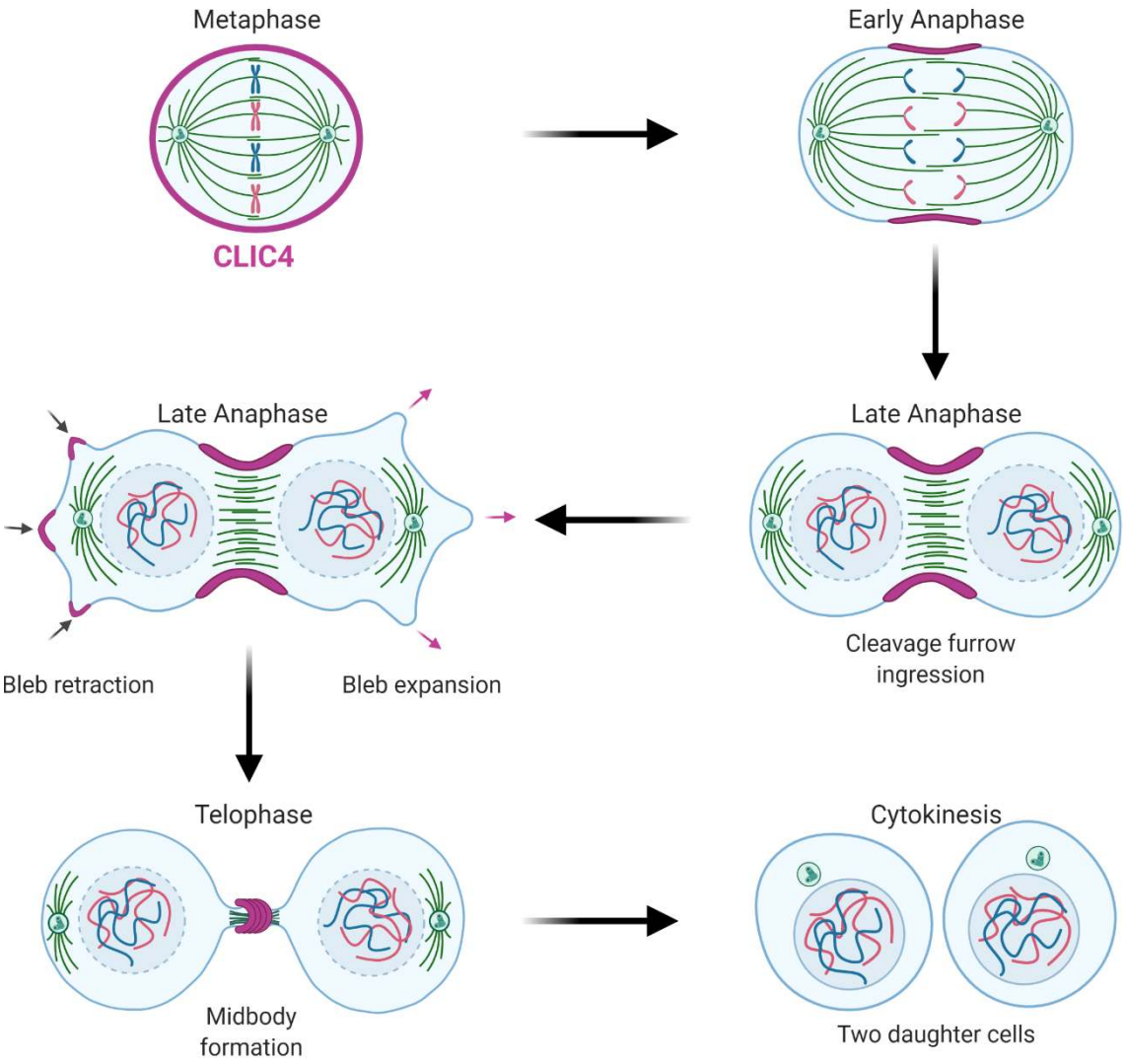

Figure 1.5: CLIC4 Localization during Mitosis

It has been demonstrated that the localization of CLIC4 to the mitotic cell surface, cleavage furrow and the midbody occurs via its conserved residues Cys35 and Phe37 in response to RhoA activation. When these residues are mutated to C35A, and F37D, respectively, the translocation of CLIC4 to the plasma membrane and cleavage furrow abolishes. Moreover, in the absence of both CLIC1/4 the cortical stability at the cleavage furrow and polar cortex cannot be maintained. Then, abnormal blebbing and the cleavage furrow regression occur resulting in cytokinesis failure. Although dividing cells cannot undergo cytokinetic abscission which leads to multinucleated cells, they can round up at the metaphase and, as a result, cleavage furrow ingression and midbody formation take place successfully (Figure 1.6) (Kagiali et al., 2020).

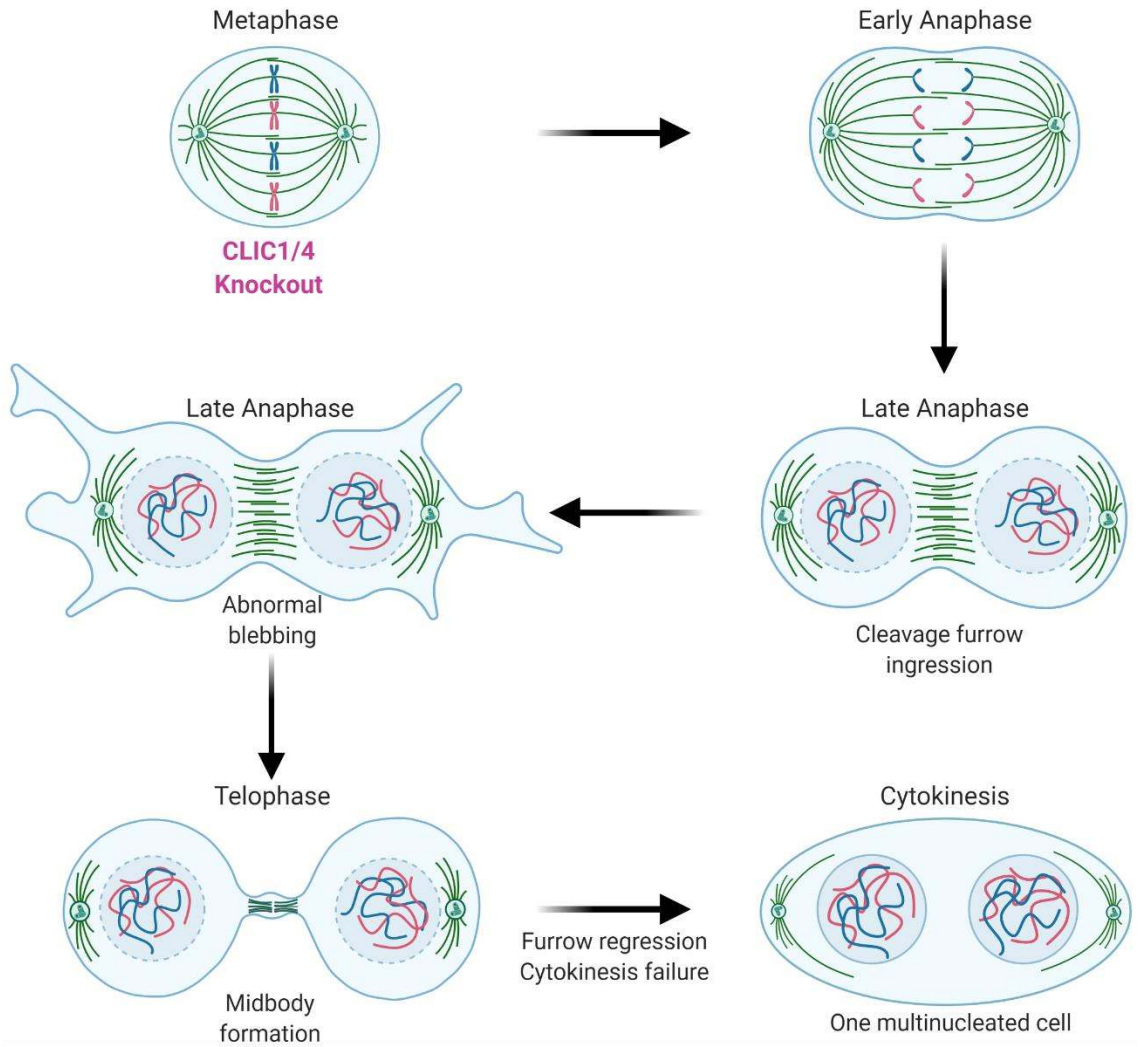

Figure 1.6: The Phenotypic Effect of CLIC1/4 Knockout during Mitosis

In the same study, the reciprocal regulation between ezrin and CLIC4 during cell cycle progression has also been discovered. It was indicated that the interaction between these two proteins and the activation of RhoA enhance the phosphorylation of ezrin and its activation which is required for the translocation of CLIC4 to the cleavage furrow. Strikingly, ezrin and CLIC4 show the same localization pattern with each other throughout mitosis (Figure 1.7). At metaphase, they both decorate the mitotic cell surface while cells progress into cytokinesis, the cleavage furrow and midbody begin to be enriched with CLIC4 and ezrin. When RhoA is activated by its RhoGEF ECT2, during cytokinesis the cytosolic CLIC4 localizes at the plasma membrane promoting the phosphorylation of ezrin at the cleavage furrow. Once ezrin is phosphorylated, it becomes active and facilitates the CLIC4 recruitment at the equatorial cortex where the cleavage

furrow forms. This co-localization provides cortical stability between the plasma membrane and actin cytoskeleton since it anchors the cortical actomyosin network and the plasma membrane at the cleavage furrow and midbody. Eventually, this mutual interaction enables successful cytokinesis forming new daughter cells (Kagiali et al., 2020).

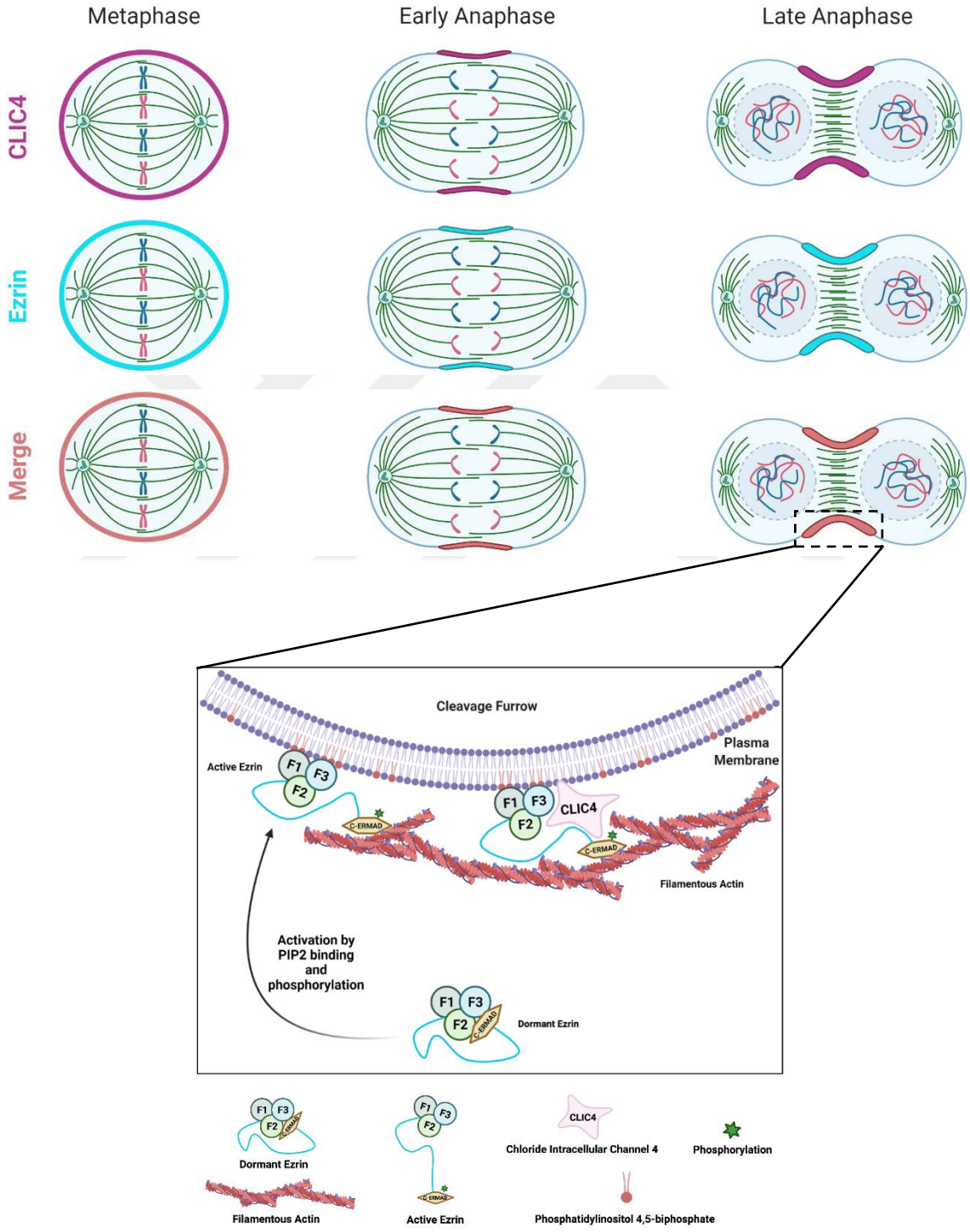

Figure 1.7: Co-localization of CLIC4 and Ezrin during Mitosis

1.4 Ezrin

Ezrin is a founding member of the evolutionarily conserved ezrin-radixin-moesin (ERM) protein family (Bretscher, 1983, 1999). The members of this protein family exhibit structural homology by sharing the total 73-81% sequence similarity. They are highly important for providing a link between the plasma membrane and the cortical actin cytoskeleton, where the connection is dynamically controlled by the RhoA family of small GTPases (Bretscher et al., 2002; Fehon et al., 2010; Neisch & Fehon, 2011). Due to the ability of this cell membrane and filamentous actin (F-actin) connection regulation, they are mostly involved in the membrane-cytoskeleton related processes including exocytosis and endocytosis. Likewise, they enable a suitable environment to transmit the extracellular signals by providing intracellular trafficking of membrane receptors (McClatchey & Fehon, 2009). Additionally, they are incorporated in the regulation of many cellular processes such as the formation of membrane protrusions, cell motility, migration and adhesion (Arpin et al., 2011; Bretscher et al., 2002; Kahsai et al., 2010). Besides the other ERM protein family members, ezrin is also essential for the determination of the surface structures, cell shape and polarity as well as phagocytosis and the entrance of virus into host cells (Bretscher et al., 2002; Liu et al., 2009; Wong & Gough, 2009). It directly participates in tumor metastasis and especially pediatric cancers (Clucas & Valderrama, 2015). In retracting cell blebbing, ezrin maintains the stabilization of actin-membrane attachment (Charras et al., 2006). There are also many cellular processes that require the activity of ezrin such as cell surface microvilli assemble, B cell migration and immunological synapse formation (Hanono et al., 2006; Lalonde et al., 2010; Pore & Gupta, 2015; Roumier et al., 2001).

Ezrin is a 586 amino acid long protein with a theoretical pI of 5.94. It is characterized by three distinct domains which are strongly conserved among ERM protein members. The first domain is the N-terminal ERM-association domain (N-ERMAD), which is also known as N-terminal FERM (band *Four*-point-one (4.1) Ezrin, Radixin, Moesin) domain. This is the domain that shares the highest similarity among the human ERM proteins, consisting of 86% sequence identity. It is located at the N-terminus building of 298 amino acid residues serving a membrane-binding site. This FERM domain has a compact cloverleaf structure with three subdomains, F1, F2 and F3. The lobe F1 possesses a ubiquitin-like fold while the lobe F2 adopts α-helical acyl-CoA-binding domain fold. In

addition, the subdomain F3 is identified as phosphotyrosine binding or pleckstrin homology domain fold. The second domain in the ezrin structure is the central α-helical domain which is located between the 298 and 497 amino acid residues including the proline-rich linker region between 470 and 497 residues. It forms coiled coil tails which are also able to interact with F-actin. The third domain is the C-terminal ERM-association domain (C-ERMAD) having approximately 71% sequence similarity between human ERMs. This domain is found in C-terminus between 497 and 586 amino acid residues containing F-actin binding sequence at the last 30 amino acid residues of the carboxyl-terminal end. Importantly, a conserved phosphorylation site, Thr567, is also positioned at C-ERMAD which is associated with ezrin activation (Figure 1.8) (Bretscher et al., 2002; Jayasundar et al., 2012; Phang et al., 2016; Ponuwei, 2016; Pore & Gupta, 2015; Smith et al., 2003).

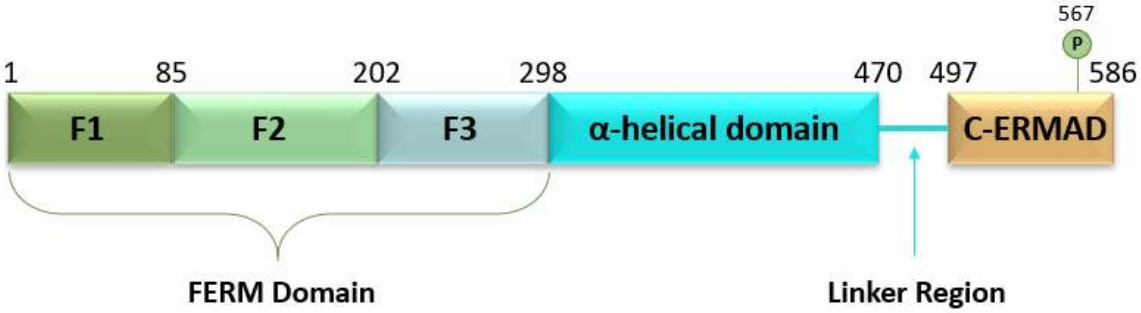

Figure 1.8: Basic Structural Motifs of Ezrin Protein

Interestingly, the activity of ERM proteins is controlled by an autoinhibitory mechanism leading to at least two physiological states, the active and the autoinhibited or dormant state (Phang et al., 2016). In the dormant state, the plasma membrane- and cytoskeleton-binding sites are masked by head-to-tail-like intramolecular connection. Through the interaction of the C-terminal region with the F2 and F3 lobes, the FERM domain cannot bind to transmembrane proteins as well as cell membrane lipids. As a result, the ezrin structure becomes closed and inactive (Gary & Bretscher, 1995; Pearson et al., 2000). In order to be converted from dormant to the active state, ezrin should undergo a conformational switch. In the first step, the first and the third lobes in the FERM domain bind to phosphatidylinositol-(4,5)-biphosphate (PIP2). Then, it is phosphorylated at its threonine (Thr567) residue in the carboxyl terminus. The interaction of ezrin with PIP2 occurs via its PIP2 binding determinants in 12-115 and 233-310 amino acid residues

whereas Lys63, Lys64, Lys253, Lys254, Lys262 and Lys263 residues provide efficient interaction. Once ezrin is activated, its self-associated structure opens and facilitates the C-ERMAD interaction with its binding partners, such as F-actin unraveling α-helical region (Barret et al., 2000; Hamada et al., 2000; Simons et al., 1998).

1.5 X-ray Crystallography

X-ray crystallography is a science of three-dimensional periodic atomic/molecular arrays, called crystals. These crystals are diffracted by X-rays, which are the type of electromagnetic radiation of high energy and extremely short wavelength. It is a powerful technique of structural biology which is utilized to determine the three-dimensional molecular structure of proteins and other biological macromolecules. These three-dimensional structural studies have provided detailed information about the activity and function of different biological molecules. For instance, unanswered questions about protein-protein interactions, protein-nucleic acid complexes, viruses and immune complexes have been addressed through structural studies. The structures of hormones reveal their binding affinity towards their receptors which has enabled the understanding of structure and nerve transmission. Similarly, the structures of enzymes and other proteins promote significant information to specify their potential interaction partners, active sites and cellular localization. The comprehensive knowledge about three-dimensional structural studies of biological molecules is also important to elucidate disease mechanisms. Since all molecules should preserve their native structure to function properly within a cell, the determination of any structural change can offer insight into how diseases occur. For the development and *de novo* engineering of potential medicines, the structure-based drug design studies and drug-repurposing utilize X-ray crystallography to observe dynamics of native and altered structures (Gawas et al., 2019; Smyth & Martin, 2000).

1.5.1 Protein Crystallization

X-ray crystallography is an anchoring tool between molecular biology and biochemistry, which aims to obtain crystal structures of biologically important macromolecules, especially proteins, and characterize their three-dimensional structures.

In this technique, the first step is to attempt to crystallize pure protein samples by applying different screening conditions. These screening conditions are also called crystallizing solutions and precipitants. The samples require optimum conditions to be chemically converted into a solid crystalline state from its liquid phase. The optimal environment for the crystallization can be achieved by altering temperature, pH, the type and the concentration of precipitant, and sample concentration. Also, specific additives can be utilized to stabilize and increase the solubility of the proteins.

The crystallization ability of the proteins depends on their saturation level. By increasing the solubility of the sample, the maximum amount of the protein can interact with crystallizing solution and become saturated. Therefore, the concentration of the protein and crystallization condition can affect the saturation level of the solution (Figure 1.9).

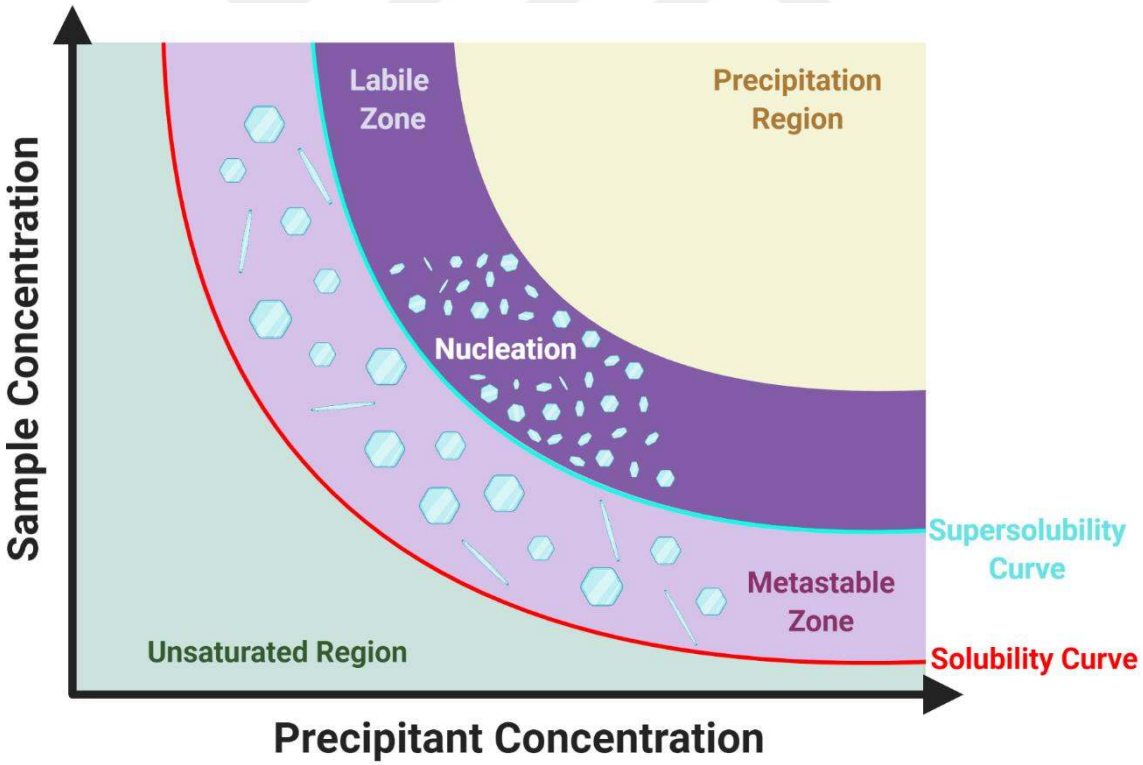

Figure 1.9: Schematic Illustration of Protein Crystallization Phase Diagram

The solubility curve shows the beginning of the saturation of the sample. The concentrations of precipitant and the protein are in equilibrium along this curve. Under this curve, crystallization never takes place since the solution is fully dissolved and not saturated. The higher concentrations of both protein and the crystallizing agent than that at equilibrium encounter with each other above the solubility curve called the supersaturation zone. In this region, the level of supersaturation is important to kinetically favor the crystallization. The amorphous aggregates are formed when excess of the sample solution separates from the mixture during the precipitation zone. The nucleation zone, also known as the labile zone, is ideal for spontaneous crystal nucleation, where the excess of the sample molecules become crystalline form. Once the nucleation is enhanced, the fast growth of crystal nuclei may take place. Then, the solution would enter the metastable zone which is the area of lower supersaturation. At the metastable zone, crystals are stable and become well-ordered larger structures, while no further nucleation occurs (Chayen, 2005; Chayen & Saridakis, 2008; Govada & Chayen, 2019). The properties of crystallized molecules interestingly are not altered by crystallization. Once the crystals form, then they are exposed to X-ray beams (Gawas et al., 2019; Smyth & Martin, 2000).

Chapter 2:
METHODS

2.1 Gene Construct Design and Cloning

2.1.1 Construct 1 and 2: CLIC4 and CLIC4 C35A

The wild type and mutant *CLIC4* constructs were generated with the following amino acid sequence by Dr. Nazan Saner from our collaborator Assoc. Prof. Nurhan Özlü's laboratory. HHHHHHSSGLVPR(Thrombin_cut_site)GSHMALSMPLNGLKEEDKEP LIELFVKAGSDGESIGNCPFSQRLFMILWLKGVVFSVTTVDLKRKPADLQNLAP GTHPPFITFNSEVKTDVNKIEEFLEEVLCPPKYLKLSPKHPESNTAGMDIFAKFSA YIKNSRPEANEALERGLLKTLKLDEYLNSPLPDEIDENSMEDIKFSTRKFLDGNE MTLADCNLLPKLHIVKVVAKKYRNFDIPKEMTGWRYLTNAYSRDEFTNTCPSD KEVEIAYSDVAKRLTK*. CLIC4 WT and CLIC4 C35A inserts were cloned into pET28a(+) bacterial vector by using NdeI and BamHI restriction sites at 5' and 3' ends, respectively. The N-terminal hexa-histidine tag was shown in green color. The thrombin cleavage site which was the part of the pET28a(+) vector was indicated in the purple sequence. The C-terminus had the in-frame stop codon shown in red asterisk.

2.1.2 Construct 3 and 4: Ezrin and Ezrin T567D

The wild type and mutant ezrin constructs were generated with the following amino acid sequence by Dr. Nazan Saner from our collaborator Assoc. Prof. Nurhan Özlü's laboratory. HHHHHHSSGLVPR(Thrombin_cut_site)GSHMPKPINVRVTTMDAELEF AIQPNTTGKQLFDQVVKTIGLREVWYFGLHYVDNKGFPTWLKLDKKVSAQEV RKENPLQFKFRAKFYPEDVAEELIQDITQKLFFLQVKEGILSDEIYCPPETAVLLG SYAVQAKFGDYNKEVHKSGYLSSERLIPQRVMDQHKLTRDQWEDRIQVWHAE HRGMLKDNAMLEYLKIAQDLEMYGINYFEIKNKKGTDLWLGVDALGLNIYEK DDKLTPKIGFPWSEIRNISFNDKKFVIKPIDKKAPDFVFYAPRLRINKRILQLCMG NHELYMRRRKPDTIEVQQMKAQAREEKHQKQLERQQLETEKKRRETVEREKE QMMREKEELMLRLQDYEEKTKKAERELSEQIQRALQLEEERKRAQEEAERLEA

DRMAALRAKEELERQAVDQIKSQEQLAAELAEYTAKIALLEEARRRKEDEVEE WQHRAKEAQDDLVKTKEELHLVMTAPPPPPPPVYEPVSYHVQESLQDEGAEPT GYSAELSSEGIRDDRNEEKRITEAEKNERVQRQLLTLSSELSQARDENKRTHNDI IHNENMRQGRDKYKTLRQIRQGNTKQRIDEFEAL*. Ezrin WT was cloned into pET28a(+) by using NdeI and EcoRI restriction sites. Then, site-directed mutagenesis was used to generate T567D mutation of ezrin and cloned into pET28a(+) bacterial vector by using NdeI and BamHI restriction sites at 5' and 3' ends, respectively. The N-terminal hexa-histidine tag was shown in green color. The thrombin cleavage site which was the part of the pET28a(+) vector was indicated in the purple sequence. The C-terminus had the in-frame stop codon shown in red asterisk.

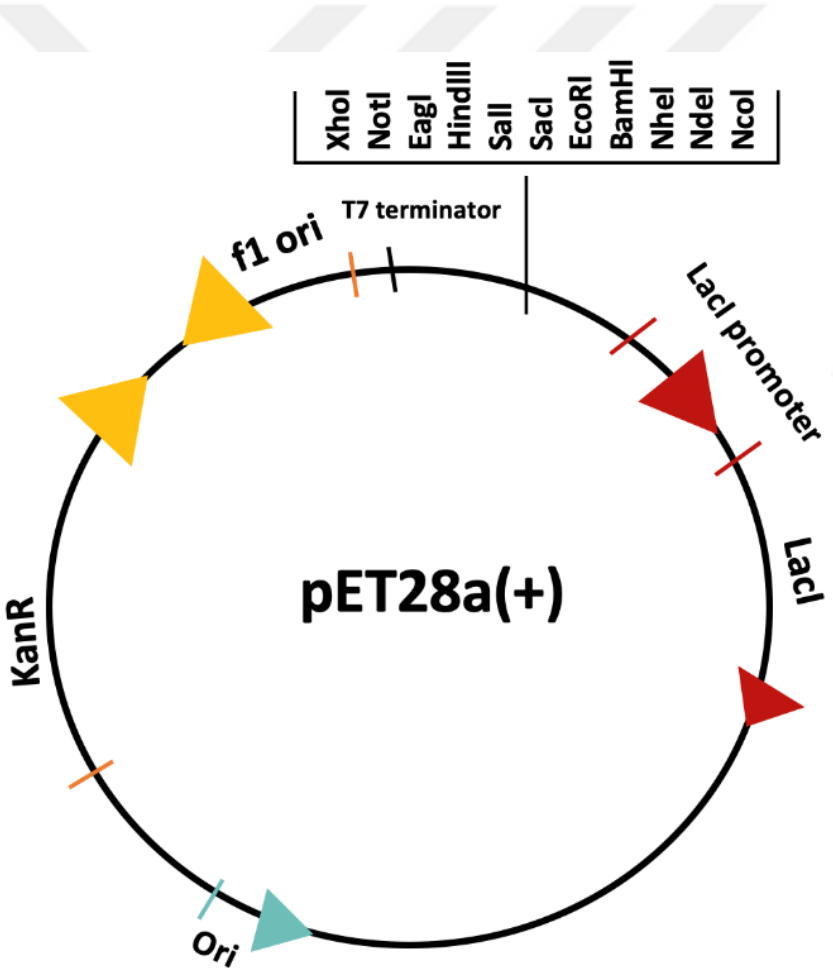

Figure 2.1: pET28a(+) Plasmid Map

2.2 *Recombinant Protein Expression*

2.2.1 CLIC4 WT and CLIC4 C35A Protein Expression in small scale

CLIC4 WT and *CLIC4 C35A* were transformed into *Escherichia coli (E. coli)* BL21 Rosetta-2 strains. 25 ml of bacterial cell cultures containing target protein genes were grown in regular LB-Miller media supplemented with 50 µg/ml Kanamycin and 35 µg/ml Chloramphenicol at 37^{O}C overnight. 750 µl of overnight cultures were mixed with 750 µl 80% Sterile Glycerol in cryogenic vials. The vials were vortexed and stored at -80^{O}C. After the preparation of their glycerol stocks, the recombinant protein expression was induced at 18^{O}C by Isopropyl β-D-1-thiogalactopyranoside (IPTG) with a final concentration of 0.4 mM for 24-, 48-, and 72-hours. The cells were harvested at 4^{O}C by using a centrifuge at 3500 rpm for 30 minutes. The cell pellets were stored at -80^{O}C, then the recombinant protein expressions were confirmed by SDS-PAGE.

2.2.2 Ezrin WT and Ezrin T567D Protein Expression in small scale

Ezrin WT and ezrin T567D were transformed into *E. coli* BL21 Rosetta-2 strains. 150 ml of bacterial cell cultures containing target protein genes were grown in regular LB-Miller media containing 50 µg/ml Kanamycin and 35 µg/ml Chloramphenicol at 37^{O}C overnight. 750 µl of overnight cultures were mixed with 750 µl 80% Sterile Glycerol in cryogenic vials, vortexed and stored at -80^{O}C. After the preparation of their glycerol stocks, the bacterial cell cultures were divided into equal amounts to test different induction temperatures. Then, protein expression was induced by 0.4 mM IPTG both at 18^{O}C for 3 days and at 37^{O}C for 24 hours. The cells were harvested at 4^{O}C by using a centrifuge at 3500 rpm for 30 minutes. The cell pellets were stored at -80^{O}C, then the recombinant protein expressions were confirmed by SDS-PAGE.

2.2.3 Protein Expression in large scale

For large scale protein expression, all target proteins, CLIC4 WT, CLIC4 C35A, ezrin WT and ezrin T567D, were inoculated from their glycerol stocks. They were first grown in 150 ml regular LB-Miller media supplemented with 50 µg/ml Kanamycin and

35 µg/ml Chloramphenicol overnight at 37^{O}C. The overnight starter culture was equally divided into the 12 liters of regular LB-Miller media with 50 µg/ml Kanamycin and 35 µg/ml Chloramphenicol at 37^{O}C. The bacterial cell cultures were grown and incubated in a shaker at 110 rpm until each culture reached OD600 about 0.8-1.2. Then, recombinant protein expression was induced by 0.4 mM IPTG. The incubation of bacterial cell cultures including CLIC4 WT and CLIC4 C35A protein genes was performed at 18^{O}C for 3 days. Ezrin WT and ezrin T567D protein production was induced at 37^{O}C for 24 hours. The cells were harvested at 4^{O}C by using a centrifuge at 3500 rpm for 30 minutes. The cell pellets were stored at -80^{O}C, and the recombinant protein expressions were confirmed by SDS-PAGE.

2.3 Pulldown Experiments

The bacterial cell pellets were dissolved in the lysis buffer containing 500 mM NaCl, 50 mM Tris-HAc (pH 7.5), 5% v/v Glycerol supplemented with 0.01% Triton-X-100 by sonication. Then, cell lysates were centrifuged at 10000 rpm for 1 hour at 4^{O}C. The pellets were collected and dissolved in the lysis buffer and stored at 4^{O}C. The clear supernatant was also collected. The Ni-NTA agarose resin beads were added into the supernatant for pulldown experiments and stored at 4^{O}C overnight. Then, to wash the beads they were centrifuged at 1000 rpm at 4^{O}C for 1 minute by washing twice with the loading buffer containing 150 mM NaCl, and 20 mM Tris-HAc (pH 7.5). After washing steps, hexa-histidine tagged proteins were eluted with the elution buffer that contains 150 mM NaCl, 20 mM Tris-HAc (pH 7.5), 250 mM Imidazole.

2.4 SDS-PAGE

The SDS-PAGE gel was poured as four gels with the following ingredients and amounts. The 12% separating gel was prepared with 7.8 ml 30% Acrylamide/ 0.8% Bisacrylamide, 6.539 ml ddH_2O, 4.875 ml 1.5 M Tris-HCl (pH 8.8), 195 µl 10% SDS, 97.5 µl 10% APS, 9.75 µl TEMED. The 4% stacking gel was prepared with 792 µl 30% Acrylamide/ 0.8% Bisacrylamide, 3.6 ml ddH_2O, 1.512ml 0.5 M Tris-HCl (pH 6.8), 60 µl 10% SDS, 30 µl 10% APS, 6 µl TEMED. The SDS-PAGE gel was run at 70 Volt for 20 minutes, then run at 90 Volt for 3 hours.

2.5 *Protein Purification*

The bacterial cell pellets were dissolved in the lysis buffer by sonication. Then, cell lysates were centrifuged by ultracentrifuge at 40000 rpm for 1 hour at 4^{O}C. After ultracentrifugation, the pellets containing membranes and insoluble debris were discarded. The clear supernatant was applied to nickel affinity chromatography by using a Ni-NTA agarose resin (Figure 2.2). First, the chromatography column was equilibrated by flowing 2 column volumes of the loading buffer. Then, the supernatant containing the overexpressed target proteins was loaded onto the Ni-NTA agarose column at the 2.5 milliliters/minute flow rate. The unbound proteins were removed by washing with 6 column volumes of the loading buffer to eliminate the non-specific bindings. After the washing step, hexa-histidine tagged proteins were eluted from the column with the elution buffer.

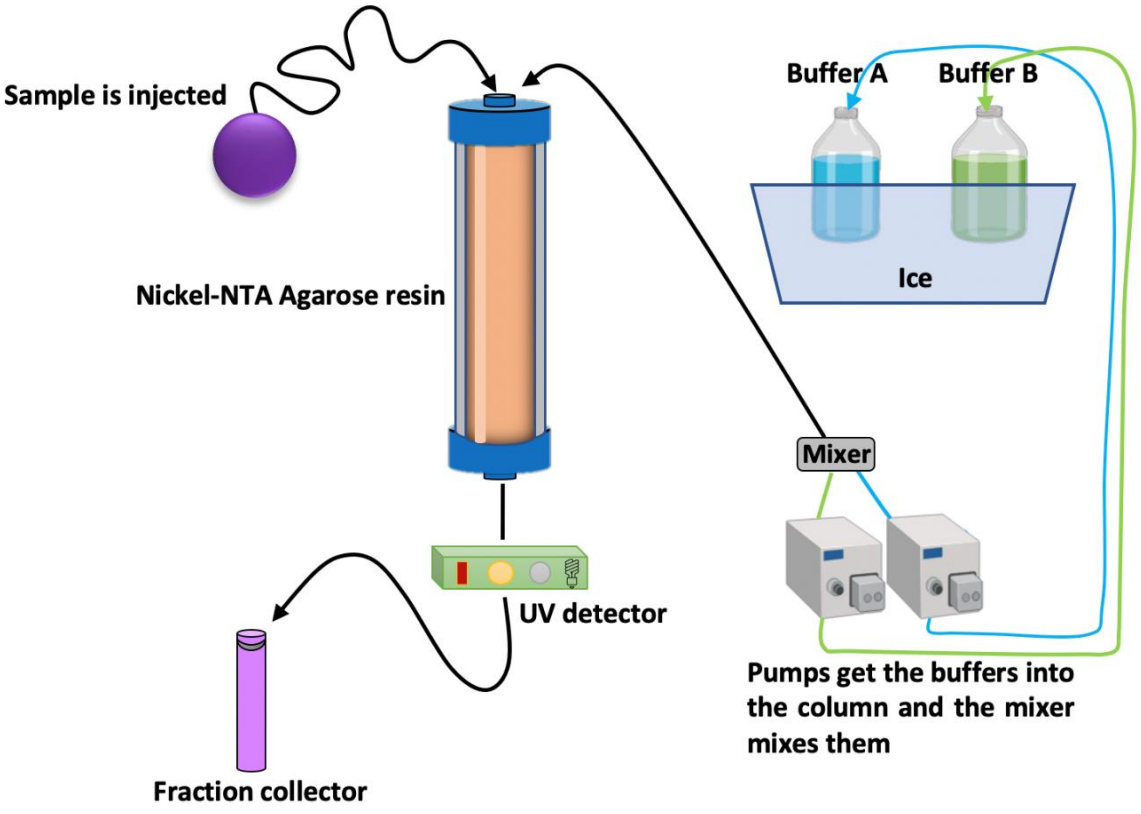

Figure 2.2: Schematic Representation of Nickel Affinity Chromatography

2.6 *Reverse Chromatography*

In order to cleave the N-terminal hexa-histidine tag of ezrin WT, CLIC4 WT and CLIC4 C35A, thrombin was applied for 3 days in 1:500 stoichiometric molar ratios at 4^{O}C. Then, purified proteins were placed in a 30 kDa cut off dialysis membrane. To remove the excess Imidazole, the proteins were dialyzed for 4 days against the buffer containing 150 mM NaCl, 20 mM Tris-HAc (pH 7.5). In the final purification step, the reverse Ni-NTA chromatography was applied to eliminate the cleaved non-specific binding proteins and hexa-histidine tag from the solution. Since the hexa-histidine tags were cleaved from the target protein, the unbound fractions having the untagged protein of interest were collected (Figure 2.3). The pure proteins were concentrated by ultrafiltration columns and stored at -80^{O}C until crystallization trials.

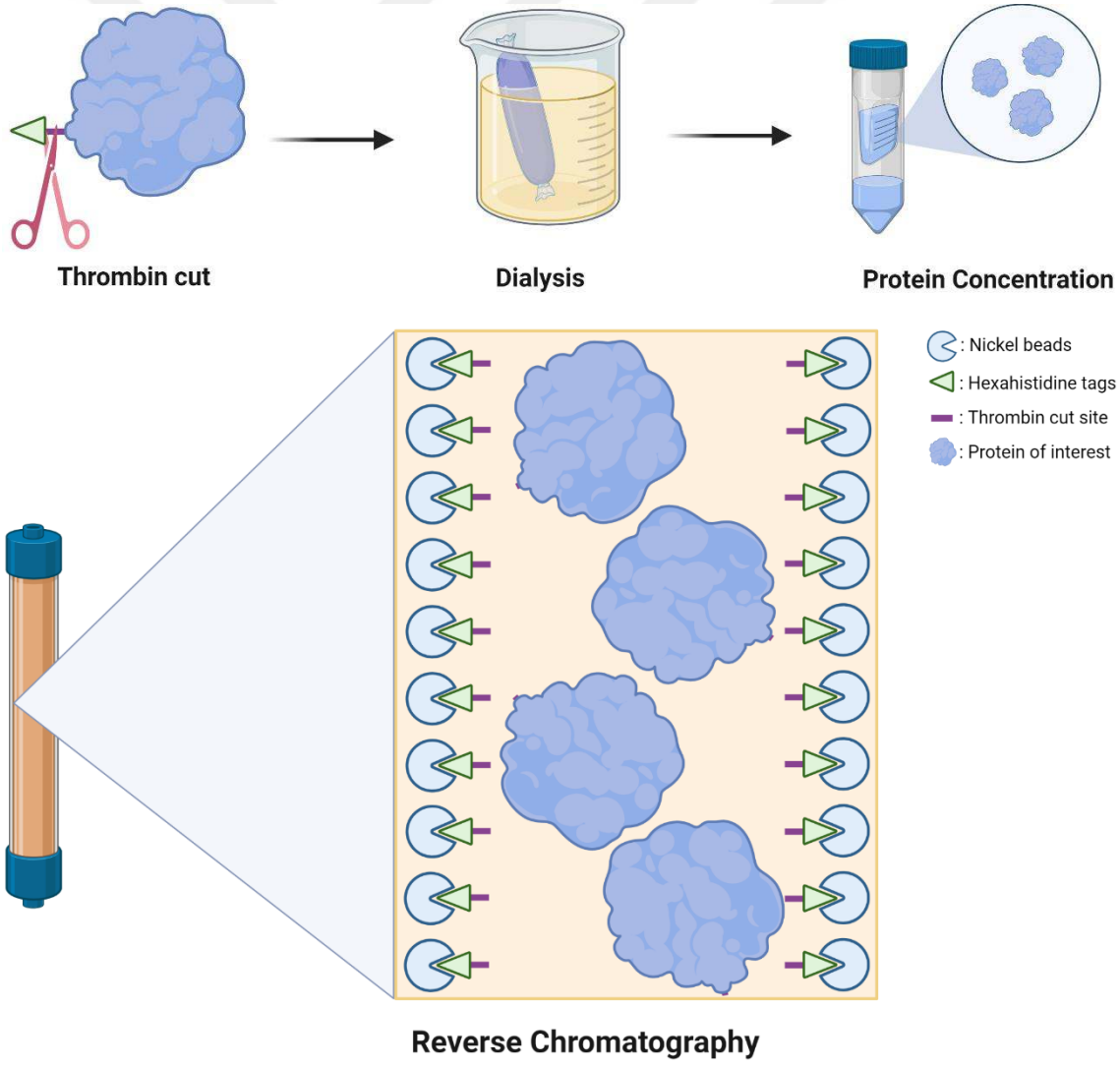

Figure 2.3: Experimental Flow of Reverse Chromatography

2.7 *Crystallization*

For the initial crystallization screening, sitting-drop microbatch under oil screening method was utilized by using 72 well Terasaki crystallization plates (Figure 2.4). During crystallization, the purified protein of interest was mixed with a 1:1 volumetric ratio with each ~3500 commercially available sparse matrix crystallization screening conditions separately. Then, the sitting solutions were covered with 16.6 µl of 100% Paraffin oil to minimize evaporation and vapor diffusion. All the crystallization experiments were performed at ambient-temperature. The growth of crystals, which were stored at room temperature, was observed under a stereo-microscope at the following time intervals: 1 week, 2 weeks and 1 month.

2.7.1 CLIC4 WT and Ezrin T567D Co-crystallization

CLIC4 WT and ezrin T567D protein samples were mixed with equal volumes to obtain a 1:1 complex. Then, the complex samples were pooled and 1 milliliter aliquots were stored at -80^{O}C until crystallization trials. Similar to other crystallization trials, the mixture was mixed with the 1:1 volumetric ratio with each ~3500 crystallization screening conditions separately and covered with 16.6 µl of 100% Paraffin oil. The crystals were stored at room temperature, and the crystals were checked weekly.

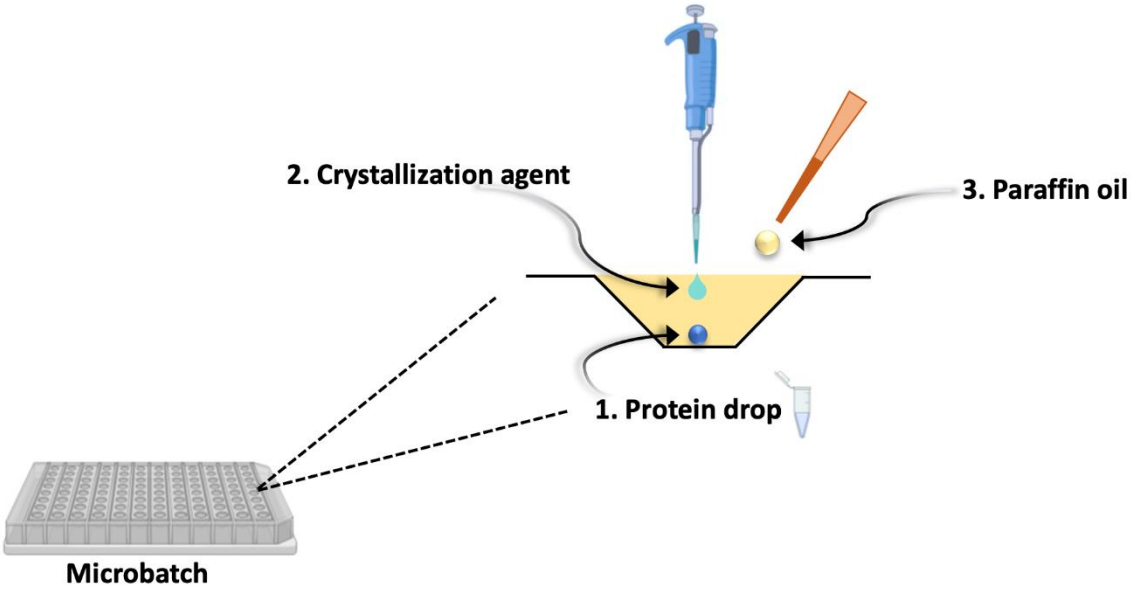

Figure 2.4: Schematic Representation of Crystallization

The ingredients of the crystallization screening conditions at which crystals formed are indicated in table 2.1-5.

Table 2.1: The Ingredients of the 41st Condition of Crystal Screen II

Condition	41st Condition of Crystal Screen II
Salt/Additive	0.01 M Nickel (II) chloride hexahydrate
Buffer	0.1 M Tris, pH 8.5
Precipitant Reagent	1.0 M Lithium sulfate monohydrate
Detergent	None
Crystallized Proteins	CLIC4 C35A

Table 2.2: The Ingredients of the 8th Condition of Midas II

Condition	8th Condition of Midas II
Salt/Additive	10% v/v Ethanol
Buffer	None
Precipitant Reagent	10% v/v Jeffamine D2000 10% v/v Jeffamine M2005
Detergent	None
Crystallized Proteins	CLIC4 WT, Ezrin WT

Table 2.3: The Ingredients of the 12th Condition of Crystal Cryo II

Condition	12th Condition of Crystal Cryo II
Salt/Additive	0.095 M Cadmium chloride hydrate
Buffer	0.095 M Sodium acetate trihydrate, pH 4.6
Precipitant Reagent	28.5% v/v Polyethylene glycol 400
Detergent	5% v/v Glycerol
Crystallized Proteins	CLIC4 WT

Table 2.4: The Ingredients of the 38th Condition of Wizard I

Condition	38th Condition of Wizard I
Salt/Additive	200 mM Lithium sulfate
Buffer	100 mM CHES/ Sodium hydroxide, pH 9.5
Precipitant Reagent	1000 mM Potassium sodium tartrate
Detergent	None
Crystallized Proteins	CLIC4 WT-Ezrin T567D co-crystals

Table 2.5: The Ingredients of the 24th Condition of Helix II

Condition	24th Condition of Helix II
Salt/Additive	0.05 M Lithium sulfate
Buffer	0.05 M HEPES
Precipitant Reagent	15% v/v PEG 350 MME, pH 6.5
Detergent	None
Crystallized Proteins	CLIC4 WT-Ezrin T567D co-crystals

2.8 Native PAGE Gel

Native PAGE gel was poured as two gel with the following ingredients and amounts. The 12% separating gel was prepared with 4 ml 30% Acrylamide/ 0.8% Bisacrylamide, 5.89 ml 0.375 M Tris-HCl (pH 8.8), 100 µl 10% w/v APS, 10 µl TEMED. The 4% stacking gel was prepared with 670 µl 30% Acrylamide/ 0.8% Bisacrylamide, 4.275 ml 0.375 M Tris-HCl (pH 8.8), 50 µl 10% w/v APS, 5 µl TEMED. The Native PAGE gel was run at 70 Volt for 30 minutes, then run at 90 Volt for 2 hours.

Chapter 3:
RESULTS

In addition to the mutual relation between ezrin and CLIC4 during cell cycle progression, their interaction has been also proposed in previous studies. For example, NHERF2 is one of the ERM binding scaffold proteins, which incorporates into the same translocation site with CLIC4 at the plasma membrane. This recruitment implies that ERMs might be directly or indirectly involved in the redistribution of CLIC4 from the cytosol to the plasma membrane (Ponsioen et al., 2009). Reciprocally, in glomerular capillary endothelial cells, ERM activation is induced by CLIC4 (Tavasoli et al., 2016). However, the mutual interaction between ezrin and CLIC4 is still not well understood. Also, it is not clear how a mutation at the conserved residue Cys35 of CLIC4 or at the phosphorylation site of ezrin changes their structures. Since this interaction might have an important role in cancer therapy, this study aimed at unveiling the mystery behind structural information of these two proteins. Although the wild type structures of CLIC4 and ezrin proteins were previously determined, the structures of their mutant forms, CLIC4 C35A and ezrin T567D, are not available. Thus, this study has been motivated to analyze the structural dynamics of wild type and mutant forms of CLIC4 and ezrin with their mutual interaction.

3.1 Mini Expression Test for CLIC4 WT and CLIC4 C35A

For the mini expression check, CLIC4 WT and CLIC4 C35A were produced in 25 ml bacterial cell cultures. Since I have also CLIC1 and CLIC4 F37D constructs for future experiments, all expression tests were applied to these two proteins, simultaneously. To determine the best induction time after the addition of IPTG, 1 ml of culture samples were taken at 24- and 48-hours intervals. Then, the remaining 23 ml cell cultures were collected the next day as 72-hours induction samples. Since the protein solubility is not known, all samples were prepared as supernatant and pellet (Figure 3.1, 3.2). As the final step, the expression level of recombinant proteins was confirmed by SDS-PAGE.

The supernatant samples were loaded on the gel as 24-, 48-, and 72-hours induction samples in the following order: marker, CLIC1, CLIC4 WT, CLIC4 C35A and CLIC4 F37D (Figure 3.1). Since the molecular weight of CLIC4, and its mutants are 29 kDa, and CLIC1 is 27 kDa, they should appear above 25 kDa, whose expected locations are shown with the red rectangle. The expression level of the proteins can be easily compared with each other based on their band densities. Since CLIC4 C35A has the thickest band, and CLIC1 has the thinnest, the descending order of the band density can be aligned as CLIC4 C35A > CLIC4 F37D > CLIC4 WT > CLIC1. For this reason, it can be concluded that CLIC4 C35A has the highest expression level since it has the thickest band among the other three proteins. Also, the CLIC1 has the lowest expression level. The CLIC4 F37D and CLIC4 WT are the second and third highly expressed proteins, respectively.

Moreover, protein expression level may depend on the induction time. To test this hypothesis, 24-, 48-, and 72-hours induction samples were loaded on the gel, respectively. The ascending order of the band thickness can be ordered as 72- < 48- = 24-hours. In brief, the band density of the CLIC4 C35A was maintained at 24- and 48-hours like the other three proteins, while it drastically decreased after 72-hours induction.

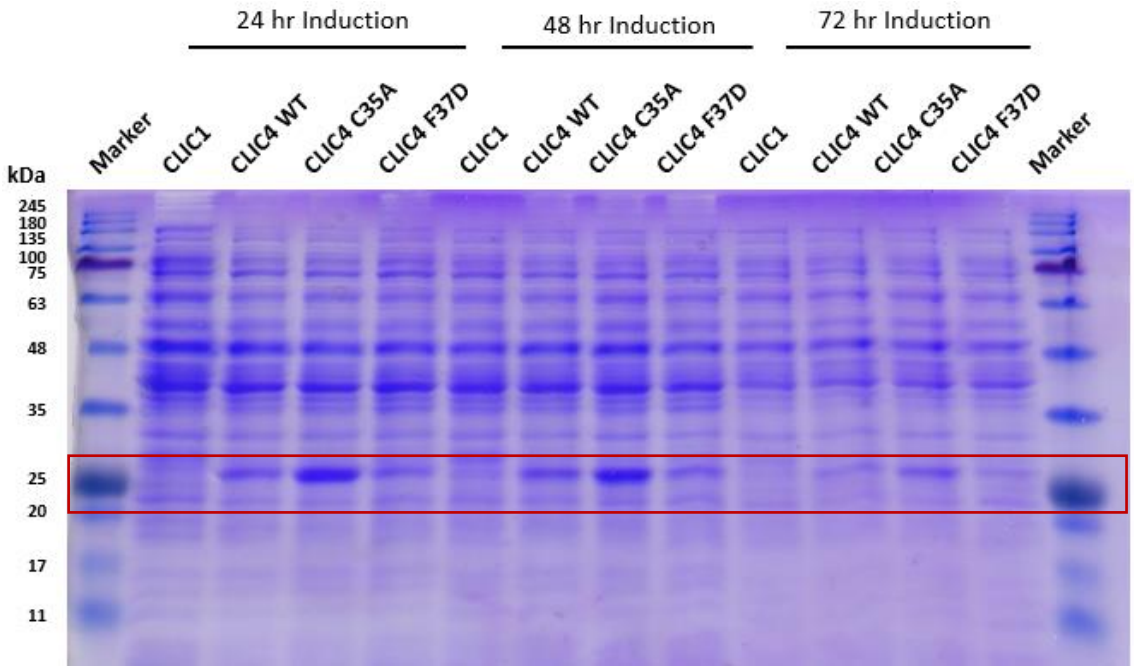

Figure 3.1: Mini Expression Test Results for Supernatant Samples of CLICs

In order to determine the protein solubility, the pellet samples of CLIC proteins were also collected and run on the gel (Figure 3.2). The expected locations of CLIC1, CLIC4 WT and its mutants are shown with the red rectangle. Although CLIC1 has no band at three induction times, the other three proteins have mild dense bands. The CLIC4 C35A has the densest band at 24-hours induction time whereas the band density of CLIC4 F37D and CLIC4 WT gradually become lighter in an order. The CLIC4 C35A and F37D have denser bands at 72-hours induction time than 48-hours, while the band density of the CLIC4 WT is higher among its mutants at these two inductions.

As a result, all CLIC proteins are usually found in the supernatant part of the solution; even though a small amount of CLIC4 WT, CLIC4 C35A and CLIC4 F37D stayed in the pellet. In comparison to the solubility of CLIC proteins according to figure 3.1 and 3.2 results, they are all highly soluble proteins.

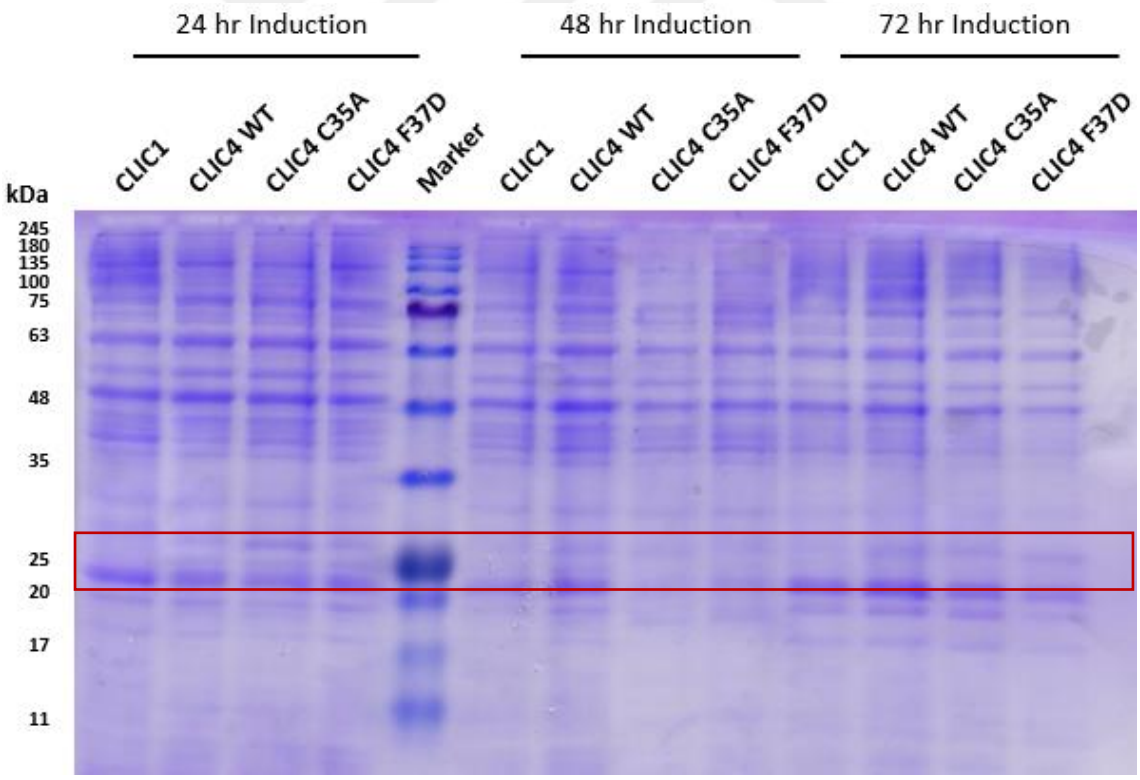

Figure 3.2: Mini Expression Test Results for Pellet Samples of CLICs

Since all constructs have the hexa-histidine tag, by using nickel-NTA resin beads the produced recombinant proteins were captured with pulldown experiments (Figure 3.3). Similar to the previous results, band densities indicate the protein expression levels. In one example, CLIC4 C35A has the highest expression level with the thickest band whereas CLIC4 WT and CLIC4 F37D are the second and third highly expressed proteins, respectively. The band density and thus, the expression level can be sorted in descending order as CLIC4 C35A > CLIC4 WT > CLIC4 F37D > CLIC1. Besides having the lowest expression level, CLIC1 has a slight band shift. Since it has the lowest molecular weight, 27 kDa, its band should be located below the other three bands, instead of being located above. The CLIC4 WT and its mutants are 29 kDa, so they are in the expected size.

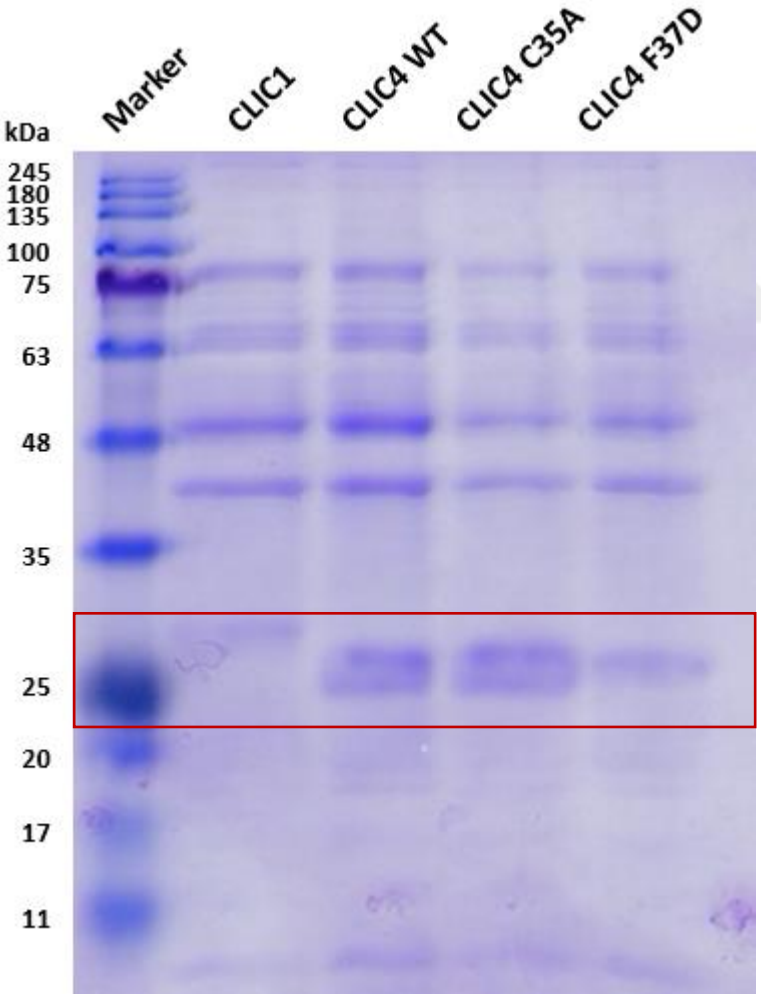

Figure 3.3: Pulldown Results for CLICs

3.2 Overexpression, Purification and Crystallization of CLIC4 C35A

Hexa-histidine tagged CLIC4 C35A proteins were purified by nickel affinity chromatography after they were overexpressed in the 12 liters culture. Then, the eluted samples were run on the gel to confirm protein expression and successful purification. Samples were loaded on the gel in the following order: marker I and II, supernatant, pellet, flow-through, 25 mM Imidazole I and II, 500 mM Imidazole I, II, III and IV (Figure 3.4). The marker I was used to estimate the size of the overexpressed protein bands, while marker II was only used to compare the band sizes with the marker I. Since the molecular weight of CLIC4 C35A is 29 kDa, its band should be above 25 kDa reference ladder band, indicated by the green band at marker I lane.

After ultracentrifugation, supernatant and pellet samples were taken to check the protein solubility. The supernatant sample has a very thick band around 29 kDa, where CLIC4 C35A is expected. Therefore, this protein is still soluble when produced at a larger scale. In the pellet sample, since DNA fragments produce a smear in the gel, no bands are observed. Moreover, the nickel-NTA resin column has a high capacity to bind the hexa-histidine tagged proteins. As seen on the supernatant lane in figure 3.4, there are also other proteins loaded on the column. Since the CLIC4 C35A has a hexa-histidine tag, even if other proteins have histidine amino acids, the target protein will have a higher affinity towards the resin beads. Therefore, it will remain in the column while other proteins are eluted. Additionally, sometimes the hexa-histidine tagged proteins might be lost because of the column capacity. Therefore, during purification, the flow-through was also collected to check whether the target protein is lost and/or how much is lost. According to the flow-through sample, there are many proteins are eluted during protein loading. Since there is a quite thin band around 29 kDa, a small amount of the target protein is lost. After all sample protein was loaded to the column, they were firstly eluted by 25 mM Imidazole. Since the eluted samples were collected into different falcon tubes, they were labelled as I, II, III, and IV, respectively. This elution provides the elimination of proteins with a low affinity towards the column. There are some proteins eluted with 25 mM Imidazole, whereas the target protein mostly remains in the column according to the comparison of 25 mM Imidazole II and 500 mM Imidazole II sample lanes. After the elution peak of 25 mM Imidazole started to decrease and stabilized, 500 mM Imidazole was loaded on the column. The highest amount of the protein is obtained at 500 mM

Imidazole II sample tube where the graph has the highest peak shown in figure 3.5. In figure 3.5, the blue line shows the UV, while the red line stands for the conductance.

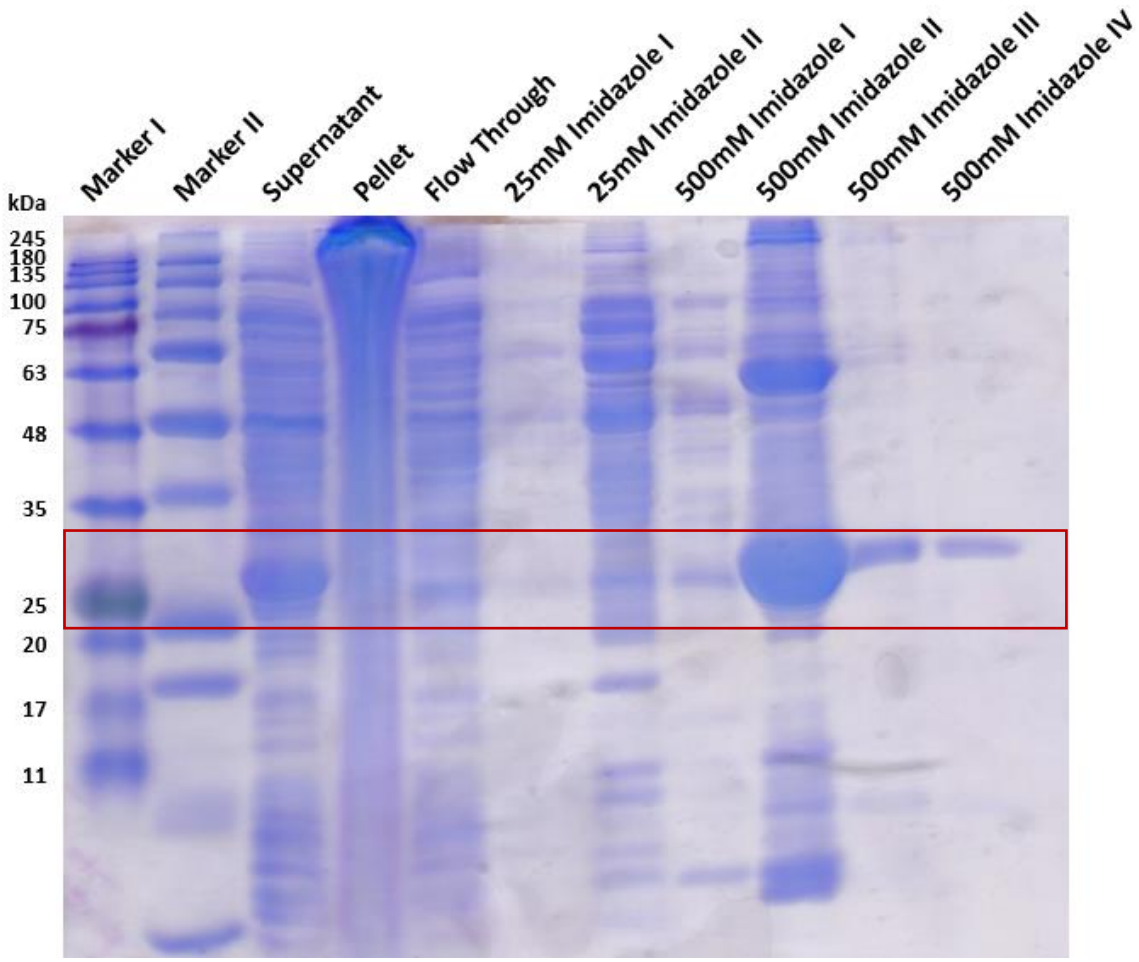

Figure 3.4: CLIC4 C35A Elution

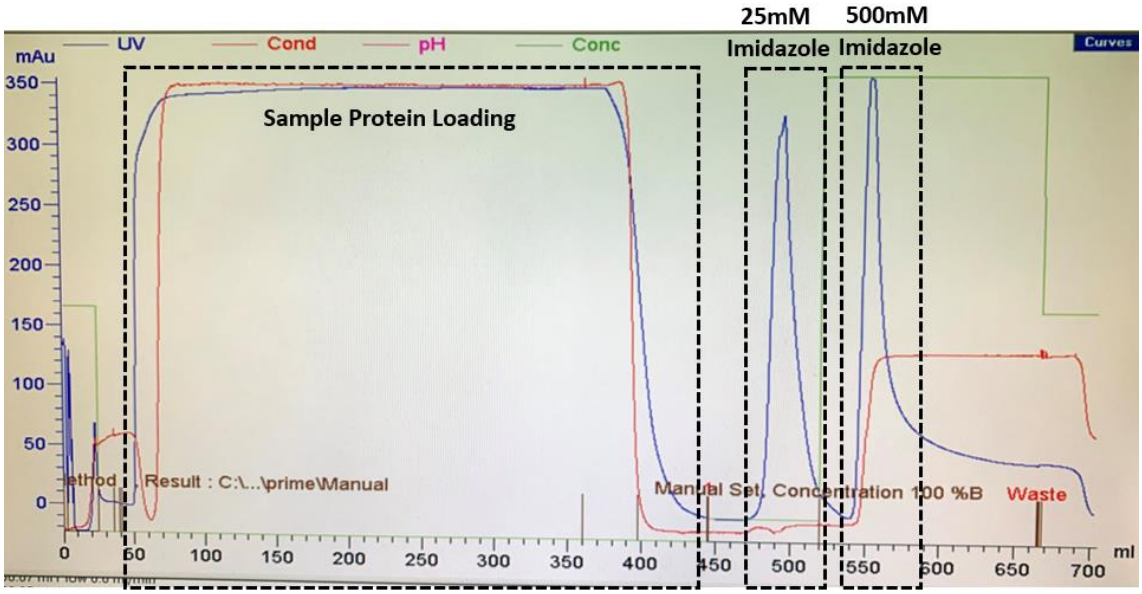

Figure 3.5: Nickel Affinity Chromatography Graph for CLIC4 C35A

After successful CLIC4 C35A purification, crystallization trials were conducted, but crystals could not be obtained. Then, the hexa-histidine tag was cleaved by thrombin from the N-terminus of the protein. In order to check whether thrombin successfully cut the hexa-histidine-tags, uncut and cut CLIC4 C35A samples were run on the gel together with thrombin itself (Figure 3.6). Different amounts of uncut and cut samples were loaded on the gel to analyze the thrombin cleavage efficiency better. This is due to the fact that, if the 6 µl of CLIC4 C35A had a very dense and thick band, the band shift after the thrombin cut would not be noticed. Contrarily, if the 2 µl of CLIC4 C35A had a very low protein amount and did not have a clear band, but the 6 µl would have. For this reason, the 2 µl, 4 µl and 6 µl of proteins were loaded on the gel. However, figure 3.6 shows that all protein amounts are enough to indicate the band shift. The presence of the band shift framed with the red rectangle implies that thrombin removed the hexa-histidine tags effectively.

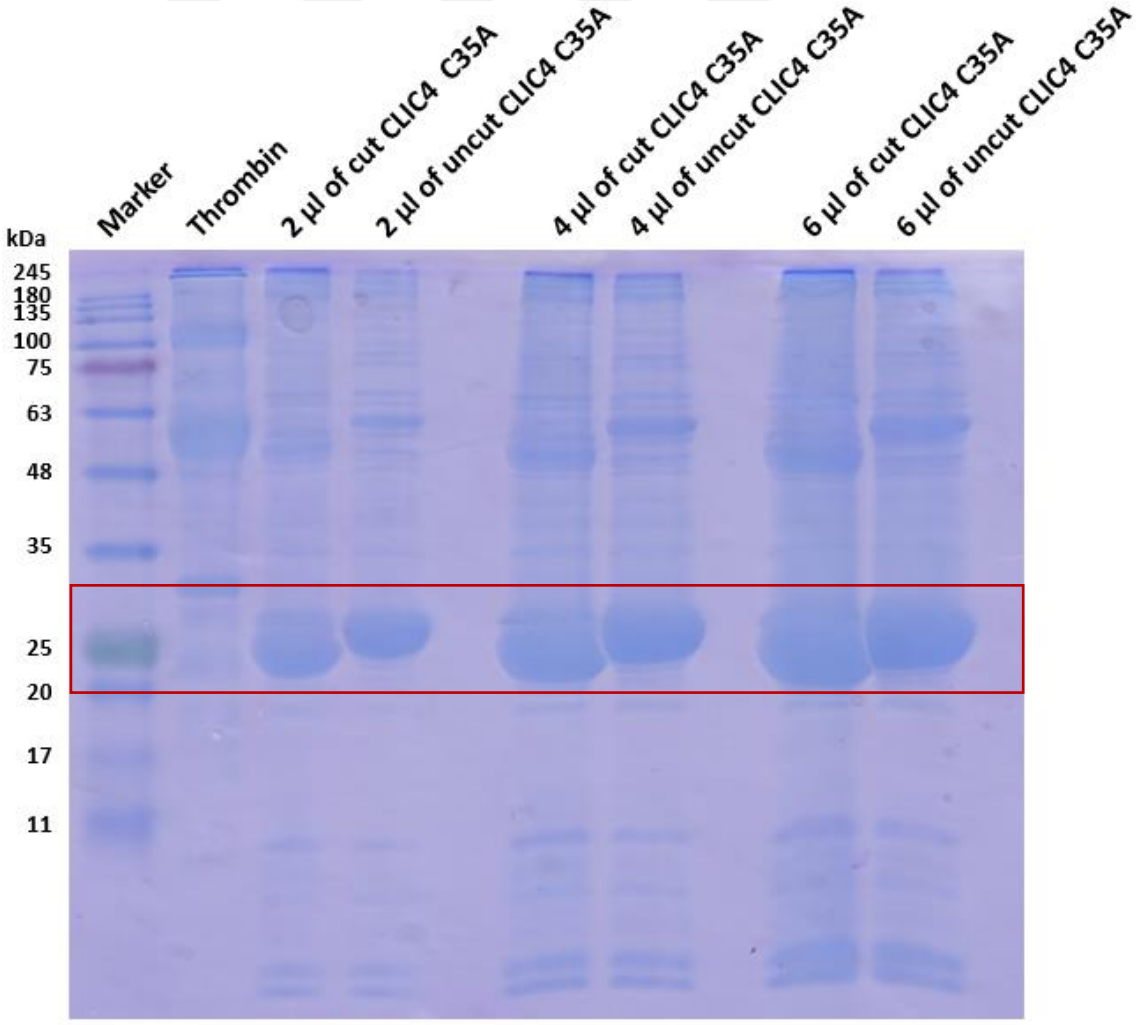

Figure 3.6: Thrombin Cut Check for CLIC4 C35A

When the hexa-histidine tag was cleaved from the N-terminus of the CLIC4 C35A, the crystallization trials were again conducted. The concentration of the crystallized protein samples was 40 mg/ml. Among the ~3500 crystallization conditions, crystals formed only at the 41st condition of Crystal Screen II. Since the obtained crystals were very soft and brittle, they are probably protein crystals. Then, to make sure whether they are protein crystals or not, the crystallization experiment was repeated with the same condition for 72 wells, and the same featured crystals were observed under a stereo-microscope (Figure 3.7).

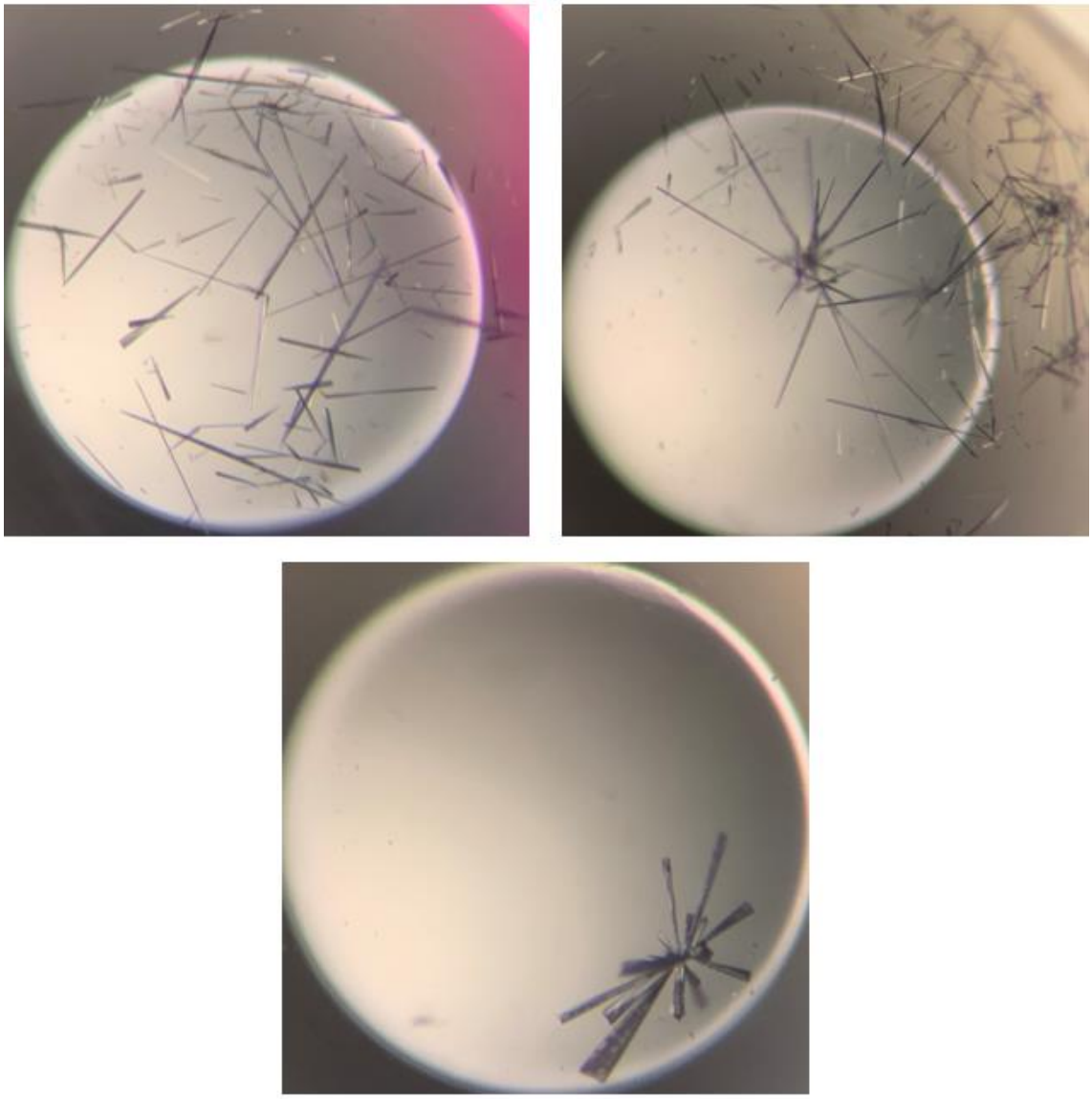

Figure 3.7: Crystals of CLIC4 C35A obtained at the 41st Condition of Crystal Screen II

The cleaved hexa-histidine tags remaining in the solution might interfere with the crystal formation. To obtain the single crystals, the cleaved hexa-histidine tags were removed from the solution by applying reverse nickel-NTA chromatography (Figure 3.8, 3.9). Since the proteins did not have hexa-histidine tags, during sample protein loading indicated in figure 3.9 the unbound samples were collected. The samples were loaded on the gel in the following order: marker, uncut, cut, and reverse nickel-NTA (Rev-NTA) samples I and II. Since the protein concentration was not known, the 1 µl, 2 µl and 6 µl of proteins were loaded on the gel. If the hexa-histidine tags were successfully removed from the protein, they will remain in the column whereas untagged protein was directly eluted from the column. As a result, Rev-NTA CLIC4 C35A I and II samples have a band around 29 kDa framed with the red rectangle, the untagged protein purified was obtained. At the final step, the 250 mM Imidazole was loaded on the column to elute the tagged proteins from the column in case of the presence of any. The small band in the last lane indicated that only a negligible amount of untagged proteins remained in the column and that most of the proteins were cut and eluted successfully.

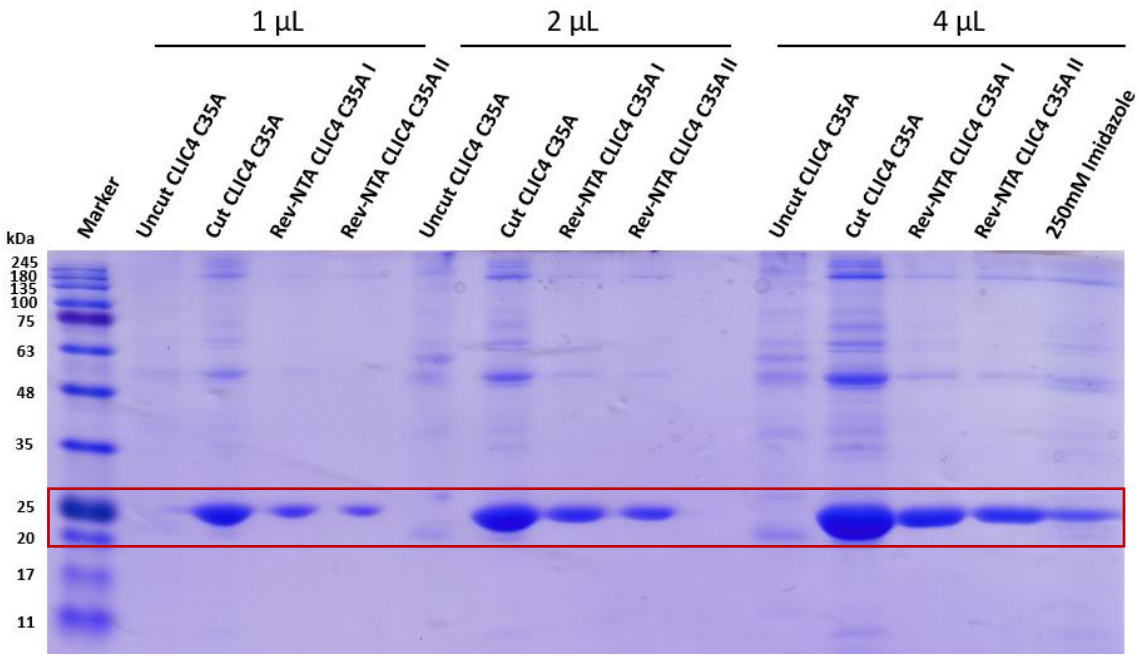

Figure 3.8: Reverse Chromatography Results for CLIC4 C35A

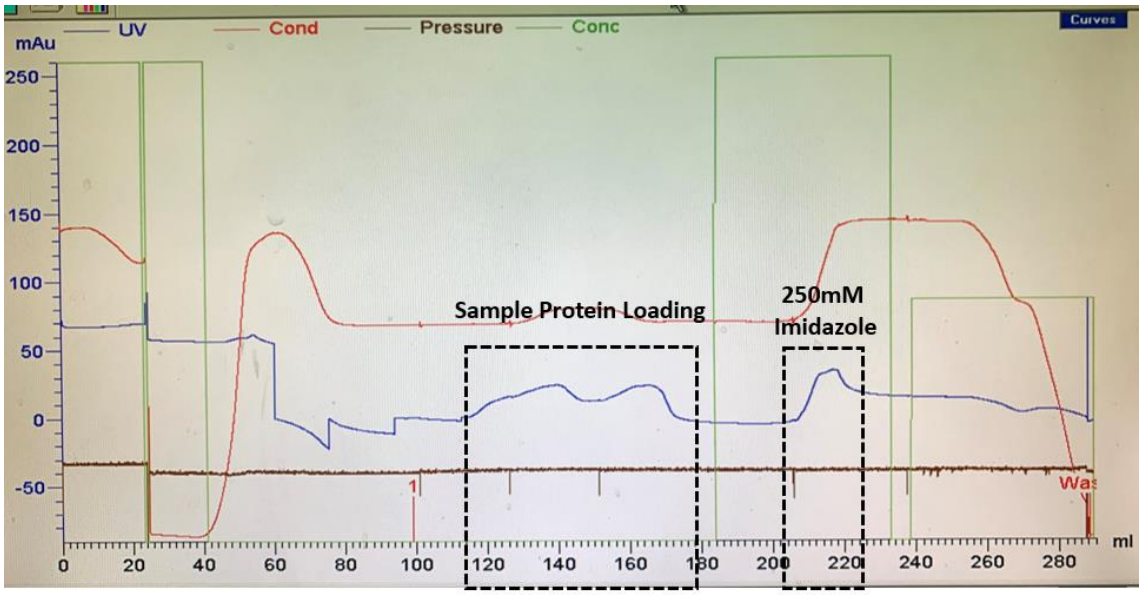

Figure 3.9: Reverse Chromatography Graph for CLIC4 C35A

The eluted untagged CLIC4 C35A proteins were concentrated because of the low concentration in the large volume. Then, the concentrated protein was run on the gel (Figure 3.10). According to the density and the thickness of the band around the 29 kDa framed with the red rectangle, the obtained protein concentration is very high.

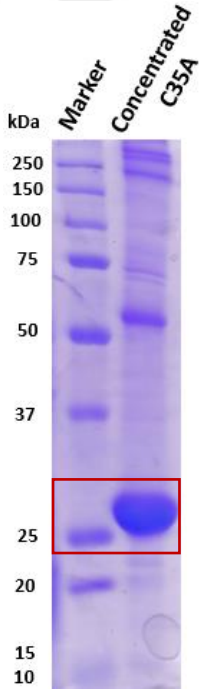

Figure 3.10: Concentrated CLIC4 C35A

After the concentration of the untagged CLIC4 C35A proteins, crystallization trials with the ~3500 crystallization conditions were again conducted to obtain single crystals. However, protein crystals could not be obtained.

3.3 Overexpression, Purification and Crystallization of CLIC4 WT

Hexa-histidine tagged CLIC4 WT proteins were overexpressed in the 12 liters culture, and a small amount of supernatant and pellet samples were taken to check the protein solubility after the ultracentrifugation. During purification, flow-through and purified protein samples were collected in the different falcon tubes labelled as 250 mM Imidazole I, II and III. To confirm protein expression and successful purification, the collected samples were run on the gel in the following order: marker, supernatant, pellet, flow-through, 50 mM Imidazole, 250 mM Imidazole I, II and III (Figure 3.11). Since the molecular weight of CLIC4 WT is 29 kDa, its band should be above the 25 kDa reference ladder band, indicated by the green band at marker lane. Moreover, to determine the addition time of the buffers, nickel affinity chromatography was utilized where the blue line shows the UV, and the red line stands for the conductance (Figure 3.12).

The supernatant sample has a very dense band around 29 kDa framed with the red rectangle, where CLIC4 WT is expected, and there are not any CLIC4 WT bands in the pellet lane. This comparison implies that the solubility of CLIC4 WT is very high and all proteins remained in the solution. Since there is also no CLIC4 WT band in the flow-through, all hexa-histidine tagged CLIC4 WT proteins were bound to the column. As seen in the flow-through lane, non-target proteins could not bind to the column and directly eluted during the sample loading step. After all samples were loaded to the column, they were eluted by 50 mM Imidazole and collected. When the first elution peak started to decrease and stabilized, the column was filled with 250 mM Imidazole. Then, the samples were collected into different falcon tubes, labelled as I, II and III, respectively. The highest amount of the CLIC4 WT is obtained at 50 mM Imidazole sample tube with the thickest band, although the first elution peak is not as high as the second peak, shown in figure 3.12. The 250 mM Imidazole I and II elution tubes have almost the same amount of protein. Since there is no CLIC4 WT band at the 250 mM Imidazole III lane, all target proteins were eluted in the column. In comparison to 50 mM and 250 mM Imidazole sample lanes, the ascending order of the protein amount is 50 mM Imidazole sample > 250 mM Imidazole I = II > III.

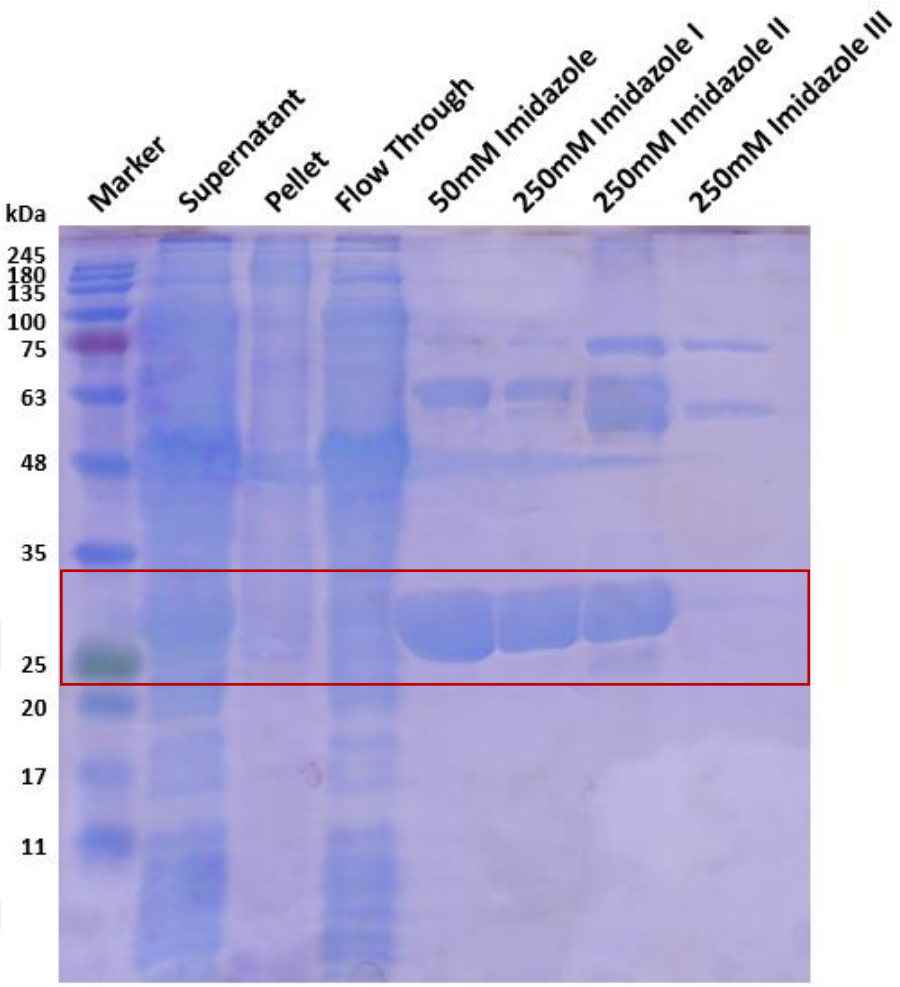

Figure 3.11: CLIC4 WT Elution

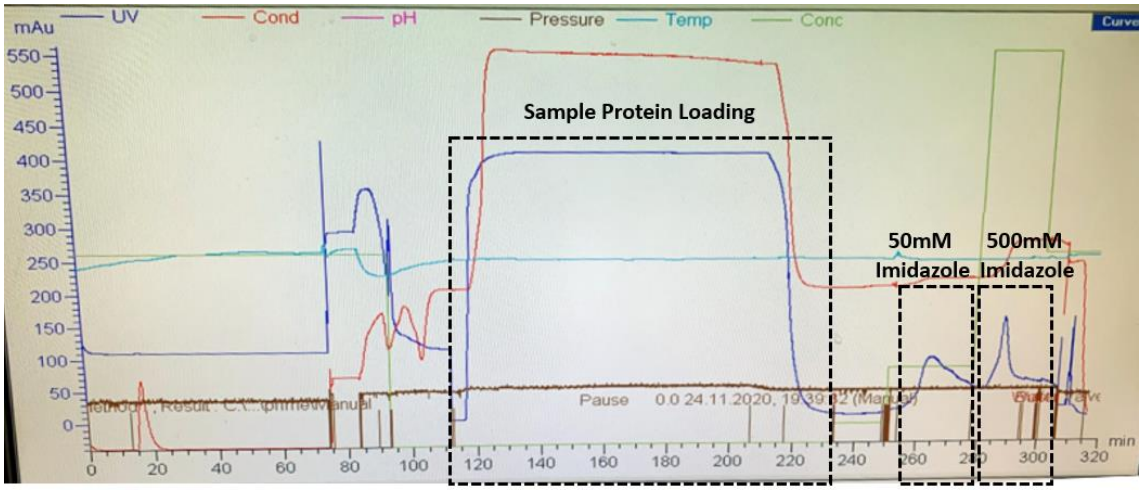

Figure 3.12: Nickel Affinity Chromatography Graph for CLIC4 WT

After the CLIC4 WT was successfully purified, crystallization was attempted, but crystals did not form. Then, the hexa-histidine tag from the N-terminus of the target protein was cut by thrombin, and reverse nickel-NTA chromatography was applied (Figure 3.13, 3.14). The samples were loaded on the gel as 5 µl and 7 µl in the following order: marker, precipitate after thrombin, supernatant after thrombin, uncut, cut, and reverse nickel-NTA (Rev-NTA) samples I, II and III. Different amounts of samples were loaded on the gel for clear bands.

When the protein solution was centrifuged after the addition of thrombin, some precipitates occurred. To determine whether all target protein or how much of it precipitated, samples from both supernatant and precipitate were taken. The smear in the precipitate lane indicates some impurities in that part. As seen on the gel result, the supernatant sample, which was loaded on the column, has the target protein around 29 kDa framed with the red rectangle. The band shift between uncut and cut samples shows that hexa-histidine tags were cleaved from the CLIC4 WT sample. Contrarily, the absence of the band around 29 kDa at the Rev-NTA sample lanes implies that the untagged CLIC4 WT could not be obtained. In addition to that, the peak during sample protein loading is almost unseeable shown in figure 3.14 with the black frame. At the last step, the tagged proteins were eluted from the column with the addition of 250 mM Imidazole. The band around 29 kDa at the last lane denotes that CLIC4 WT was collected at this step.

The collected CLIC4 WT with 250 mM Imidazole elution was concentrated and run on the gel with the uncut sample (Figure 3.15). The concentrated CLIC4 WT has a band shift, framed with the red rectangle, in comparison to the uncut sample.

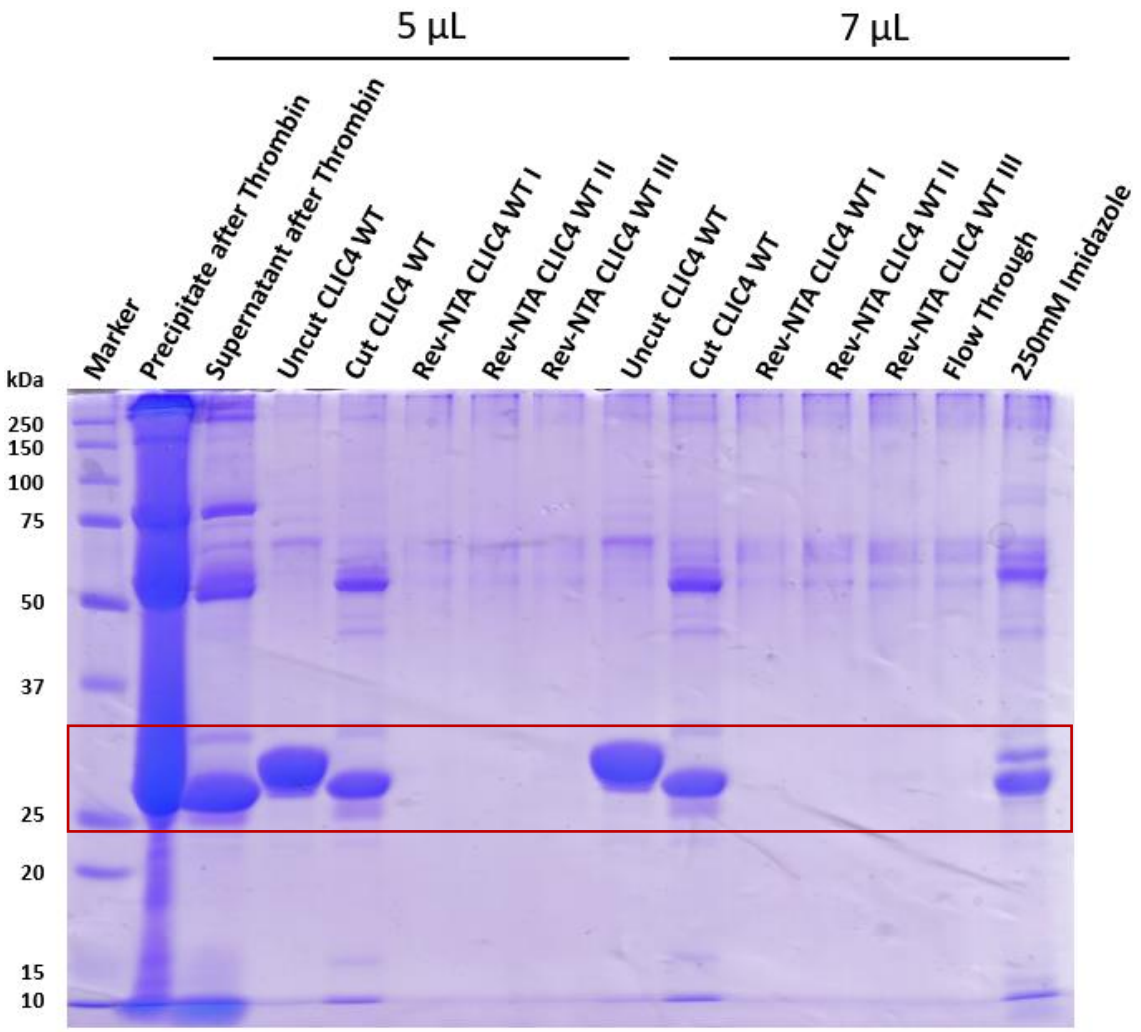

Figure 3.13: Reverse Chromatography for CLIC4 WT

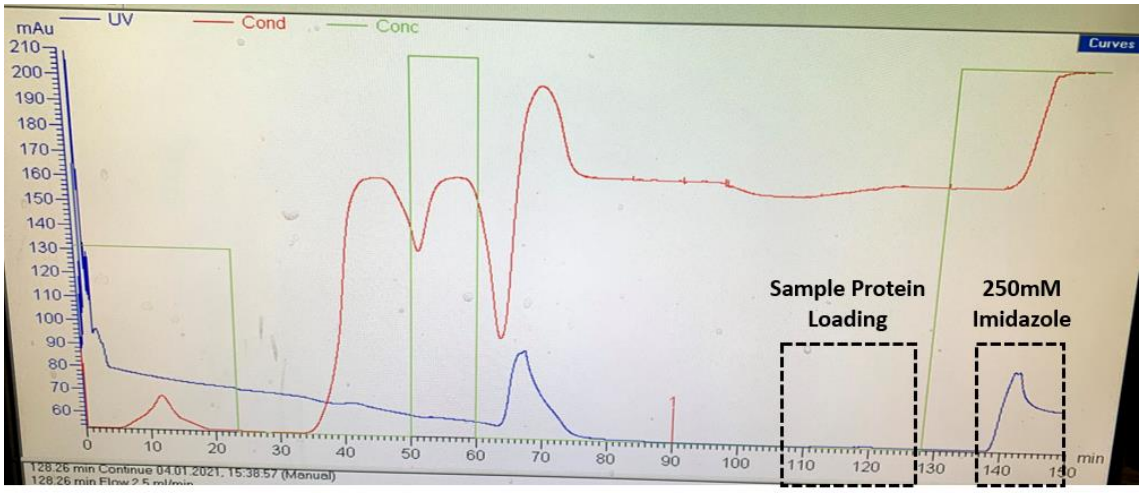

Figure 3.14: Reverse Chromatography Graph for CLIC4 WT

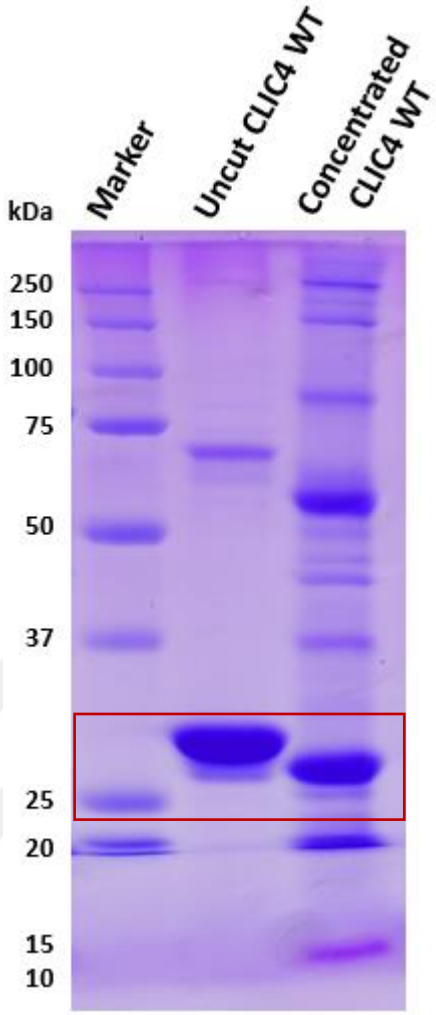

Figure 3.15: Concentrated CLIC4 WT

The crystallization trials were conducted on concentrated CLIC4 WT protein. The concentration of the crystallized protein samples was 3 mg/ml. Among the ~3500 crystallization conditions, crystals formed at two conditions, the 8th condition of Midas II, and the 12th condition of Crystal Cryo II. Then, the protein crystallization was repeated with the same conditions for 72 wells, and crystals were observed under a stereo-microscope (Figure 3.16, and 17). While the crystals obtained at the Crystal Cryo II were soft and very brittle, the crystals at Midas II were very solid.

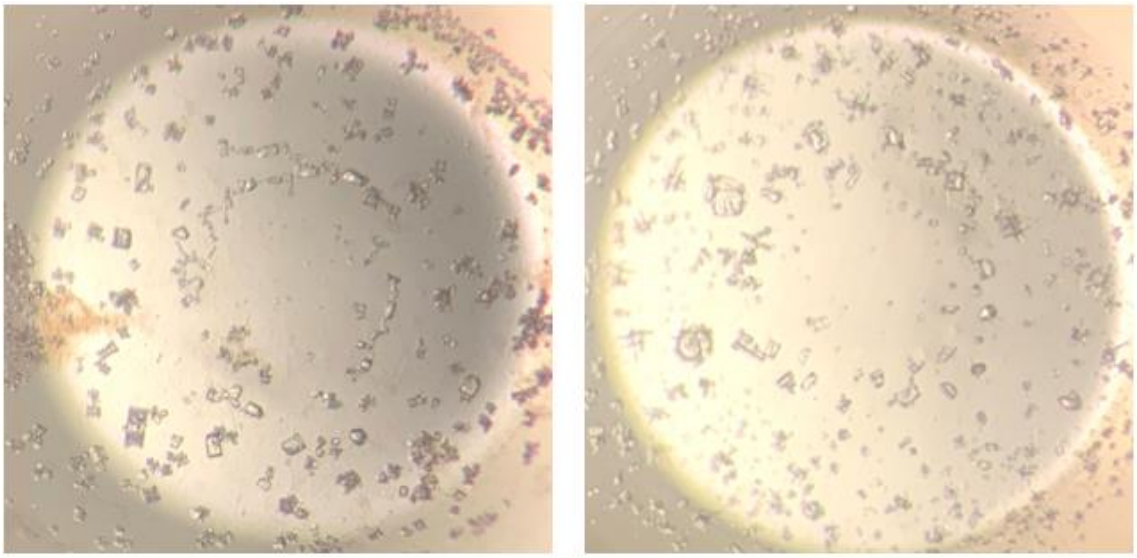

Figure 3.16: Crystals of CLIC4 WT obtained at the 8th Condition of Midas II

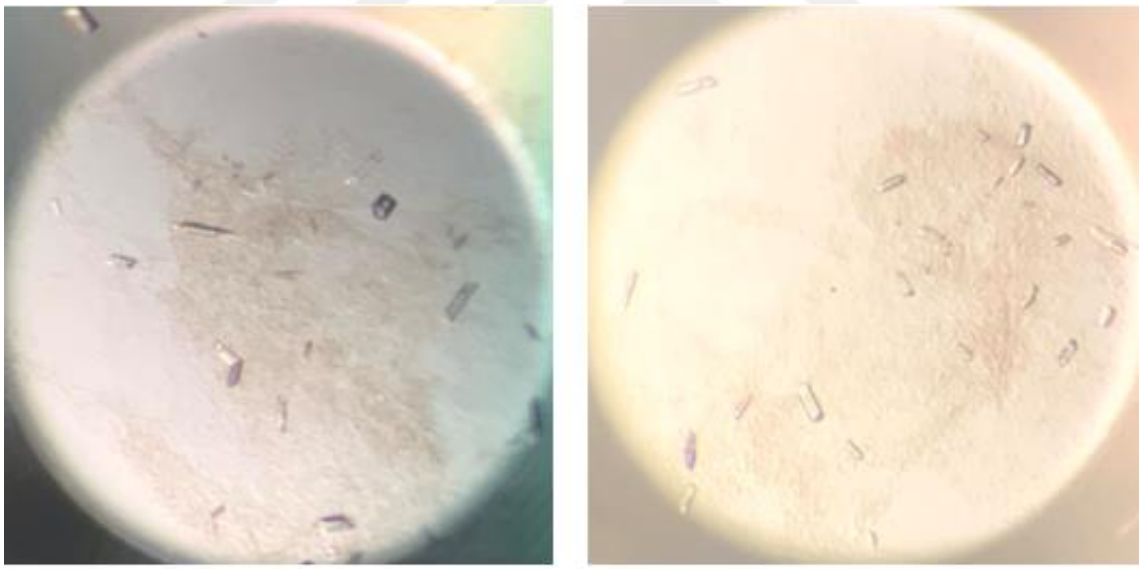

Figure 3.17: Crystals of CLIC4 WT obtained at the 12th Condition of Crystal Cryo II

3.4 Mini Expression Test for Ezrin WT and Ezrin T567D

The mini expression test was also conducted for both ezrin WT and its mutant form, ezrin T567D (Figure 3.18 and 3.19, respectively). The molecular weight of these two proteins is approximately 70 kDa whose expected locations are framed by the red rectangle. To differentiate their SDS-PAGE results, the marker was placed at the fourth lane in the ezrin T567D gel, and at the first lane in the wild type gel. For their expression tests, the whole cell lysate (WCL), pellet and supernatant samples were respectively loaded on the gel, as well as pulldown samples. Additionally, to determine the best induction temperature, the samples were induced at $18^{O}C$ and $37^{O}C$, separately.

Both ezrin WT and ezrin T567D proteins show the same expression pattern which can be proposed by comparing their SDS-PAGE results. Their before induction samples have almost no expression band, while there is a very thin and light band in the pulldown samples. When these proteins are induced by IPTG, the band density of the WCL samples does not change regardless of their induction temperature. However, ezrin has different band densities at the pellet and supernatant samples due to different induction temperatures. When it is induced at $37^{O}C$, the band density becomes higher than the samples induced at $18^{O}C$. Since supernatant and pellet samples have very light and thin bands at $18^{O}C$, it can be concluded that at $18^{O}C$ this protein is not expressed very well. Moreover, at this induction temperature, ezrin T567D slightly passes to the pellet increasing the thickness of the band. Thus, the band density of its supernatant is lighter than the pellet. When ezrin T567D is induced at $37^{O}C$, its supernatant density becomes thicker and darker than the pellet density.

Since the pulldown experiment directly shows the expression level of the target proteins by specifically capturing their hexa-histidine tag, the best induction temperature can be estimated based on these results. Both ezrin WT and ezrin T567D have the highest expression level at $37^{O}C$ since they have the thickest band at this temperature. The band density of the target proteins is lower at $18^{O}C$ while there is a very thin and light band at the before induction lane. Therefore, the expression level of the target proteins can be sorted in descending order as samples induced at $37^{O}C > 18^{O}C >$ before induction. As a result, the best induction temperature is $37^{O}C$ for both ezrin WT and ezrin T567D proteins.

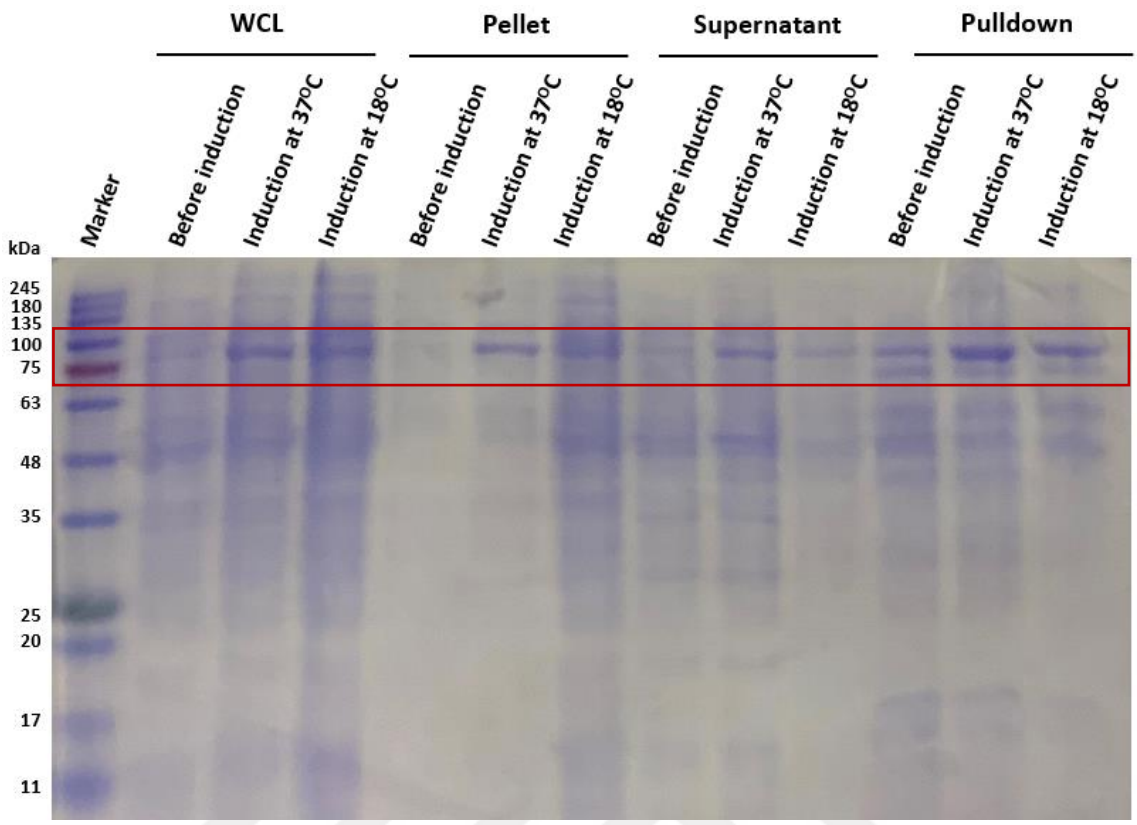

Figure 3.18: Mini Expression Test for Ezrin WT

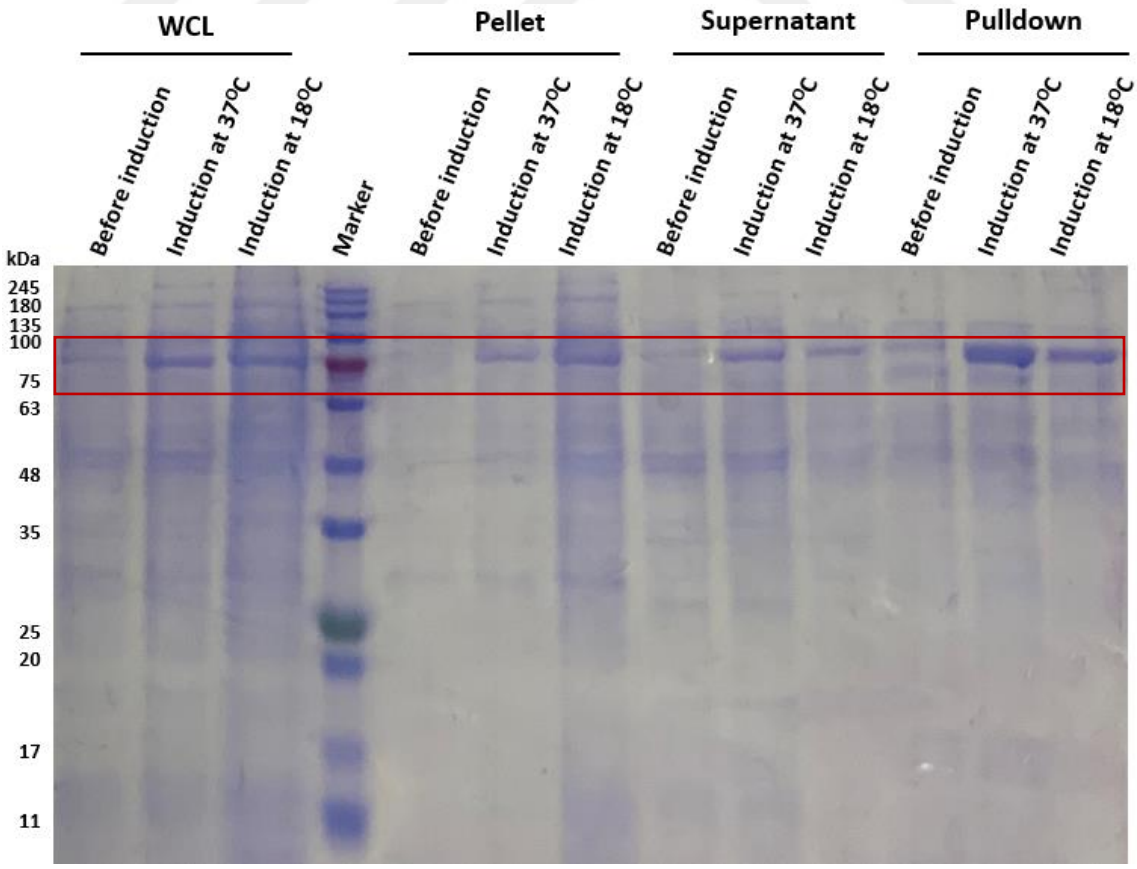

Figure 3.19: Mini Expression Test for Ezrin T567D

3.5 Overexpression, Purification and Crystallization of Ezrin

Hexa-histidine tagged ezrin WT proteins were produced and overexpressed in the 12 liters culture. A small amount of pellet was taken to check the protein solubility after the ultracentrifugation. The purified protein samples were collected in the different falcon tubes with respect to Imidazole concentration. Also, during purification flow-through was collected to check whether the target protein is lost or not. Then, protein expression and purification were confirmed with SDS-PAGE. The samples were loaded on the gel in the following order: marker, pellet, flow-through, 12.5 mM Imidazole I and II, 250 mM Imidazole I, II and III (Figure 3.20). The expected location of the ezrin WT is around 70 kDa framed with the red rectangle in figure 3.20. The nickel affinity chromatography graph was utilized to determine the exact time to add the buffers. In the graph in figure 3.21, the blue line shows the UV, and the red line stands for the conductance.

As seen in figure 3.20, the flow-through sample enlarged the SDS-PAGE. Based on this enlargement and high band density it can be concluded that flow-through has the highest protein concentration among all other samples. Thus, most of the ezrin WT proteins did not bind to the column, so that a high amount of the target protein was lost during the sample loading step. Also, there is a small amount of ezrin WT remained in the pellet while most of the proteins are soluble and purified with Imidazole. Besides the flow-through and the target protein band in the pellet samples, most of the proteins were purified. Firstly, proteins were purified with 12.5 mM Imidazole. In the first elution labelled as 12.5 mM Imidazole I, a higher amount of proteins are obtained compared with the second tube. Then, 250 mM Imidazole was loaded to the column following the stabilization of the first elution peak. Among all elution bands, the 250 mM Imidazole I elution sample has the thickest band with the highest amount of the ezrin WT which enlarged the gel as similar to flow-through. In comparison to 12.5 mM and 250 mM Imidazole sample lanes, the descending order of the protein concentration is 250 mM Imidazole sample I > II > 250 mM Imidazole I > II > 250 mM Imidazole III.

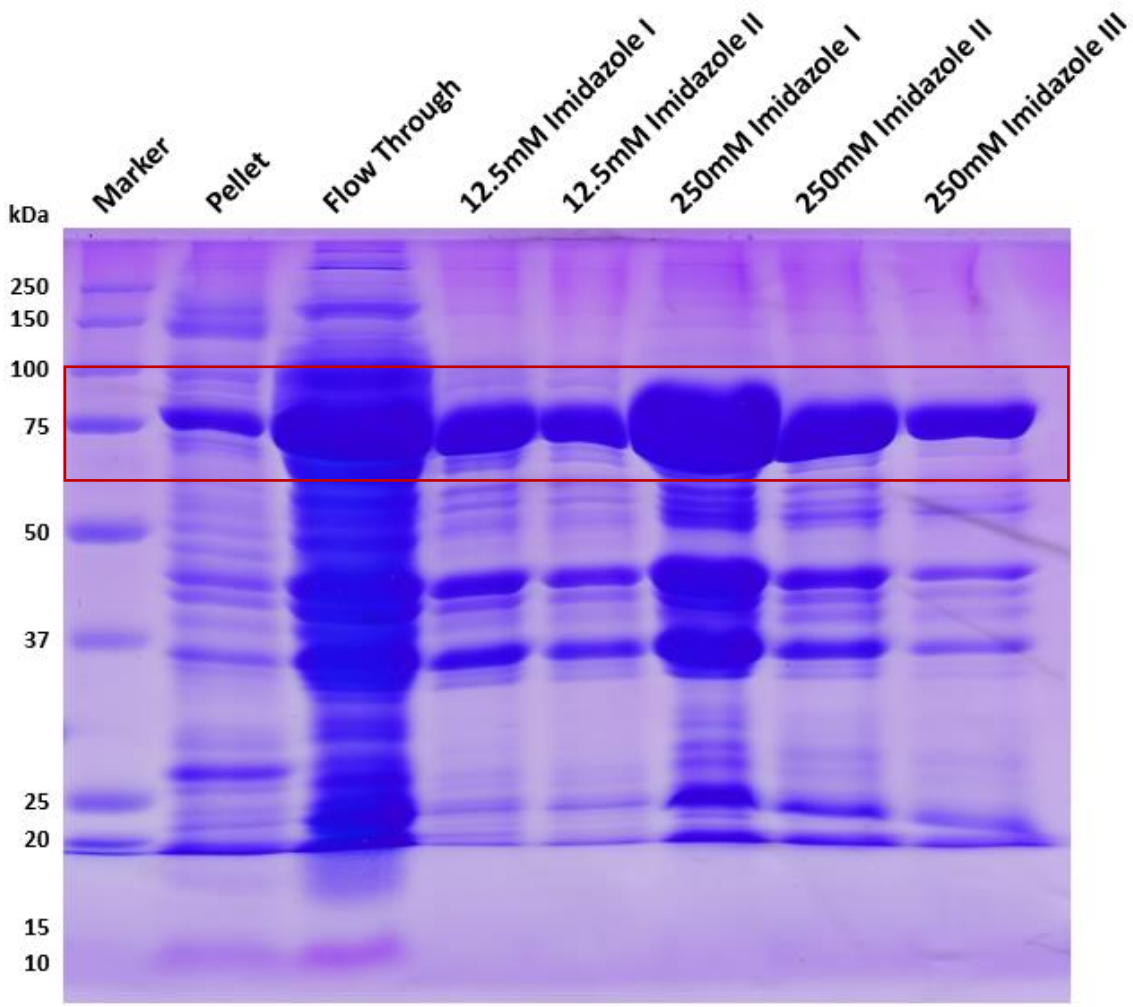

Figure 3.20: Ezrin WT Elution

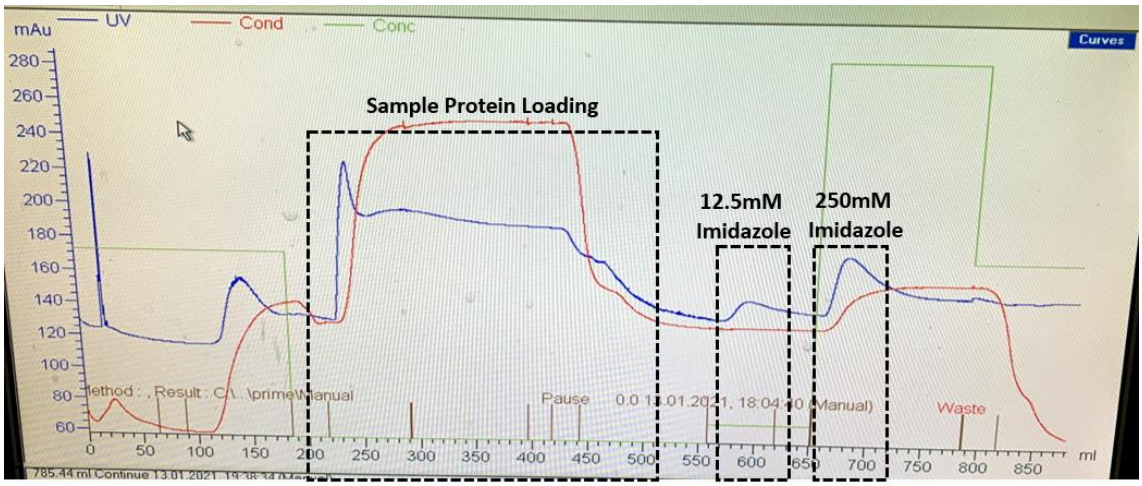

Figure 3.21: Nickel Affinity Chromatography Graph for Ezrin WT

After successful purification of ezrin WT proteins, all five elution samples were pooled and concentrated. The concentration of the crystallized protein samples was 1.1 mg/ml. Then, the crystallization trials were conducted with the ~3500 crystallization conditions. Crystals formed at the 8th condition of Midas II. Then, the protein crystallization was repeated with the same condition for 72 wells, and crystals were observed under a stereo-microscope (Figure 3.22). However, the obtained crystals were very solid.

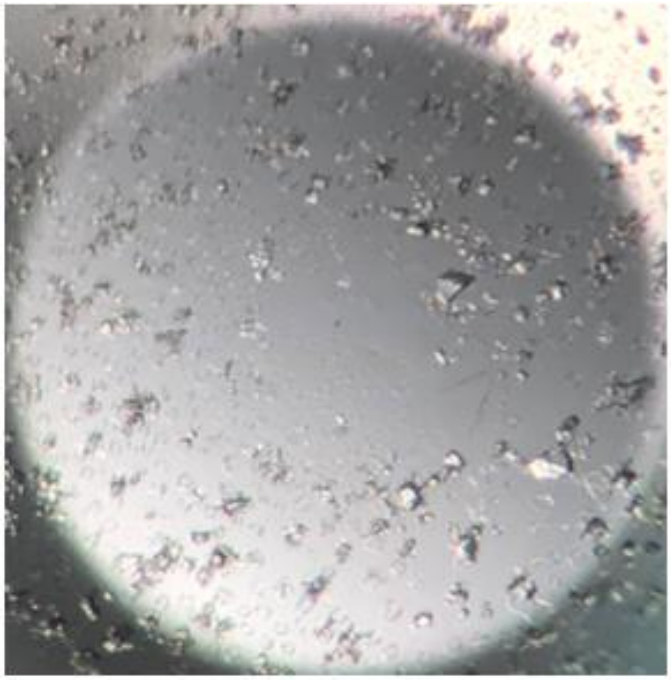

Figure 3.22: Crystals of Ezrin WT obtained at the 8th Condition of Midas II

The hexa-histidine tags of the concentrated ezrin WT proteins were cleaved by thrombin and removed from the solution with reverse nickel-NTA chromatography (Figure 3.23, 3.24). Then, the untagged proteins were collected throughout the sample loading. Before the addition of thrombin, the sample solution was centrifuged, and some part of the solution precipitated. To determine whether all target protein or how much of it precipitated the two phases of the sample were taken and labelled as uncut precipitate and supernatant. As seen in figure 3.23, the uncut precipitate has the thickest target protein band around 70 kDa framed with the red rectangle indicating the precipitation of ezrin WT in high amounts. Since there is still an adequate amount of the target protein remaining in the uncut supernatant, it was utilized for the cleavage of the hexa-histidine tags. After the addition of thrombin, the color of the solution became blurry. To specify the constituent part of the turbidity, the sample was loaded on the 6^{th} lane on the gel as the cut mixture. Then, the sample solution was centrifuged, and two phases formed as supernatant and precipitate. These phases were named as cut supernatant and precipitate, respectively. They were loaded on the gel to check the remaining protein concentration as well as the lost amount. Also, since the cut mixture consisted of these two phases, it was named as the cut mixture: supernatant and precipitate. Then, the supernatant part with a sufficient amount of the ezrin WT was utilized to be loaded on the column, although the cut precipitate has a very dense target protein band. Because of the thick bands in the uncut and cut samples, the band shift resulting from the cleavage of hexa-histidine tags cannot be differentiated.

During reverse nickel-NTA chromatography, if the hexa-histidine tags were successfully removed from the protein, they will remain in the column whereas untagged target protein was directly eluted from the column. The untagged proteins were collected in five falcon tubes labelled as Rev-NTA ezrin WT I, II, III, IV, V, and loaded on the gel in the same order. It can be inferred from their bands around 70 kDa that hexa-histidine tags were cleaved and the untagged ezrin WT proteins were successfully collected. Among all Rev-NTA samples, Rev-NTA ezrin WT I has the lowest protein concentration with the thinnest band, while the other four samples have adequate and almost the same protein amount. After all samples were loaded to the column, the tagged target protein was eluted with 250 mM Imidazole. As seen from the last three lanes on the gel, many ezrin WT proteins with tags remained in the column whereas no peak formation occurred in figure 3.24 with the addition of the 250 mM Imidazole.

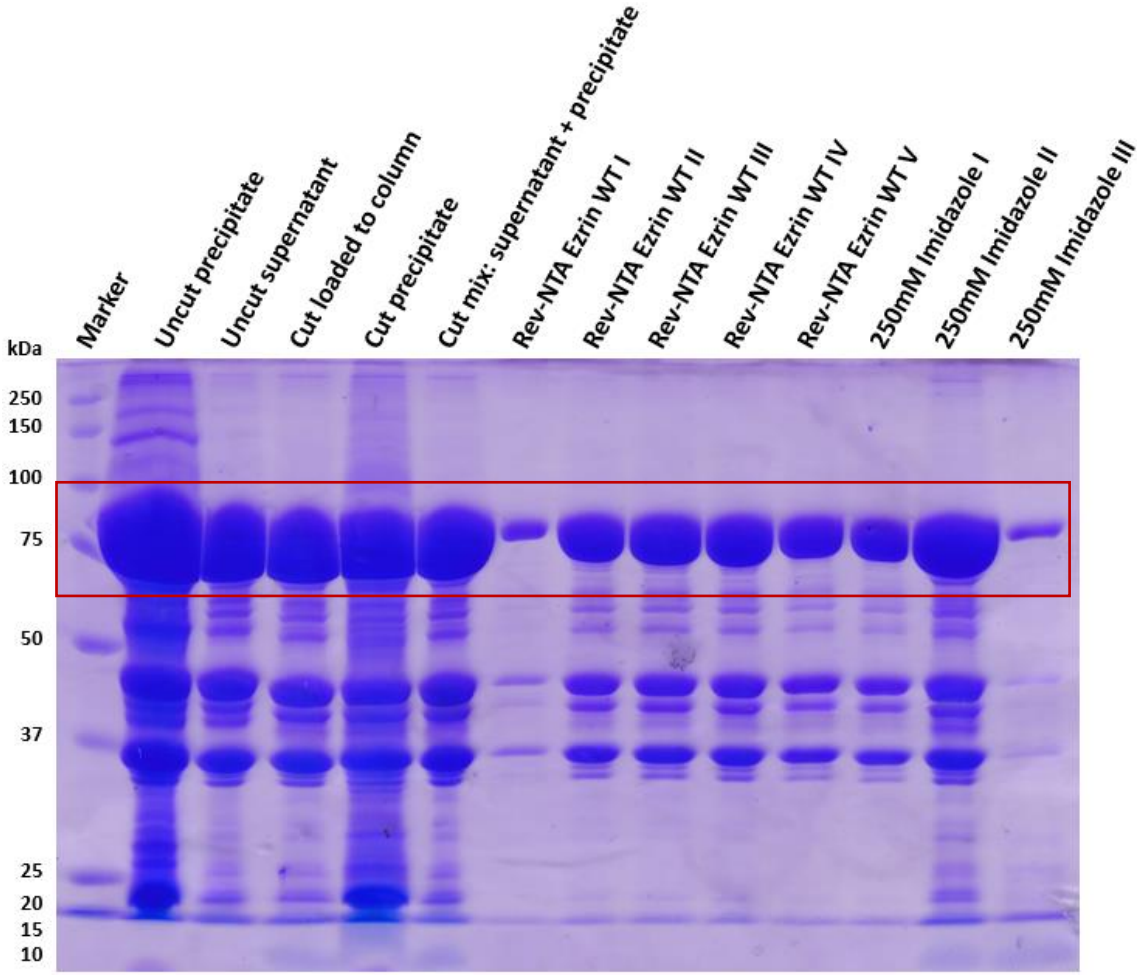

Figure 3.23: Reverse Chromatography for Ezrin WT

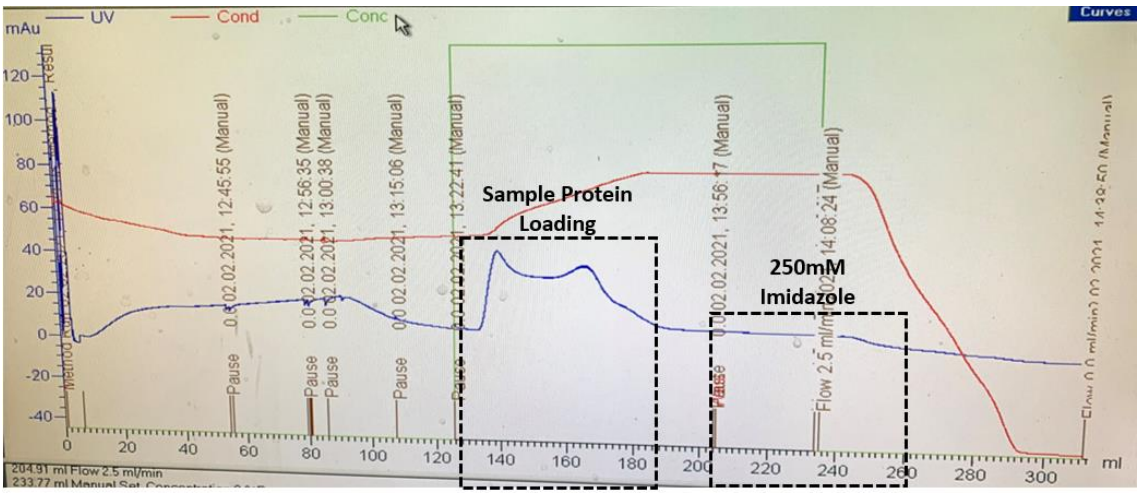

Figure 3.24: Reverse Chromatography Graph for Ezrin WT

Since the band density was very high in uncut and cut samples, the band shift could not be differentiated in figure 3.23. For this reason, uncut and cut ezrin WT samples were loaded on the new gel in a low amount (Figure 3.25). The expected size of the target protein is framed with the red rectangle. There is a minor band shift between uncut and cut samples regardless of the thick bands which implies that hexa-histidine tags were cleaved from the ezrin WT sample.

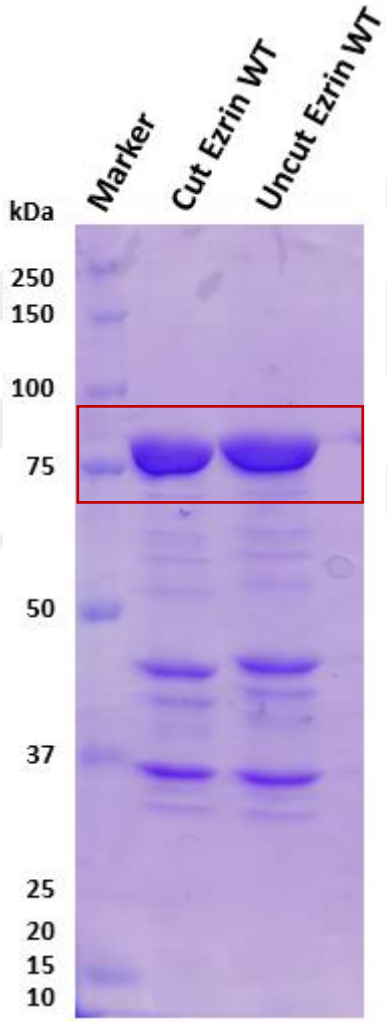

Figure 3.25: Thrombin Cut Check for Ezrin WT

After the removal of hexa-histidine tags from the solution with reverse chromatography, since Rev-NTA ezrin WT I sample has the lowest protein concentration among the other Rev-NTA samples, the other four elution samples were pooled and concentrated. The concentrated untagged ezrin WT samples were run on the gel (Figure 3.26). According to the density and the thickness of the band which is indicated with the red rectangle, the concentration of ezrin WT protein is very high.

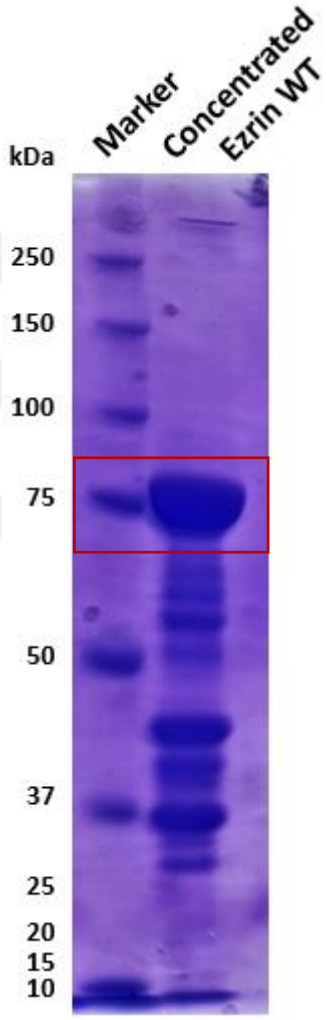

Figure 3.26: Concentrated Ezrin WT

3.6 Overexpression, Purification and Crystallization of Ezrin T567D

Hexa-histidine tagged ezrin T567D proteins were produced and overexpressed in the 12 liters culture. After the ultracentrifugation, the samples were taken from supernatant and pellet to check the protein solubility. Then, the nickel-NTA chromatography was applied to purify the target protein from the supernatant. During the sample loading, flow-through was stored to determine whether ezrin T567D proteins are lost or not. Then, elution samples were collected in different falcon tubes with respect to Imidazole concentration. Finally, SDS-PAGE was performed to confirm protein expression and purification. The samples were loaded on the gel in the following order: marker, supernatant, pellet, flow-through, 25 mM Imidazole I, II, III, 250 mM Imidazole I, II, III, and IV (Figure 3.27). The expected location of the ezrin T567D is around 70 kDa shown with the red rectangle in figure 3.27. The nickel affinity chromatography graph was utilized to determine the exact time to add the buffers. In this graph in figure 3.28, the blue line shows the UV, and the red line stands for the conductance.

As seen in figure 3.27, the ezrin T567D band in the supernatant sample enlarged its lane due to its high concentration while a small amount of it remained in the pellet resulting in a very thin band. Also, the difference in band thickness in supernatant and pellet implies the high solubility of ezrin T567D protein. The target protein was eluted with 25 mM and 250 mM Imidazole. Firstly, the 25 mM Imidazole was loaded on the column. This elution provides the elimination of non-target proteins with a low affinity towards the column. There are some proteins eluted with 25 mM Imidazole, whereas the target protein mostly remained in the column compared with the 250 mM Imidazole II sample lane. Also, the elution peak at 25 mM Imidazole is not as high as the 250 mM Imidazole peak shown in figure 3.28 with the black frame. The 250 mM Imidazole was loaded to the column when the first elution peak started to decrease and stabilized. Ezrin T567D protein has the highest concentration at the 250 mM Imidazole II elution lane with the thickest band around 70 kDa. In comparison to 25 mM and 250 mM Imidazole sample lanes, the descending order of the protein concentration is 250 mM Imidazole sample II > III > I > IV > 25 mM Imidazole III > II > I. Since the highest amount of ezrin T567D protein was purified at 250 mM Imidazole II sample, this sample was utilized for further experiments.

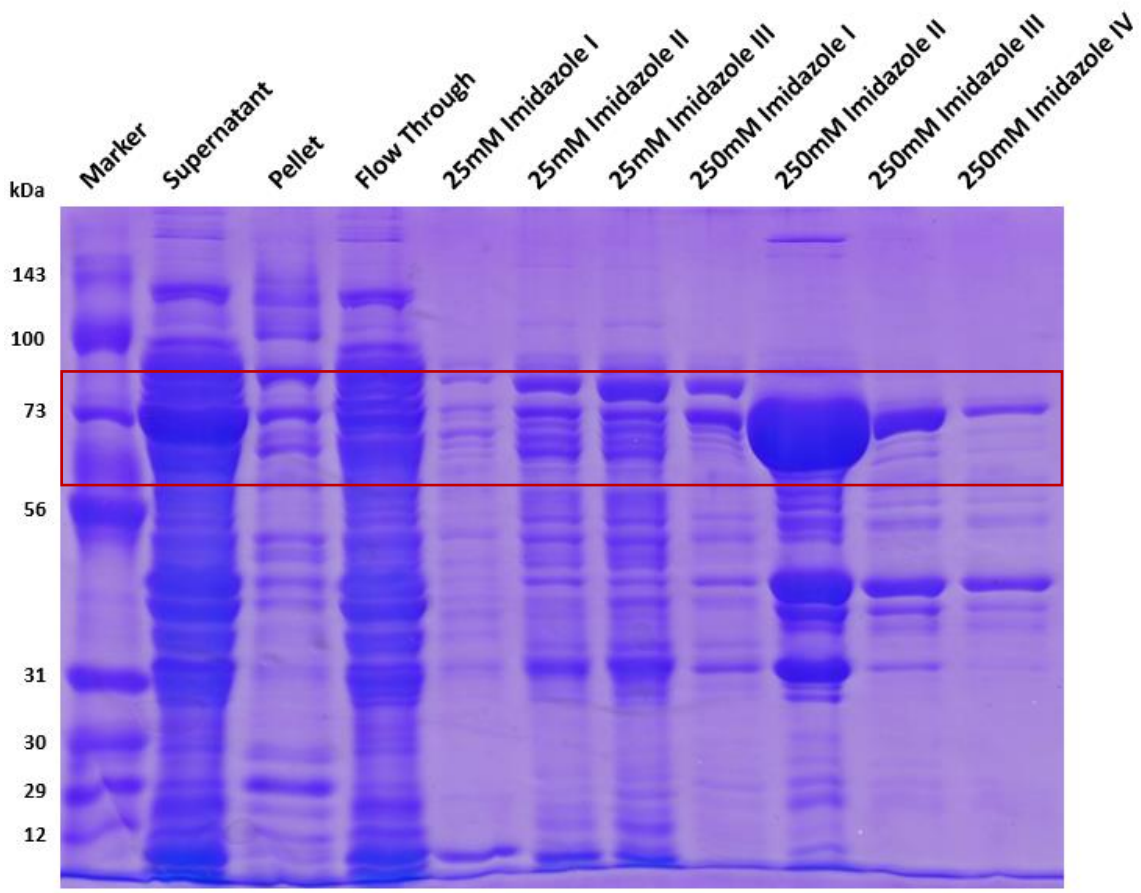

Figure 3.27: Ezrin T567D Elution

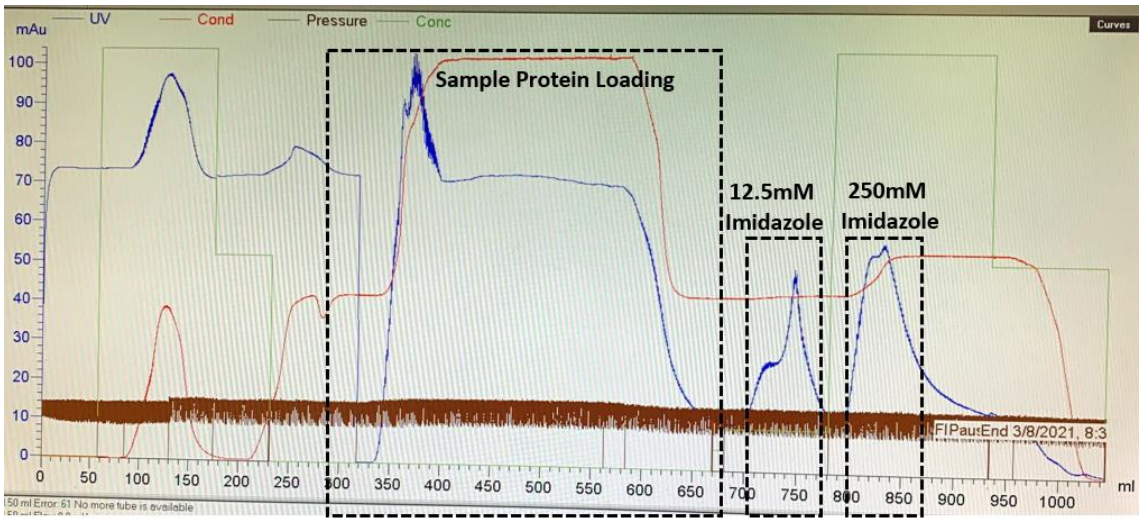

Figure 3.28: Nickel Affinity Chromatography Graph of Ezrin T567D

3.7 Native Gel for CLIC and Ezrin Proteins

After all pure proteins were successfully obtained, a native gel was conducted to determine any possible interactions between these purified proteins. If there is an interaction, the extra band should be seen above the ezrin proteins' bands since ezrin has the highest molecular weight. The proteins were loaded on the gel in the following order: Ezrin, Ezrin T567D, CLIC4 WT, CLIC4 WT/Ezrin WT, CLIC4 WT/Ezrin T567D, CLIC1 WT, CLIC1 WT/Ezrin WT, CLIC1 WT/Ezrin T567D, CLIC4 C35A, CLIC4 C35A/Ezrin WT, CLIC4 C35A/Ezrin T567D, CLIC4 WT/CLIC1 WT/Ezrin T567D, CLIC4 WT/CLIC1 WT/Ezrin WT, CLIC4 C35A/CLIC1 WT/Ezrin T567D (Figure 3.29). The samples with only one protein were loaded on the gel as the control, whereas two or three protein mixtures were utilized for any possible interactions between them. All samples have the clear band, unfortunately, there is no extra band above ezrin bands. Therefore, it can be suggested that there is no interaction between any of these proteins.

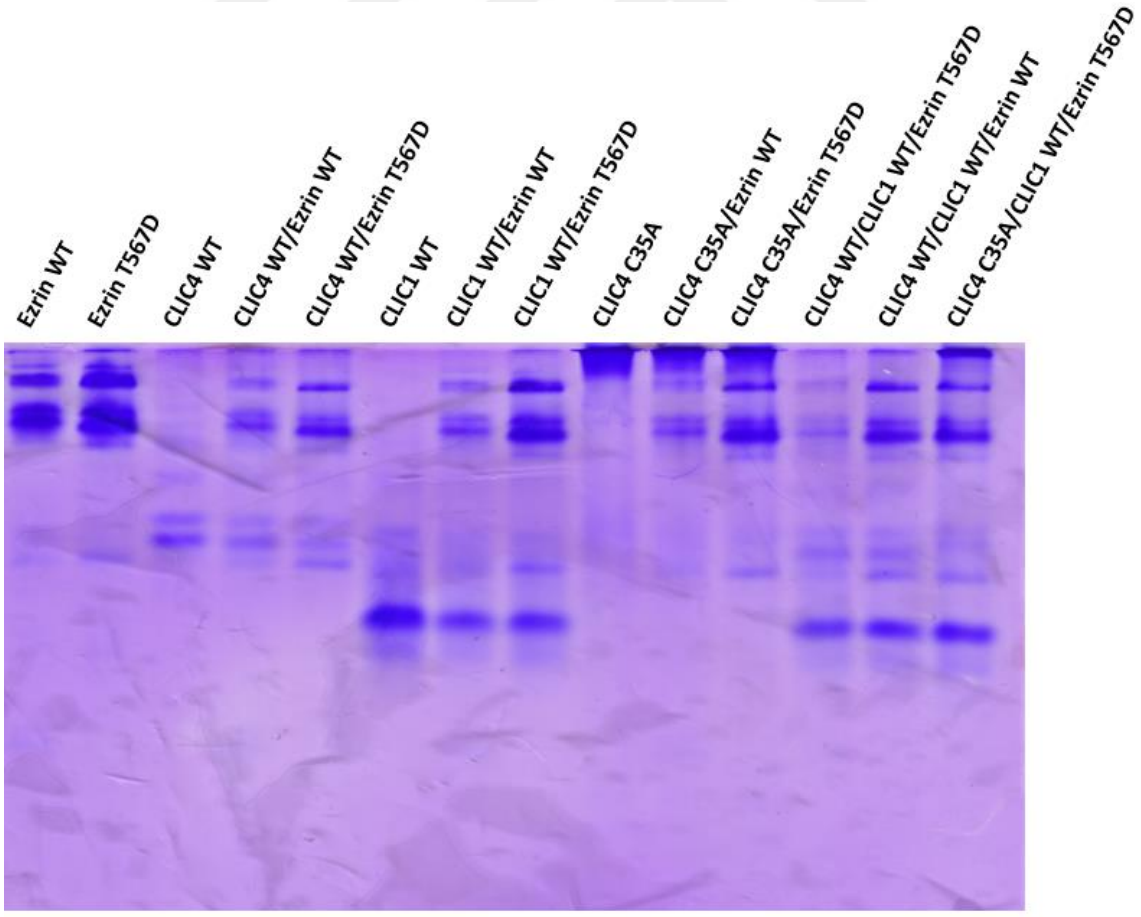

Figure 3.29: Native Gel Result for CLIC and Ezrin Proteins

3.8 Co-Crystallization of CLIC4 WT and Ezrin T567D

An equal amount of pure CLIC4 WT and pure ezrin T567D protein mixture was experimented to obtain co-crystals of these two proteins. The total concentration of the co-crystallized protein samples was 3.3 mg/ml. Among the ~3500 crystallization conditions, crystals formed at two conditions, the 38th condition of Wizard I and the 24th condition of Helix II. Then, the protein crystallization was repeated with the same conditions for 72 wells, and crystals were observed under a stereo-microscope (Figure 3.30, and 31). The obtained crystals were very soft and brittle at both conditions.

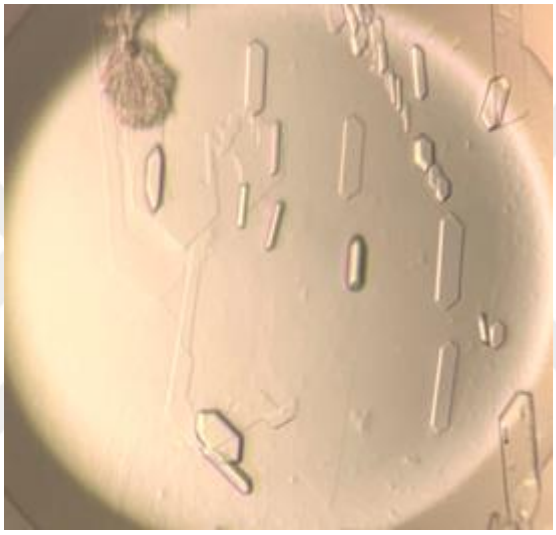

Figure 3.30: Co-crystals of CLIC4 WT and Ezrin T567D obtained at the 38th Condition of Wizard I

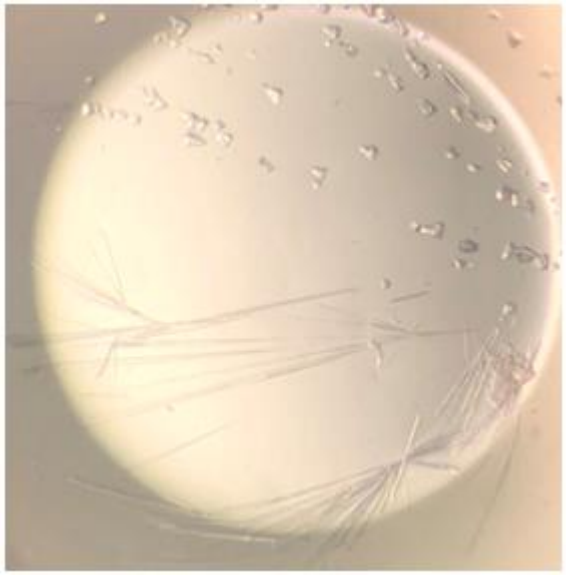

Figure 3.31: Co-crystals of CLIC4 WT and Ezrin T567D obtained at the 24th Condition of Helix II

3.9 CLIC4 and Ezrin Docking Study

In order to provide information about how CLIC4 and ezrin interact with each other, the docking study was conducted by using Haddock web server based on the active sites (Van Zundert et al., 2016). For the docking study, the known information was very limited. While these two proteins co-localize at the plasma membrane, their interaction sites are not known in contrast to the PIP2 binding sites of ezrin. Thus, based on the PIP2 binding determinants on ezrin, 12-115 and 233-310 amino acid residues, two PIP2 molecules were used to dock CLIC4 and ezrin. Since the maximum number of active sites should be 200 residues, the input parameters for ezrin were chosen as 63-115, and 233-298. For the input parameters of CLIC4 its active sites Cys35, Phe37, Pro76, Asp87, Phe122 and Tyr244 were utilized. Additionally, CLIC4 and ezrin interact with each other when ezrin is in the active state. Therefore, the active structure of ezrin (PDB ID: 4RMA) belonging to its FERM domain was docked with CLIC4 (PDB ID: 2AHE) and two PIP2 molecules (Figure 3.32). The root mean square deviation (RMSD) of the docked structure from the overall lowest energy structure is 1.8 with a z-score of -2.0. The structure of CLIC4 and PIP2 are represented in pink and slate, respectively. The FERM domain of ezrin with F1, F2 and F3 is colored as smudge, pale green, pale cyan, respectively. In figure 3.33, the putative interaction sites, determined by the docking study between ezrin-PIP2 and ezrin-CLIC4 is demonstrated.

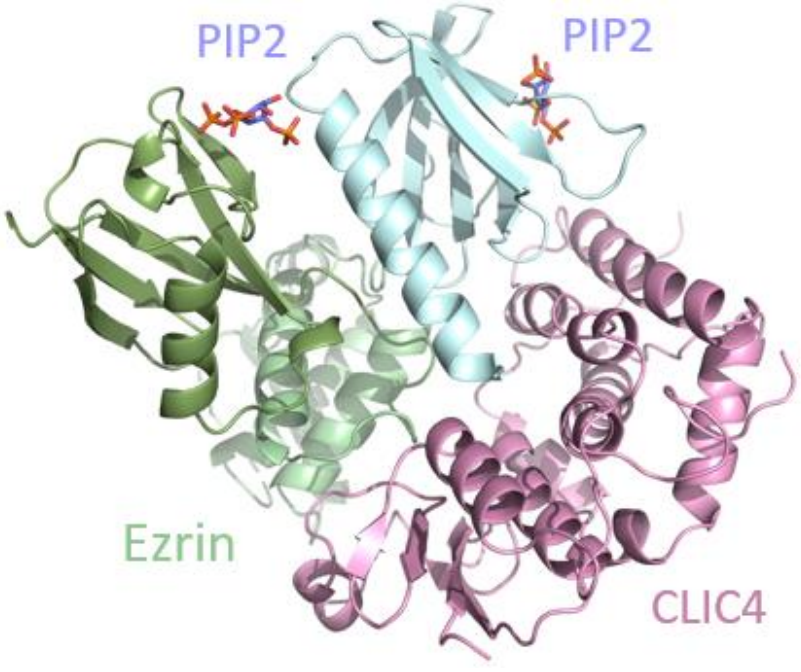

Figure 3.32: Docked Structure of CLIC4 and Ezrin

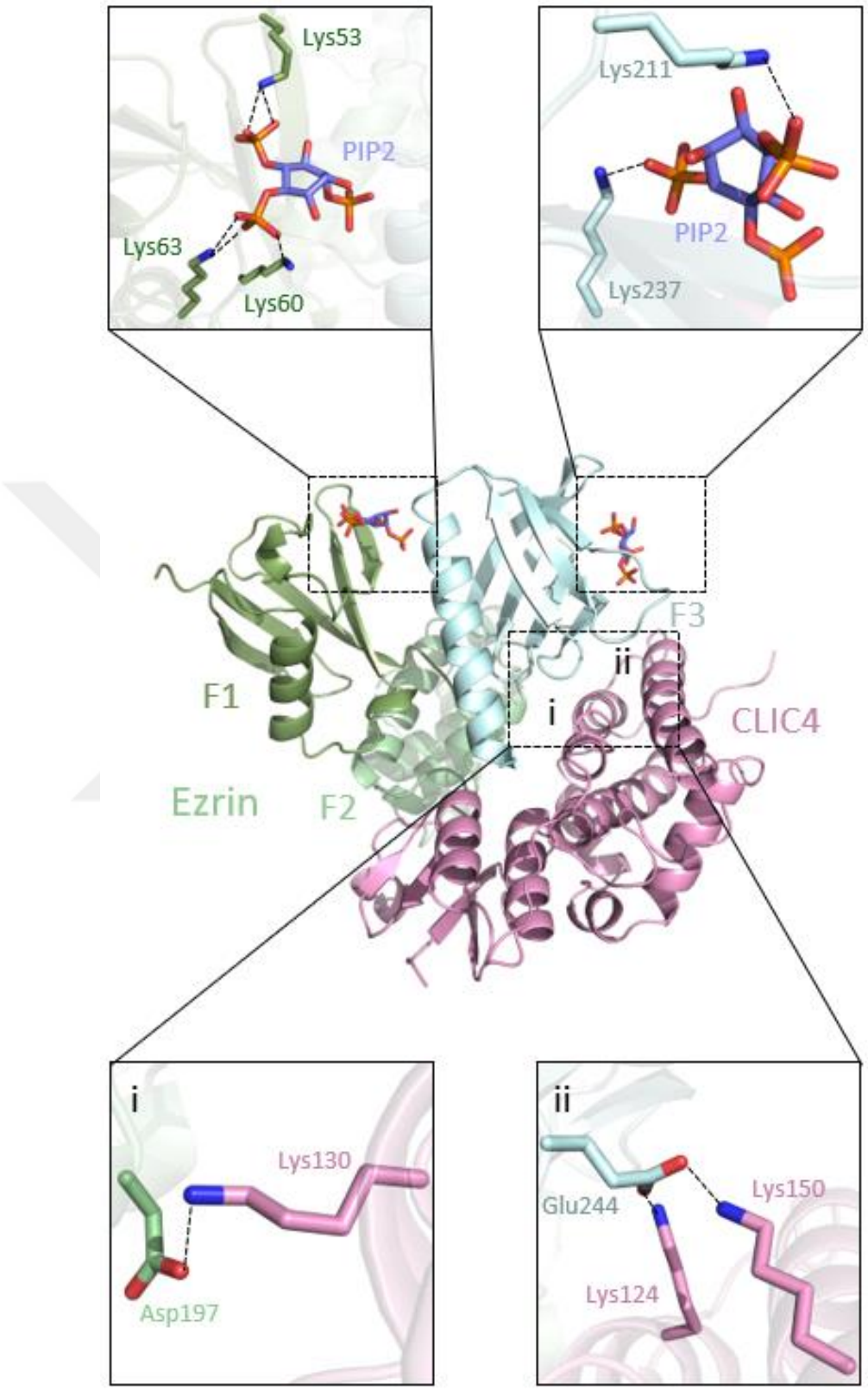

Figure 3.33: Representation of Interaction between Ezrin-PIP2 and Ezrin-CLIC4

Chapter 4:
CONCLUSION/DISCUSSIONS

The Chloride Intracellular Channel Protein 4 (CLIC4) and ezrin proteins are very important for successful cell division. The interaction between these two proteins at the cleavage furrow and midbody provides a bridge between the cortical actomyosin network and the plasma membrane. Additionally, they enable the cortical stability between the plasma membrane and actin cytoskeleton. While the CLIC4 and ezrin have X-ray crystal structures (PDB ID: 2AHE and 4RM9, respectively), the structures of their mutant forms, CLIC4 C35A and ezrin T567D, are not available. The structure of CLIC4 is represented in pink color in figure 4.1.

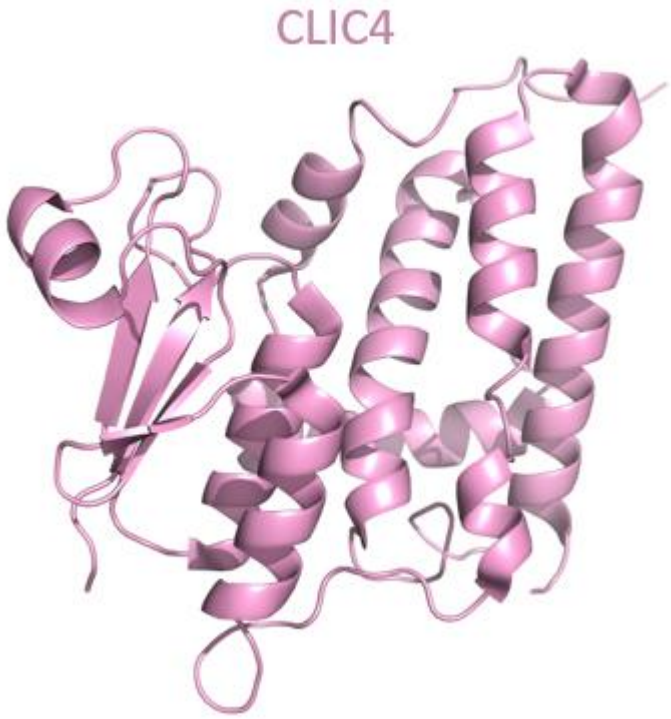

Figure 4.1: Cartoon Representation of CLIC4
PDB ID: 2AHE

CLIC4 has a reactive cysteine at the 35th amino acid residue. The Cys35 serves as a putative enzymatic site for CLIC4 promoting its translocation and interaction with other proteins. In the recent study, it was demonstrated that CLIC4 WT and CLIC4 C35A have different interactomes. When Cys35 is mutated to C35A, due to abolished plasma

membrane and cleavage furrow translocation, the mutant CLIC4 is less likely to interact with plasma membrane proteins with respect to CLIC4 WT. Importantly, ezrin was one of those proteins that interact with only CLIC4 WT at the plasma membrane (Kagiali et al., 2020). However, as seen in figure 4.3, the only difference between the wild type and the mutant version is the sulfur in the side chain of the wild type. The conversion of the 35th amino acid from cysteine to alanine eliminates the side chain effect which concludes that this reactive cysteine residue provides the potential-substrate binding site as well as its function.

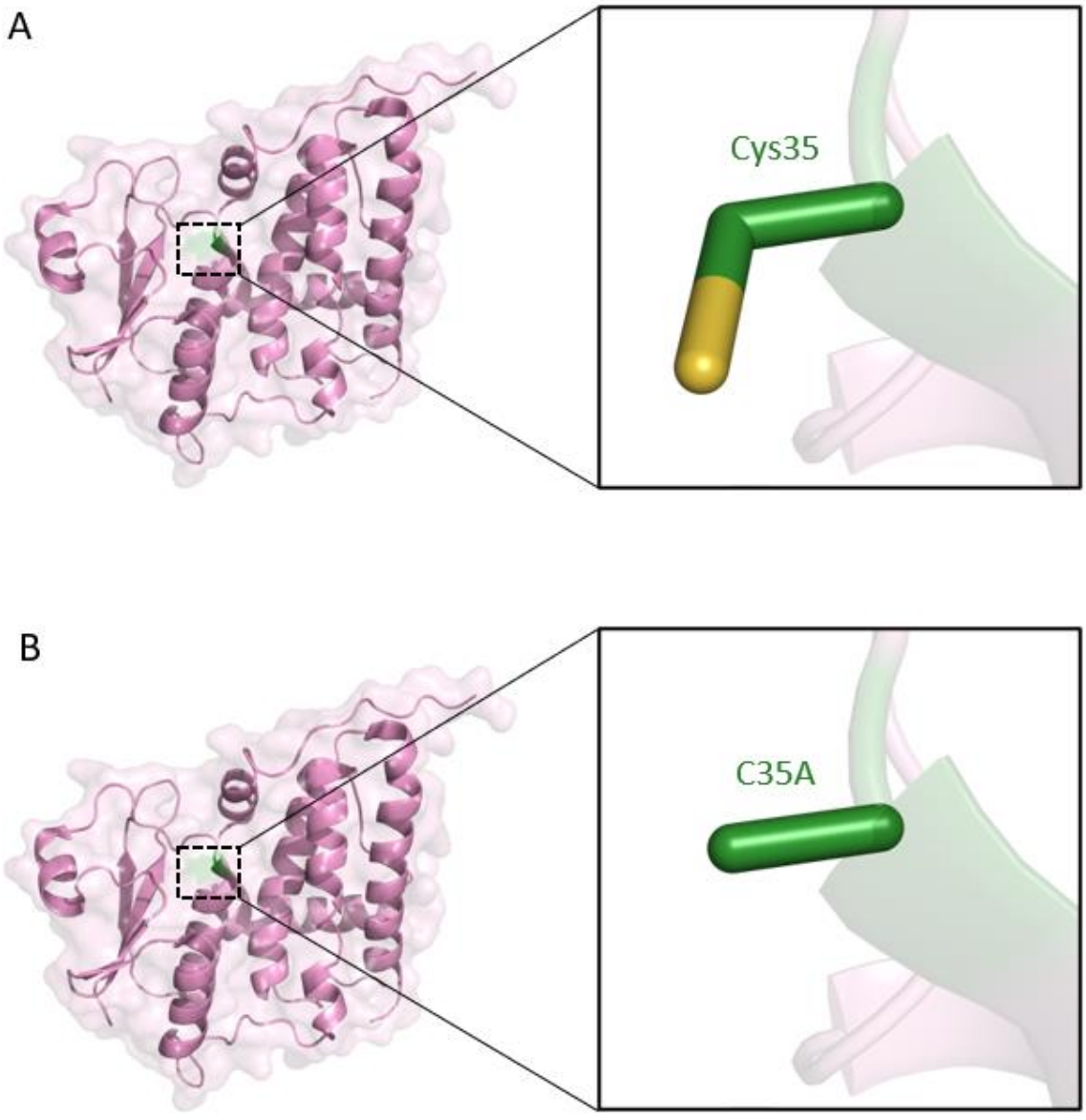

Figure 4.2: Representation of Side Chain of Cys35 in CLIC4 WT and CLIC4 C35A

The structure of the ezrin FERM:C-terminal domain complex was represented in figure 4.2. The FERM domain with F1, F2 and F3 is colored as smudge, pale green, pale cyan, respectively, and the C-terminal is colored in light orange.

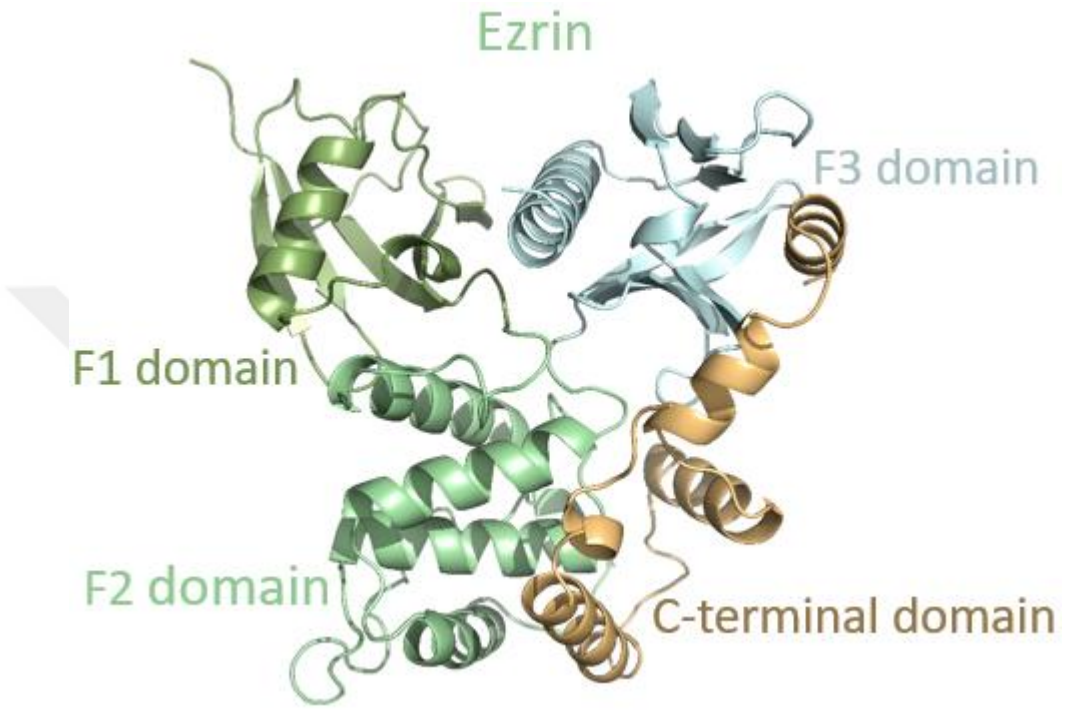

Figure 4.3: Cartoon Representation of Ezrin FERM:C-terminal Domain Complex PDB ID: 4RM9

In order to interact with its interaction partners in the active state, ezrin needs to be converted from a dormant state to an active state. To undergo a conformational switch, it should first bind to PIP2 through the F1 and F3 lobes in the FERM domain shown in the smudge and the pale cyan in figure 4.2. Then, it is phosphorylated at its threonine (Thr567) residue in the carboxyl terminus. Once ezrin is activated, its self-associated structure opens and facilitates the C-ERMAD interaction with its binding partners (Barret et al., 2000; Hamada et al., 2000; Simons et al., 1998). The side chain difference of Thr567 in wild type and phosphomimetic mutant of ezrin, ezrin T567D is shown in figure 4.4.

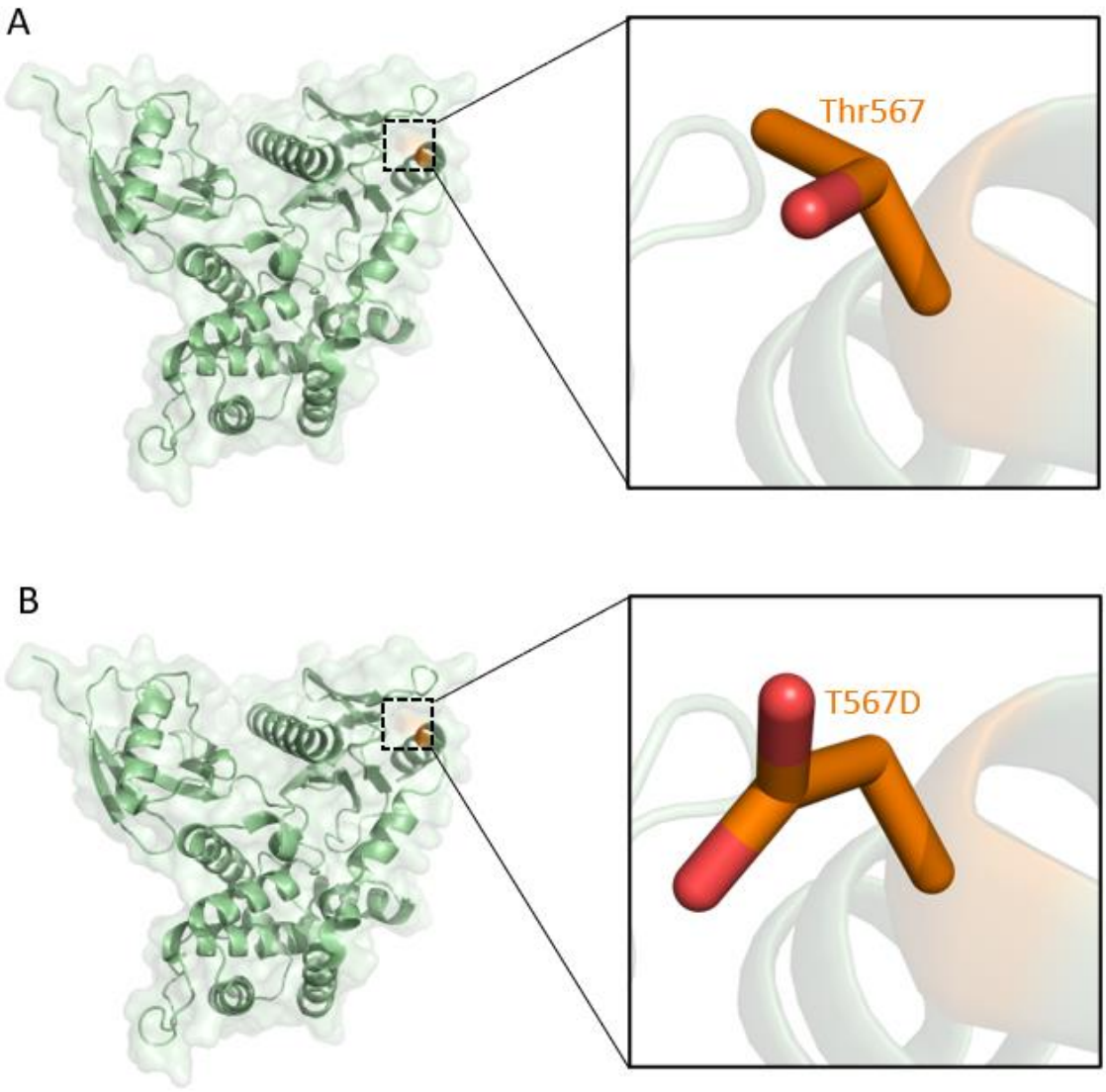

Figure 4.4: Representation of Side Chain of Thr567 in Ezrin WT and Ezrin T567D

In order to obtain crystals of the target proteins, they should be overexpressed and produced at a larger scale for higher amounts of proteins. The solubility of the protein is very important for the experiment design. The insoluble proteins remain in the pellet as well as aggregated proteins which form the inclusion body in the pellet. They should be solubilized with refolding experiments. Despite insoluble proteins, soluble proteins stay in the supernatant part of the solution. Since all target proteins are obtained in the supernatant, they all are soluble.

All protein production was induced by IPTG. After IPTG induction, the bacterial cell cultures grow, producing more target proteins with the expanding cell numbers. For instance, there is almost no protein expression for before induction samples of ezrin WT and ezrin T567D proteins except at pulldown ones. This implies that recombinant protein production requires the IPTG induction to express the target proteins in excess amounts. The mini expression check cultures of CLIC proteins grew for three days which was expected to increase expressed protein amounts. However, in figure 3.1, protein bands in the 72-hours induction have the lowest expression level, while there is no difference between the 24- and 48-hours induction samples. This is due to the fact that the 72-hours samples were obtained from 23 ml cell cultures, and 24- and 48-hours samples were taken from 1 ml cultures, the protein samples were diluted as 23-fold at 72-hours induction samples with the increasing supernatant volume.

In addition to the induction time, the induction temperature is also important to adjust a suitable environment for target protein expression. While all CLIC proteins were induced at $18^{O}C$, both ezrin and its mutant showed the highest expression level at $37^{O}C$. Moreover, at $37^{O}C$ a small amount of ezrin T567D passes to the pellet increasing the thickness of the band. Thus, it may imply that ezrin T567D becomes slightly insoluble at this induction temperature.

The pulldown of CLIC1 has a slight band shift which is not seen at supernatant samples. This may be resulted from taken some resin beads. Moreover, if the expression level of the CLIC proteins is compared between each other, the CLIC4 C35A is highly expressed while the CLIC1 has the lowest expression level. Also, the CLIC4 C35A and the CLIC4 F37D have higher expression levels than the CLIC4 WT. In addition, the pulldown results of the mini expression test of ezrin and ezrin T567D show that ezrin T567D is expressed more than the wild type. The higher expression level of the mutant version of these proteins compared to the wild type implies that mutant versions of these proteins may benefit bacterial cell growth resulting in more mutant protein production.

During the 12 liters cell culture purification of the target proteins, the nickel-NTA column was used to purify hexa-histidine tagged proteins. The nickel-NTA resin column has a capacity based on the charged resin beads to bind the hexa-histidine tagged proteins. As seen on the supernatant samples obtained after the 12 liters cell culture purification, there are also other proteins loaded on the column. Since the target proteins have hexa-histidine tags, even if other proteins have histidine amino acids, the target protein will

have a higher affinity towards the resin beads. Therefore, they will remain in the column while other proteins are eluted. However, sometimes the hexa-histidine tagged proteins might be lost because of the decreased column capacity. For example, during ezrin WT purification, a very high amount of it was lost during the flow-through. Therefore, during purification, the flow-through was also collected to check whether the target protein is lost and/or how much is lost.

Furthermore, the principle of reverse nickel-NTA chromatography is to collect the untagged proteins. Since hexa-histidine tags have a higher affinity towards resin beads, while cleaved tags bind to the resin beads remaining at the column, untagged proteins should be directly eluted. Since the hexa-histidine tags of CLIC4 C35A and ezrin WT were successfully removed, they directly eluted during sample protein loading. Contrarily, as shown in figure 3.13, the CLIC4 WT has a band size difference between its uncut and cut samples. Based on this band shift, it can be suggested that the hexa-histidine tag was cut by thrombin from the target protein. However, during sample protein loading the untagged protein could not be collected. Then, the CLIC4 WT was purified by 250 mM Imidazole. This may be caused by an inefficient amount of thrombin. Since the CLIC4 WT proteins with hexa-histidine tags remained on the column and purified with 250 mM Imidazole, there is a possibility that thrombin could not cleave all hexa-histidine tags in CLIC4 WT samples. However, if a small amount of hexa-histidine tag of the protein would be cleaved, there should have been a protein band in the collected reverse chromatography samples. Additionally, the amino acid sequence of CLIC4 was checked and it does not have any thrombin cut site which eliminates the possibility of truncation of CLIC4 protein by thrombin. As a result, the untagged proteins could not be obtained, while tagged CLIC4 WT remained on the column. After this experiment, the eluted CLIC4 WT with 250 mM Imidazole was concentrated and run on the gel with the uncut sample. As seen in figure 3.15, the concentrated CLIC4 WT had an unexplainable band shift in comparison to the uncut sample.

In addition to that, native page gel has clear bands indicating the expected locations of the proteins in the complex. However, the CLIC4 C35A does not have a band at the expected location. The CLIC4 C35A protein sample was taken from the stock utilized for crystallization experiments which was stored in the fridge for four months, the protein may be aggregated.

Moreover, during crystallization trials, not only protein crystals but also salt crystals were obtained. Since most of the crystallization conditions are comprised of a high amount of salts, the salts can also be crystallized in a favorable environment. The salt and protein crystals can be differentiated from their softness. While protein crystals are more prone to be soft and brittle, the salts are very solid. For this reason, when the protein crystals are touched, they are easily shattered. Contrarily, the salt crystals are highly crispy and hard to break when pressure is applied. Based on this information, all obtained crystals were shattered, and the soft ones were replicated in 72 wells with the same condition. The crystals of CLIC4 C35A and CLIC4 WT obtained at the 12^{th} condition of Crystal Cryo II are very brittle and resemble protein crystals. Also, co-crystals are similar to protein crystals. Additionally, ezrin WT and CLIC4 WT crystallized at the same condition, which is the 8^{th} condition of Midas II. Since all proteins require different conditions to be chemically converted into a solid crystalline state from its liquid phase, the optimal environment depends on various factors such as pH and the type of the precipitant. There is a possibility to be crystallized at the same conditions for these two proteins, but it is extremely unlikely to have the same size and shape crystals. Since the formed crystals are solid and very similar to each other, they are salt crystals.

As mentioned before, CLIC4 and ezrin interaction was implied in the earlier studies. When the cysteine residue of CLIC4 is mutated to C35A, the interaction between ezrin and CLIC4 is abolished according to their interactome analysis. Thus, the wild type CLIC4 is required for the interaction with ezrin. Moreover, ezrin binds to the CLIC4 when it is at the active state which requires the PIP2 binding and phosphorylation at its conserved phosphorylation site Thr567. Therefore, the phosphomimetic mutant of ezrin was produced to determine its interaction with CLIC4 WT. In this study, since CLIC4 WT and ezrin T567D were expected to directly interact with each other, the native gel was conducted to demonstrate their interaction (Figure 3.29), but any interaction band could not be observed. However, co-crystals were obtained, which increases the likelihood of their interaction. The obtained co-crystals were collected as well as other protein crystals and will be shipped to the Linac Coherent Light Source at SLAC, Stanford University to take X-ray snapshots of the molecules. Then, their molecular refinements will be conducted to determine whether they are protein crystals or not and also to reveal the mystery behind their structural information. Moreover, the docking study was conducted to represent any possible interaction between CLIC4-ezrin-PIP2. To start the

modelling of the interaction, the cluster which has the lowest energy, RMSD value, and z-score was preferred. The lowest energy shows the stability of the cluster, whereas the low z-score indicates the standard deviation of the HADDOCK score of any given cluster. As seen in figure 3.33, ezrin binds to PIP2 via both Lys53, Lys60 and Lys63 at the F1 domain, and Lys211 and Lys237 at the F3 domain. Also, there are two putative interaction sites between ezrin and CLIC4. The Asp197 residue of ezrin at the F2 domain forms hydrogen bods with Lys130 residue at CLIC4, and Glu244 of ezrin at the F3 domain involves in interaction with two different amino acid residues, Lys124 and Lys150, at CLIC4. Since the exact mechanism of how CLIC4 and ezrin communicate with each other is still elusive, thanks to the docking study the possible interaction model can be represented in figure 4.5.

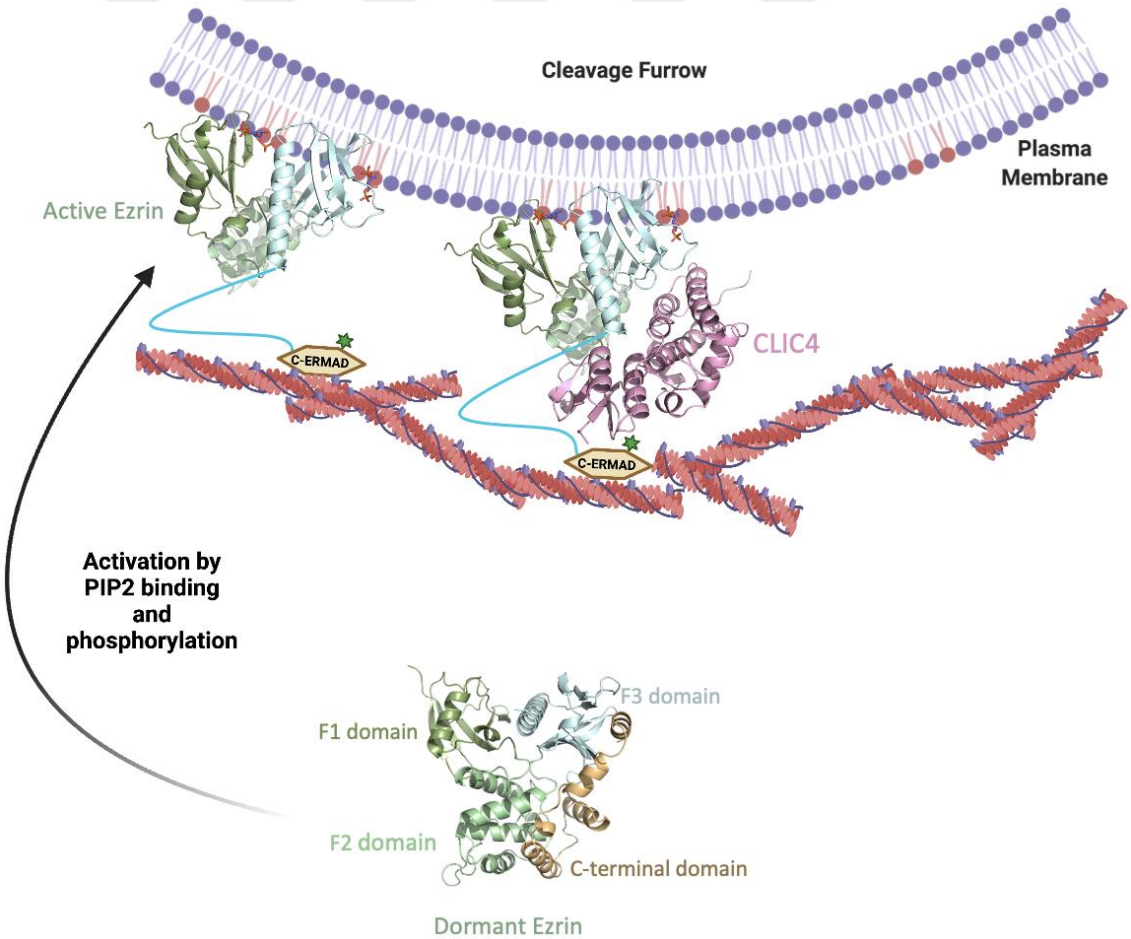

Figure 4.5: Interaction Model for CLIC4 and Ezrin

BIBLIOGRAPHY

Álvarez-Fernández, M., & Malumbres, M. (2014). Preparing a cell for nuclear envelope breakdown: Spatio-temporal control of phosphorylation during mitotic entry. *BioEssays*, *36*(8), 757–765. https://doi.org/10.1002/bies.201400040

Argenzio, E., Klarenbeek, J., Kedziora, K. M., Nahidiazar, L., Isogai, T., Perrakis, A., Jalink, K., Moolenaar, W. H., & Innocenti, M. (2018). Profilin binding couples chloride intracellular channel protein CLIC4 to RhoA–mDia2 signaling and filopodium formation. *Journal of Biological Chemistry*, *293*(50), 19161–19176. https://doi.org/10.1074/jbc.RA118.002779

Argenzio, E., Margadant, C., Leyton-Puig, D., Janssen, H., Jalink, K., Sonnenberg, A., & Moolenaar, W. H. (2014). CLIC4 regulates cell adhesion and β1 integrin trafficking. *Journal of Cell Science*, *127*(24), 5189–5203.

Arpin, M., Chirivino, D., Naba, A., & Zwaenepoel, I. (2011). Emerging role for ERM proteins in cell adhesion and migration. *Cell Adhesion and Migration*, *5*(2), 199–206. https://doi.org/10.4161/cam.5.2.15081

Barret, C., Roy, C., Montcourrier, P., Mangeat, P., & Niggli, V. (2000). Mutagenesis of the phosphatidylinositol 4,5-bisphosphate (PIP2) binding site in the NH2-terminal domain of ezrin correlates with its altered cellular distribution. *Journal of Cell Biology*, *151*(5), 1067–1079. https://doi.org/10.1083/jcb.151.5.1067

Bartek, J., & Lukas, J. (2001). Mammalian G1- and S-phase checkpoints in response to DNA damage. *Current Opinion in Cell Biology*, *13*(6), 738–747. https://doi.org/10.1016/S0955-0674(00)00280-5

Berryman, M. A., & Goldenring, J. R. (2003). CLIC4 Is Enriched at Cell-Cell Junctions and Colocalizes With AKAP350 at the Centrosome and Midbody of Cultured Mammalian Cells. *Cell Motility and the Cytoskeleton*, *56*(3), 159–172. https://doi.org/10.1002/cm.10141

Board, P. G., Coggan, M., Chelvanayagam, G., Easteal, S., Jermiin, L. S., Schulte, G. K., Danley, D. E., Hoth, L. R., Griffor, M. C., Kamath, A. V., Rosner, M. H., Chrunyk, B. A., Perregaux, D. E., Gabel, C. A., Geoghegan, K. F., & Pandit, J. (2000). Identification, characterization, and crystal structure of the omega class glutathione transferases. *Journal of Biological Chemistry*, *275*(32), 24798–24806. https://doi.org/10.1074/jbc.M001706200

Bretscher, A. (1983). Purification of an 80,000-dalton protein that is a component of the isolated microvillus cytoskeleton, and its localization in nonmuscle cells. *The Journal of Cell Biology*, *97*(2), 425–432. https://doi.org/10.1083/jcb.97.2.425

Bretscher, A. (1999). Regulation of cortical structure by the ezrin-radixin-moesin protein family. *Current Opinion in Cell Biology*, *11*(1), 109–116. https://doi.org/10.1016/S0955-0674(99)80013-1

Bretscher, A., Edwards, K., & Fehon, R. G. (2002). ERM proteins and merlin: Integrators at the cell cortex. *Nature Reviews Molecular Cell Biology*, *3*(8), 586–599. https://doi.org/10.1038/nrm882

Burke, B., & Ellenberg, J. (2002). Remodelling the walls of the nucleus. *Nature Reviews Molecular Cell Biology*, *3*(7), 487–497. https://doi.org/10.1038/nrm860

Charras, G. T., Hu, C. K., Coughlin, M., & Mitchison, T. J. (2006). Reassembly of contractile actin cortex in cell blebs. *Journal of Cell Biology*, *175*(3), 477–490. https://doi.org/10.1083/jcb.200602085

Chayen, N. E. (2005). Methods for separating nucleation and growth in protein crystallisation. *Progress in Biophysics and Molecular Biology*, *88*(3), 329–337. https://doi.org/10.1016/j.pbiomolbio.2004.07.007

Chayen, N. E., & Saridakis, E. (2008). Protein crystallization: From purified protein to diffraction-quality crystal. *Nature Methods*, *5*(2), 147–153. https://doi.org/10.1038/nmeth.f.203

Chou, S. Y., Hsu, K. S., Otsu, W., Hsu, Y. C., Luo, Y. C., Yeh, C., Shehab, S. S., Chen, J., Shieh, V., He, G. A., Marean, M. B., Felsen, D., Ding, A., Poppas, D. P., Chuang, J. Z., & Sung, C. H. (2016). CLIC4 regulates apical exocytosis and renal tube luminogenesis through retromer- and actin-mediated endocytic trafficking. *Nature Communications*, *7*. https://doi.org/10.1038/ncomms10412

Chuang, J.-Z., Chou, S.-Y., & Sung, C.-H. (2010). Chloride Intracellular Channel 4 Is Critical for the Epithelial Morphogenesis of RPE Cells and Retinal Attachment. *Molecular Biology of the Cell*, *21*, 3017–3028. https://doi.org/10.1091/mbc.E09

Chuang, J.-Z., Milner, T. A., Zhu, M., & Sung, C. H. (1999). A 29 kDa intracellular chloride channel p64H1 is associated with large dense-core vesicles in rat hippocampal neurons. *Journal of Neuroscience*, *19*(8), 2919–2928. https://doi.org/10.1523/jneurosci.19-08-02919.1999

Clucas, J., & Valderrama, F. (2015). Correction to ERM proteins in cancer progression

[J. Cell Sci. 127, (2015), 267-275]. *Journal of Cell Science*, *128*(6), 1253. https://doi.org/10.1242/jcs.170027

Dulhunty, A., Gage, P., Curtis, S., Chelvanayagam, G., & Board, P. (2001). The Glutathione Transferase Structural Family Includes a Nuclear Chloride Channel and a Ryanodine Receptor Calcium Release Channel Modulator. *Journal of Biological Chemistry*, *276*(5), 3319–3323. https://doi.org/10.1074/jbc.M007874200

Duncan, R. R., Westwood, P. K., Boyd, A., & Ashley, R. H. (1997). Rat brain p64H1, expression of a new member of the p64 chloride channel protein family in endoplasmic reticulum. *Journal of Biological Chemistry*, *272*(38), 23880–23886. https://doi.org/10.1074/jbc.272.38.23880

Edwards, J. C., & Kahl, C. R. (2010). Chloride channels of intracellular membranes. *FEBS Letters*, *584*(10), 2102–2111. https://doi.org/10.1016/j.febslet.2010.01.037

Eggert, U. S., Mitchison, T. J., & Field, C. M. (2006). Animal cytokinesis: From parts list to mechanisms. *Annual Review of Biochemistry*, *75*, 543–566. https://doi.org/10.1146/annurev.biochem.74.082803.133425

Evans, T., Rosenthal, E. T., Youngblom, J., Distel, D., & Hunt, T. (1983). Cyclin: A protein specified by maternal mRNA in sea urchin eggs that is destroyed at each cleavage division. *Cell*, *33*(2), 389–396. https://doi.org/10.1016/0092-8674(83)90420-8

Fehon, R. G., McClatchey, A. I., & Bretscher, A. (2010). Organizing the cell cortex: The role of ERM proteins. *Nature Reviews Molecular Cell Biology*, *11*(4), 276–287. https://doi.org/10.1038/nrm2866

Fernández-Salas, E., Sagar, M., Cheng, C., Yuspa, S. H., & Weinberg, W. C. (1999). P53 and Tumor Necrosis Factor A Regulate the Expression of a Mitochondrial Chloride Channel Protein. *Journal of Biological Chemistry*, *274*(51), 36488–36497. https://doi.org/10.1074/jbc.274.51.36488

Gary, R., & Bretscher, A. (1995). Ezrin Self-Association Involves Binding of an N-Terminal Domain to a Normally Masked C-Terminal Domain that Includes the F-Actin Binding Site. *Molecular Biology of the Cell*, *6*, 1061–1075. https://doi.org/10.1091/mbc.e12-02-0152

Gawas, U. B., Mandrekar, V. K., & Majik, M. S. (2019). Structural analysis of proteins using X-ray diffraction technique. In *Advances in Biological Science Research: A*

Practical Approach. Elsevier Inc. https://doi.org/10.1016/B978-0-12-817497-5.00005-7

Govada, L., & Chayen, N. E. (2019). Choosing the method of crystallization to obtain optimal results. *Crystals*, *9*(2). https://doi.org/10.3390/cryst9020106

Güttinger, S., Laurell, E., & Kutay, U. (2009). Orchestrating nuclear envelope disassembly and reassembly during mitosis. *Nature Reviews Molecular Cell Biology*, *10*(3), 178–191. https://doi.org/10.1038/nrm2641

Hamada, K., Shimizu, T., Matsui, T., Tsukita, S., Tsukita, S., & Hakoshima, T. (2000). Structural basis of the membrane-targeting and unmasking mechanisms of the radixin FERM domain. *EMBO Journal*, *19*(17), 4449–4462. https://doi.org/10.1093/emboj/19.17.4449

Hanono, A., Garbett, D., Reczek, D., Chambers, D. N., & Bretscher, A. (2006). EPI64 regulates microvillar subdomains and structure. *Journal of Cell Biology*, *175*(5), 803–813. https://doi.org/10.1083/jcb.200604046

Harashima, H., Dissmeyer, N., & Schnittger, A. (2013). Cell cycle control across the eukaryotic kingdom. *Trends in Cell Biology*, *23*(7), 345–356. https://doi.org/10.1016/j.tcb.2013.03.002

Hunt, T., Nasmyth, K., & Novák, B. (2011). The cell cycle. *Philosophical Transactions of the Royal Society B: Biological Sciences*, *366*(1584), 3494–3497. https://doi.org/10.1098/rstb.2011.0274

Iyama, T., & Wilson III, D. M. (2013). DNA repair mechanisms in dividing and non-dividing cells. *Natural Institutes of Health*, *12*(6), 620–636. https://doi.org/10.1038/jid.2014.371

Jayasundar, J. J., Ju, J. H., He, L., Liu, D., Meilleur, F., Zhao, J., Callaway, D. J. E., & Bu, Z. (2012). Open conformation of ezrin bound to phosphatidylinositol 4,5-bisphosphate and to F-actin revealed by neutron scattering. *Journal of Biological Chemistry*, *287*(44), 37119–37133. https://doi.org/10.1074/jbc.M112.380972

Jiang, L., Phang, J. M., Yu, J., Harrop, S. J., Sokolova, A. V., Duff, A. P., Wilk, K. E., Alkhamici, H., Breit, S. N., Valenzuela, S. M., Brown, L. J., & Curmi, P. M. G. (2014). CLIC proteins, ezrin, radixin, moesin and the coupling of membranes to the actin cytoskeleton: A smoking gun? *Biochimica et Biophysica Acta - Biomembranes*, *1838*(2), 643–657. https://doi.org/10.1016/j.bbamem.2013.05.025

Kagiali, Z. C. U., Saner, N., Akdag, M., Sanal, E., Degirmenci, B. S., Mollaoglu, G., &

Ozlu, N. (2020). CLIC4 and CLIC1 bridge plasma membrane and cortical actin network for a successful cytokinesis. *Life Science Alliance*, *3*(2), 1–19. https://doi.org/10.26508/lsa.201900558

Kahsai, A. W., Zhu, S., & Fenteany, G. (2010). G Protein-Coupled Receptor Kinase 2 Activates Radixin, Regulating Membrane Protrusion and Motility in Epithelial Cells. *Natural Institutes of Health*, *1803*(2), 300–310. https://doi.org/10.1016/j.bbamcr.2009.11.002.G

Lalonde, D. P., Garbett, D., & Bretscher, A. (2010). A regulated complex of the scaffolding proteins PDZK1 and EBP50 with ezrin contribute to microvillar organization. *Molecular Biology of the Cell*, *21*(9), 1519–1529. https://doi.org/10.1091/mbc.E10-01-0008

Littler, D. R., Harrop, S. J., Goodchild, S. C., Phang, J. M., Mynott, A. V., Jiang, L., Valenzuela, S. M., Mazzanti, M., Brown, L. J., Breit, S. N., & Curmi, P. M. G. (2010). The enigma of the CLIC proteins: Ion channels, redox proteins, enzymes, scaffolding proteins? *FEBS Letters*, *584*(10), 2093–2101. https://doi.org/10.1016/j.febslet.2010.01.027

Liu, Y., Belkina, N. V., & Shaw, S. (2009). HIV infection of t cells: Actin-in and actin-out. *Science Signaling*, *2*(66), 1–4. https://doi.org/10.1126/scisignal.266pe23

Lukas, J., Lukas, C., & Bartek, J. (2004). Mammalian cell cycle checkpoints: Signalling pathways and their organization in space and time. *DNA Repair*, *3*(8–9), 997–1007. https://doi.org/10.1016/j.dnarep.2004.03.006

McClatchey, A. I., & Fehon, R. G. (2009). Merlin and the ERM proteins – regulators of receptor distribution and signaling at the cell cortex. *Natural Institutes of Health*, *19*(5), 198–206. https://doi.org/10.1016/j.tcb.2009.02.006.Merlin

Neisch, A. L., & Fehon, R. G. (2011). Ezrin, Radixin and Moesin: Key regulators of membrane-cortex interactions and signaling. *Natural Institutes of Health*, *23*(4), 377–382. https://doi.org/10.1016/j.ceb.2011.04.011.Ezrin

Özlü, N., Qureshi, M. H., Toyoda, Y., Renard, B. Y., Mollaoglu, G., Özkan, N. E., Bulbul, S., Poser, I., Timm, W., Hyman, A. A., Mitchison, T. J., & Steen, J. A. (2015). Quantitative comparison of a human cancer cell surface proteome between interphase and mitosis. *The EMBO Journal*, *34*(2), 251–265. https://doi.org/10.15252/embj.201385162

Padmakumar, V. C., Speer, K., Pal-Ghosh, S., Masiuk, K. E., Ryscavage, A., Dengler,

S. L., Hwang, S., Edwards, J. C., Coppola, V., Tessarollo, L., Stepp, M. A., & Yuspa, S. H. (2012). Spontaneous skin erosions and reduced skin and corneal wound healing characterize CLIC4 NULL mice. *American Journal of Pathology*, *181*(1), 74–84. https://doi.org/10.1016/j.ajpath.2012.03.025

Pearson, M. A., Reczek, D., Bretscher, A., & Karplus, P. A. (2000). Structure of the ERM protein moesin reveals the FERM domain fold masked by an extended actin binding tail domain. *Cell*, *101*(3), 259–270. https://doi.org/10.1016/S0092-8674(00)80836-3

Peters, J. M. (2006). The anaphase promoting complex/cyclosome: A machine designed to destroy. *Nature Reviews Molecular Cell Biology*, *7*(9), 644–656. https://doi.org/10.1038/nrm1988

Phang, J. M., Harrop, S. J., Duff, A. P., Sokolova, A. V., Crossett, B., Walsh, J. C., Beckham, S. A., Nguyen, C. D., Davies, R. B., Glöckner, C., Bromley, E. H. C., Wilk, K. E., & Curmi, P. M. G. (2016). Structural characterization suggests models for monomeric and dimeric forms of full-length ezrin. *Biochemical Journal*, *473*(18), 2763–2782. https://doi.org/10.1042/BCJ20160541

Pines, J., & Rieder, C. L. (2001). Re-staging mitosis: A contemporary view of mitotic progression. *Nature Cell Biology*, *3*(1). https://doi.org/10.1038/35050676

Ponsioen, B., van Zeijl, L., Langeslag, M., Berryman, M., Littler, D., Jalink, K., & Moolenaar, W. H. (2009). Spatiotemporal Regiulation of Chloride Intracellular Channel Protein CLIC4 by RhoA. *Molecular Biology of the Cell*, *20*, 4664–4672. https://doi.org/10.1091/mbc.E09

Ponuwei, G. A. (2016). A glimpse of the ERM proteins. *Journal of Biomedical Science*, *23*(1), 4–9. https://doi.org/10.1186/s12929-016-0246-3

Pore, D., & Gupta, N. (2015). Ezrin-Radixin-Moesin family proteins in the regulation of B cell immune response. *Natural Institutes of Health*, *35*(1), 15–31.

Proutski, I., Karoulias, N., & Ashley, R. H. (2002). Overexpressed chloride intracellular channel protein CLIC4 (p64H1) is an essential component of novel plasma membrane anion channels. *Biochemical and Biophysical Research Communications*, *297*(2), 317–322. https://doi.org/10.1016/S0006-291X(02)02199-X

Roumier, A., Olivo-Marin, J. C., Arpin, M., Michel, F., Martin, M., Mangeat, P., Acuto, O., Dautry-Varsat, A., & Alcover, A. (2001). The membrane-microfilament linker

ezrin is involved in the formation of the immunological synapse and in T cell activation. *Immunity*, *15*(5), 715–728. https://doi.org/10.1016/S1074-7613(01)00225-4

Salazar-Roa, M., & Malumbres, M. (2017). Fueling the Cell Division Cycle. *Trends in Cell Biology*, *27*(1), 69–81. https://doi.org/10.1016/j.tcb.2016.08.009

Shukla, A., Malik, M., Cataisson, C., Ho, Y., Friesen, T., Suh, K. S., & Yuspa, S. H. (2009). TGF-β signalling is regulated by Schnurri-2-dependent nuclear translocation of CLIC4 and consequent stabilization of phospho-Smad2 and 3. *Nature Cell Biology*, *11*(6), 777–784. https://doi.org/10.1038/ncb1885

Simons, P. C., Pietromonaco, S. F., Reczek, D., Bretscher, A., & Elias, L. (1998). C-terminal threonine phosphorylation activates ERM proteins to link the cell's cortical lipid bilayer to the cytoskeleton. *Biochemical and Biophysical Research Communications*, *253*(3), 561–565. https://doi.org/10.1006/bbrc.1998.9823

Smith, W. J., Nassar, N., Bretscher, A., Cerione, R. A., & Karplus, P. A. (2003). Structure of the active N-terminal domain of ezrin: Conformational and mobility changes identify keystone interactions. *Journal of Biological Chemistry*, *278*(7), 4949–4956. https://doi.org/10.1074/jbc.M210601200

Smyth, M. S., & Martin, J. H. J. (2000). X-Ray Crystallography. *Journal of Clinical and Molecular Pathology*, *53*, 8–14. https://doi.org/10.1016/B978-0-12-374984-0.01657-0

Suginta, W., Karoulias, N., Aitken, A., & Ashley, R. H. (2001). Chloride intracellular channel protein CLIC4 (p64H1) binds directly to brain dynamin I in a complex containing actin, tubulin and 14-3-3 isoforms. *Biochemical Journal*, *359*(July), 55–64. https://doi.org/10.1042/0264-6021

Suh, K. S., Mutoh, M., Gerdes, M., & Yuspa, S. H. (2005). CLIC4, an intracellular chloride channel protein, is a novel molecular target for cancer therapy. *The Journal of Investigative Dermatology. Symposium Proceedings / the Society for Investigative Dermatology, Inc. [and] European Society for Dermatological Research*, *10*(2), 105–109. https://doi.org/10.1111/j.1087-0024.2005.200402.x

Suh, K. S., Mutoh, M., Nagashima, K., Fernandez-Salas, E., Edwards, L. E., Hayes, D. D., Crutchley, J. M., Marin, K. G., Dumont, R. A., Levy, J. M., Cheng, C., Garfield, S., & Yuspa, S. H. (2004). The Organellular Chloride Channel Protein CLIC4/mtCLIC Translocates to the Nucleus in Response to Cellular Stress and

Accelerates Apoptosis. *Journal of Biological Chemistry*, *279*(6), 4632–4641. https://doi.org/10.1074/jbc.M311632200

Tavasoli, M., Al-Momany, A., Wang, X., Li, L., Edwards, J. C., & Ballermann, B. J. (2016). Both CLIC4 and CLIC5A activate ERM proteins in glomerular endothelium. *American Journal of Physiology - Renal Physiology*, *311*(5), F945–F957. https://doi.org/10.1152/ajprenal.00353.2016

Ulmasov, B., Bruno, J., Gordon, N., Hartnett, M. E., & Edwards, J. C. (2009). Chloride intracellular channel protein-4 functions in angiogenesis by supporting acidification of vacuoles along the intracellular tubulogenic pathway. *American Journal of Pathology*, *174*(3), 1084–1096. https://doi.org/10.2353/ajpath.2009.080625

Vader, G., & Lens, S. M. A. (2008). The Aurora kinase family in cell division and cancer. *Biochimica et Biophysica Acta - Reviews on Cancer*, *1786*(1), 60–72. https://doi.org/10.1016/j.bbcan.2008.07.003

Van Zundert, G. C. P., Rodrigues, J. P. G. L. M., Trellet, M., Schmitz, C., Kastritis, P. L., Karaca, E., Melquiond, A. S. J., Van Dijk, M., De Vries, S. J., & Bonvin, A. M. J. J. (2016). The HADDOCK2.2 Web Server: User-Friendly Integrative Modeling of Biomolecular Complexes. *Journal of Molecular Biology*, *428*(4), 720–725. https://doi.org/10.1016/j.jmb.2015.09.014

Vermeulen, K., Van Bockstaele, D. R., & Berneman, Z. N. (2003). The cell cycle: A review of regulation, deregulation and therapeutic targets in cancer. *Cell Proliferation*, *36*(3), 131–149. https://doi.org/10.1046/j.1365-2184.2003.00266.x

Walczak, C. E., Cai, S., & Khodjakov, A. (2010). Mechanisms of chromosome behaviour during mitosis. *Nature Reviews Molecular Cell Biology*, *11*(2), 91–102. https://doi.org/10.1038/nrm2832

Wong, W., & Gough, N. R. (2009). Focus issue: The protein dynamics of cell signaling. *Science Signaling*, *2*(66), 2–5. https://doi.org/10.1126/scisignal.266eg4